POLARIMETRY OF MAGNETIC CATACLYSMIC VARIABLES

Mark Cropper

A thesis submitted in partial fulfilment
for the degree of Doctor of Philosophy
at the University of Cape Town

March 1985

DECLARATION

All work in this thesis which is not referenced or disclaimed, is my own.

Signed by candidate

ABSTRACT

The design and construction of an astronomical polarimeter is described and an evaluation made of its performance. Extensive observations of cataclysmic variables with emphasis on the AM Her and DQ Her classes are then presented.

After consideration of the basic principles involved in the development of an efficient and accurate polarimeter, a design using two super-achromatic retarders (a ¼ wave and a ½ wave) rotating above a fixed analyser was adopted. This permitted simultaneous linear and circular polarisation measurements, or, by rearranging the order of the retarders in the beam, linear polarisation measurements alone, or circular polarisation measurements alone, with enhanced efficiency. The polarimeter was found to have extremely low instrumental polarisations and, because of the superachromatic retarders used, the efficiency correction factors were very close to 1 at all wavelengths. The polarisations are calculated at the telescope and the light curve at a higher time resolution may also be recorded if this is required.

Extensive sets of observations using the polarimeter were obtained for six of the ten AM Her variables (or "polars"). EF Eri and E1405-451 were observed most. Evidence was found in E1405-451 for movement of the apparent location of the accretion region on the primary star and the inclination and magnetic dipole offset from the rotation axis was determined. This allowed a comparison to be made between the competing models for the cyclotron emission, showing that those which take into account the temperature structure of the accretion region provide the best results. Observations and an analysis of the polarisation data from HO139-68, E2003+225, VV Puppis and PG1550+191 are also presented in some

detail. A final chapter presents results from observations made to detect a modulation in the polarisation at the rotation period of the primary in the DQ Her variables. Upper limits are set for 4 members of the class and the implications of the results are discussed.

ACKNOWLEDGEMENTS

Over the past four years many people have helped me get to this point. My sincere thanks are due to:

- Tony Back who designed and built the polarimeter optical module from the roughest of my sketches.

- Luis Balona for permitting his assembler programs to be used as a basis for mine and for his help in the early stages of software development.

- The staff of the S.A.A.O. Electronics Workshop - Guy Woodhouse, Bill Pearson, Dave Carter, Jim Wilson and Tony Riddick for their friendliness, hospitality and help at all times.

- Penny Dobbie for typing the manuscript.

- Darragh O'Donoghue, Santiago Tapia and Don Kurtz for their interest, help and encouragement.

- The C.S.I.R. and U.C.T. for personal financial support, and the C.S.I.R. for providing funds for the polarimeter.

- Prof. M. Feast for his generous allocation of telescope time at the S.A.A.O.

- Erika, who helped me fulfil the rest of the requirements for a Ph.D. degree.

- Brian Warner, who supervised this thesis, with whom I have had many clarifying discussions and who provided me with the environment within which it was possible to make the most of these opportunities.

CONTENTS

INTRODUCTION

Cataclysmic Variables (CVs) are semi-detached binary stars with white dwarf primary and lower main sequence secondary components (see reviews by Warner 1976, Robinson 1976, Cordova and Mason 1983). Until relatively recently, however, the effects of magnetic fields in these objects had hardly been investigated, despite the discovery of a fairly large number of strongly magnetised single white dwarfs (Angel 1977). The discovery by Tapia (1977) of strongly polarised light (both linear and circular) from AM Her and subsequent discoveries of polarisation in other CV's by a variety of investigators, established the existence of a class of CV's with a strongly magnetic primary ($B \gtrsim 10^7 G$), and no evidence of an accretion disk. The primary source of light in these objects appears to be cyclotron radiation (although most of the accretion energy is liberated as X-rays). In addition, the existence of magnetic fields has been invoked to explain the characteristics of another class of CV's, the DQ Her stars (or alternatively, but not entirely synonomously, the "Intermediate Polars"). For more details on the above classes, see Liebert and Stockman (1984), Mason (1985) and Warner (1982), Warner (1984).

Because the Astronomy Department at the University of Cape Town specialises largely in CV's, there was an urgent requirement for a polarimeter. The description of the design and the presentation of the observations made with the new instrument and their analysis and interpretation is set out in this thesis.

Chapter 1 presents an overview of the concepts involved in the optimum design of a polarimeter. Chapter 2 is a description of the design finally adopted, and an evaluation of the capabilities of the instrument. Details of the electronic circuitry and software have been left out, in order to reduce the bulk of the thesis. As can be imagined, however, considerable time and effort was spent in the design, construction and programming of the instrument - the reduction program alone (QUARTZ) is more than 250 pages of assembler code. Initially it was intended to include the Technical Manual, Users Manual and Manual for the Analysis Package as appendices in the thesis: however it was judged that Plate 1, showing details of the instrument provided enough information in this regard.

Chapters 3 to 6 deal with the observations themselves. Chapter 3 contains an investigation into the polarisation behaviour of EF Eri, the shortest period and probably most enigmatic AM Her star. Chapter 4 presents a large data set obtained with the collaboration of Drs. J. Menzies and S. Tapia and some relatively successful investigations into the properties of E1405-451. Both chapters were originally written in paper form: the former has been published in *Mon. Not. R. astr. Soc., 212,* and the latter has been recently submitted. Chapter 5 contains data on and investigations into four other AM Her stars, while the last chapter deals with a variety of cataclysmic variables, principally DQ Her stars.

The photometric observations obtained in collaboration with B. Warner during the initial years of this thesis during the construction phase of the polarimeter are not included. They are available as follows:-

a) Warner, B. and Cropper, M. "High Speed Photometry of the Dwarf Nova V2051 Oph", *Mon. Not. R. astr. Soc., 203*, 909, June 1983.

b) Warner, B. and Cropper, M. "High Speed Photometry of the Intermediate Polar V1223 Sgr", *Mon. Not. R. astr. Soc., 206*, 261, January 1984.

c) McHardy, I.M., Pye, J.P., Fairall, A.P., Warner, B., Cropper, M., and Allen, S. "Identification of 3A0729+103 with an Intermediate Polar Type Cataclysmic Variable", *Mon. Not. R. astr. Soc., 210*, 663, October 1984.

REFERENCES

Angel, J.R.P., 1977. *Astrophys. J., 216,* 1.

Cordova, F.A. and Mason, K.O., 1983 in Accretion Driven Stellar X-Ray Sources, ed. Lewin, W.H.G. and van den Heuvel, E.P.J., Cambridge University Press, England, P. 147.

Liebert, J. and Stockman, H.S., 1984. Steward Observatory Preprint no. 441.

Mason, K.O., 1985. University College London Preprint.

Robinson, E.L., 1976. *Ann. Rev. Astr. Astrophys., 14,* 119.

Tapia, S., 1977. *Astrophys. J., 212,* L125.

Warner, B., 1976. *I.A.U. Symp., 73,* 85.

Warner, B., 1982. *I.A.U. Coll., 72,* 155.

Warner, B., 1984. In Cataclysmic Variables and Low Mass X-ray Binaries, eds. Lamb, D.Q. and Patterson, J., Cambridge, Massachusetts. In press.

CHAPTER 1

CONCEPTS

1.1 General Principles

The basis for the optimum design of an optical polarimeter is set out in two important papers by Serkowski (Serkowski 1973, 1974). There he splits the designs of astronomical polarimeters into two classes:-

(a) Polarimeters without rapid modulation of the signal;

(b) Polarimeters with rapid modulation of the signal.

1.1.1 Polarimeters without Rapid Modulation of the Signal

In case (a) above a measurement is made of the intensity of a beam passing through an analyser at (at least) two different orientations of the analyser. Circular polarisation measurements are taken by inserting a quarter wave retarder in the beam and proceeding as for linear polarisation. These polarimeters are shown (Serkowski 1974) to be less efficient than polarimeters with rapid modulation of signal, and to be inherently less accurate. This is a result of atmospheric scintillation effects and of variations in the sky conditions during the integrations. Efficiencies can be improved by inserting depolarisers in the beam but this leads to clumsy mechanical arrangements where the entire instrument has to be rotated. As the case (a) polarimeters are inferior in every respect they were not investigated further.

1.1.2 Polarimeters with Rapid Modulation of the Signal

If the modulation rate is faster than the rate at which atmospheric conditions can change or guiding errors can take place, rapid modulation of the signal reduces errors caused in this way. The highest frequency variations caused the atmosphere are a result of scintillation. The resulting errors can be diminished by a factor (Serkowski 1974)

$$SF = (f/f_c)^{5/6}$$

where f = modulation frequency

f_c = cut off frequency $f_c = V/(\pi D)$

and D = telescope diameter

V = speed at which the wind moves the shadow pattern across the aperture of the telescope.

Typical values are f_c = 5 hz for a 2m telescope and 10 hz for a 1m telescope. Modulation at a rate of 60 hz thus reduces the scintillation by factors of approximately 8 and 4.5 for 2 and 1m telescopes respectively. Clearly at this modulation rate, errors caused by scintillation will be much reduced.

The rapid modulation can be achieved in three ways:-

(a) Rotating an analyser rapidly in the beam, so that the extinction axis moves through 360 degrees perpendicular to the beam. Because of movement of the image on the detector photocathode and because photomultipliers can be more sensitive to light linearly polarised in one orientation than another this is not very satisfactory. Introducing depolariser into the beam (Serkowski 1974) ameliorates the former

problem but does nothing for the latter.

(b) Rotation of a retarder of fixed retardance in the beam about an axis perpendicular to the fast axis of the retarder. The emergent beam is passed through an analyser and the resultant intensity recorded. The intensity is modulated by the rotation of the retarder in such a way that the polarisation information can be calculated (see section 1.5).

(c) Using a variable retarder in front of an analyser. Varying the retardance on the retarder modulates the intensity from the analyser and the polarisation information again can be calculated.

The instrument therefore requires a fixed analyser and a rotating or variable retarder. Greater flexibility and better separation of the polarisation information is obtained, however, by using two retarders instead of one in front of the analyser. Use of three retarders provides very little extra flexibility at the expense of more light absorption, extra complexity and cost. It was therefore not considered.

Rapid modulation of the light passing to the detector reduces all but one major source of error - that of photon statistics. This can be countered only by collecting a larger number of photons and maximizing the efficiency of the detector. Small errors are introduced by imperfect retarders. These can be minimized by careful optical and mechanical design. Other small errors such as those resulting from variable sky background, unnecessary reflections, and instrumental polarisations can also be minimized by taking the prescribed precautions (Serkowski 1974).

1.2 Description of Polarised Light

The polarisation state of light is generally described by four Stokes parameters, usually written I,Q,U and V.

If a simple electromagnetic wave is propagating in the z direction, the components of the electric vector E at some point along the wave are given by (Serkowski 1962)

$$E_x = E_{xo}\sin(\omega t-\varepsilon_x) \tag{1.2}$$

$$E_y = E_{yo}\sin(\omega t-\varepsilon_y) \tag{1.3}$$

The Stokes parameters are then defined as (Chandrasekhar 1950)

$$I = E_{xo}^2 + E_{yo}^2 \tag{1.4}$$

$$Q = E_{xo}^2 - E_{yo}^2 \tag{1.5}$$

$$U = -2E_{xo}E_{yo}\cos(\varepsilon_x-\varepsilon_y) \tag{1.6}$$

$$V = 2E_{xo}E_{yo}\sin(\varepsilon_x-\varepsilon_y) \tag{1.7}$$

The Stokes parameters describing a *beam* of light are sums of the individual waves making up the beam. The light beam is then generally partially polarised and is considered as consisting of an unpolarised component with Stokes parameters

$$\{I - (Q^2+U^2+V^2)^{\frac{1}{2}},0,0,0\} \tag{1.8}$$

and a fully polarised component

$$\{Q^2+U^2+V^2)^{\frac{1}{2}},Q,U,V \tag{1.9}$$

(Chandrasekhar 1950). The beam can thus still be characterized by the four Stokes parameters.

The polarisation state can also be described by four other parameters - intensity I (same as the Stokes I), degree of linear polarisation p, position angle θ in the equatorial co-ordinate system, and degree of circular polarisation q. The transformation equations are (Serkowski 1974)

$$I = I \tag{1.10}$$

$$p = (Q^2+U^2)^{\frac{1}{2}}/I \qquad Q = Ipcos2\theta \tag{1.11}$$

$$\theta = \tfrac{1}{2}tan^{-1}(U/Q) \qquad U = Ipsin2\theta \tag{1.12}$$

$$q = V/I \qquad V = Iq \tag{1.13}$$

Both sets of parameters are used in observational astronomy.

1.3 Mueller Matrix Description of the System

In Section (1.1.2) it was found that the instrument would use an optical arrangement of two retarders and a fixed analyser. The emergent intensity of the beam (as a function of the initial Stokes parameters I,Q,U and V, the retardances τ_1 and τ_2, and optic axis position angles ψ_1 and ψ_2) is found by means of Mueller matrix calculations.

The matrix for a perfect analyser at any position angle ϕ is (Shurcliff 1962)

$$\tfrac{1}{2}\begin{Bmatrix} 1 & cos2\phi & sin2\phi & 0 \\ cos2\phi & cos^2 2\phi & \tfrac{1}{2}sin4\phi & 0 \\ sin2\phi & \tfrac{1}{2}sin4\phi & sin^2 2\phi & 0 \\ 0 & 0 & 0 & 0 \end{Bmatrix} \tag{1.14}$$

The matrix for a perfect retarder of retardance τ and fast axis at position angle ψ is

$$\begin{Bmatrix} 1 & 0 & 0 & 0 \\ 0 & G+Hcos4\psi & Hsin4\psi & -sin\tau sin2\psi \\ 0 & Hsin4\psi & G-Hcos4\psi & sin\tau cos2\psi \\ 0 & sin\tau sin2\psi & -sin\tau cos2\psi & cos\tau \end{Bmatrix} \tag{1.15}$$

where $G = \frac{1}{2}(1+\cos\tau)$ $H = \frac{1}{2}(1-\cos\tau)$. Multiplying these matrices in the appropriate manner, two important equations are obtained for the final intensity emerging from the analyser (Serkowski 1974):

(a) For a single retarder with optic axis at position angle ψ followed by an analyser with principal plane at position angle $\phi = 0^{o}$ (upper signs) or $\phi = 90^{o}$ (lower signs):

$$I' = \tfrac{1}{2}[I \pm Q(G+H\cos 4\psi) \pm UH\sin 4\psi \mp V\sin\tau\sin 2\psi] \qquad (1.16)$$

(b) For two retarders in series, retardances τ_1, τ_2 and fast axes at position angles ψ_1, ψ_2, followed by an analyser with principal plane at position angle $\phi = 0^{o}$ (upper signs) or $\phi = 90^{o}$ (lower signs):

$$\begin{aligned} I' = \tfrac{1}{2}\{ & I \pm Q[G_1G_2+H_1H_2\cos 4(\psi_1-\psi_2)+H_1G_2\cos 4\psi_1 \\ & +G_1H_2\cos 4\psi_2-\sin\tau_1\sin\tau_2\sin 2\psi_1\sin 2\psi_2] \\ & \pm U[H_1H_2\sin 4(\psi_1-\psi_2)+H_1G_2\sin 4\psi_1+ \\ & G_1H_2\sin 4\psi_2+\sin\tau_1\sin\tau_2\cos 2\psi_1\sin 2\psi_2] \\ & \mp V[H_2\sin\tau_1\sin(2\psi_1-4\psi_2)+G_2\sin\tau_1\sin 2\psi_1 \\ & +\cos\tau_1\sin\tau_2\sin 2\psi_2]\} \end{aligned} \qquad (1.17)$$

The variables in these two equations provide for a great deal of flexibility in the modulation of the incoming beam as a function of τ and ψ.

1.4 The Polarisation Convertors

As the retarders are the most critical optical elements in the polarimeter, some time was spent in evaluating them.

1.4.1 Variable Retarders

A detailed investigation was first made into the properties of variable retarders as they have the following advantages:-

(a) They can be modulated very rapidly;

(b) They avoid the problem of rotating optics, with motors, drive belts, heavy currents, image motion etc.

(c) As no accelerations and decelerations have to take place some variable retarders can be modulated in a more complicated way then rotating retarders (for example see Baur *et al.* 1974).

In addition, it seemed that variable retarders have more development potential than fixed retarders, and that greater benefit in the long run would be obtained from using them. These reasons initially made the variable retarders seem more attractive.

Two types of variable retarders are available commercially: Pockels cells and photoelastic modulators. The former have been used extensively by Angel and Landstreet 1970, Tomaszewski *et al.* (1980) and recently by McLean *et al.* (1984). The latter have been used by Kemp, Wolstencroft and Swedlund (1972) and Wolstencroft, Smith, Cormack and Campbell (1983). All of these designs use one variable retarder only. Designs with two retarders are limited to solar instruments (e.g. Baur *et al.* 1974), where two Pockels cells are used. In the Pockels cell (Billings 1952) a crystal, KDP or ADP, changes its retardance in phase with a rapidly changing high voltage applied between transparent electrodes at each surface.

The photoelectric modulator uses stress birefringence caused by acoustic vibrations set up in an isotropic material (Kemp 1969).

A scheme using two variable retarders was investigated where the efficiency of the polarimeter for detecting circular or linear polarisation could be varied continuously from 100% efficiency for circular and 0% efficiency for linear polarisation to 100% linear and 0% circular. It was felt that this would introduce a great deal of flexibility into the observing. Before a solution was found, however, it became apparent that there were severe problems:

(a) The variable retarders are not achromatic;

(b) The Pockels cells absorb too much light;

(c) The variable retarders are extremely expensive;

(d) Pockels cells need high voltages (up to 5 kV), which, for maximum efficiency, should be square wave at a high modulation rate ($\sim$1 khz);

(e) Photoelastic modulators rely on standing waves to cause the retardance and therefore cannot be square wave modulated. The amount of modulation falls off from a maximum in the centre towards the edges of the aperture.

The above together with the realisation that the variable efficiency idea proposed above would not, after all, result in any advantage, led to the demise of the variable retarder as a viable modulating element for the polarimeter. The most important consideration was point (a). The applied voltage to the Pockels cell is determined by the required

retardation at the specified wavelength (see Goldstein 1968). The polarisation efficiency falls off as $\sin\left(\frac{\lambda}{\lambda_0}\cdot\frac{\pi}{2}\right)$ (Angel 1981). For two cells in series this would be $\sin^2\left(\frac{\lambda}{\lambda_0}\cdot\frac{\pi}{2}\right)$. If the voltage was set for retardation τ (for 4000Å) this would result in a modulation efficiency of 95% and 90% respectively at 5000Å. This wavelength dependent efficiency is the major reason only one cell is used for broadband work. Different voltages have to be applied for a constant retardation at different wavelengths and a wavelength dependent modulation efficiency correction factor applied. It was decided that until achromatic variable retarders become available it is preferable to use non-variable retarders which can be made achromatic.

1.4.2 Rotating Retarders

By using one retarder of retardance $\tau_1 = \pi/4$ and another with retardance $\tau_2 = \pi/2$ a number of convenient optical schemes can be developed for modulating the incident beam. These retarders are commercially available in a "Superachromatic" form from B. Halle, Berlin. They are made from three pairs of quartz and MgF_2 achromatic plates and have a path difference of $\pi/2$ (half wave plate) $\pm 1\%$ and $\pi/4$ (quarter wave plate) $\pm$ 2% over a spectral range 3100Å to 11000Å (Serkowski 1973, Title 1975). These retarders are almost perfect over the entire visual passband and have even been used (although at a lower modulation efficiency) in the infra red (Bailey and Hough 1982). Although expensive it was felt that their excellence over the entire band, together with ease of operation (no changing of

retarders for different filters) justified their purchase.

Four possible optical schemes are possible with the above two retarders:-

a) ½ wave plate only

b) ¼ wave plate only

c) ¼ then ½ wave plate

d) ½ then ¼ wave plate

Substitution into equations 1.16 and 1.17 gives

a) $$I' = \tfrac{1}{2}(I \pm Q\cos 4\psi \pm U\sin 4\psi) \qquad (1.18)$$

b) $$I' = \tfrac{1}{2}(I \pm \tfrac{1}{2}Q \pm \tfrac{1}{2}Q\cos 4\psi \pm \tfrac{1}{2}U\sin 4\psi \mp V\sin 2\psi) \qquad (1.19)$$

c) $$I' = \tfrac{1}{2}\{I \pm \tfrac{1}{2}Q[\cos 4(\psi_1-\psi_2)+\cos 4\psi_2] \pm \tfrac{1}{2}U[\sin 4(\psi_1-\psi_2)+\sin 4\psi_2] \mp V\sin(2\psi_1-4\psi_2)\} \qquad (1.20)$$

d) $$I' = \tfrac{1}{2}\{I \pm \tfrac{1}{2}Q[\cos 4(\psi_1-\psi_2)+\cos 4\psi_1] \pm U[\sin 4(\psi_1-\psi_2)+\sin 4\psi_2] \pm V\sin 2\psi_2\} \qquad (1.21)$$

In scheme (a) modulation in the emergent intensity will occur if the immergent beam is linearly polarised, while in schemes (b) to (d) modulation will occur if the immergent beam is polarised in any way. It is evident that simply by changing the element arrangement in the beam a flexible instrument can be constructed which is able to measure linear polarisation alone or both linear and circular polarisation simultaneously. Measuring circular polarisation alone requires acceleration and deceleration of one of the waveplates (see Section 1.5.3 and 2.5.2) but this can be controlled automatically without difficulty.

A number of optical arrangements are listed in Serkowski (1974) and an analysis is made in terms of efficiency, ratios of modulation to mechanical rotation frequencies and availability

of components. The arrangements that perform best are:-

a) Linear - ½ wave plate continually rotating.

b) Circular - ½ wave plate continually rotating asynchronously followed by ¼ wave plate rotating in 90° steps.

c) Simultaneous - ¼ wave plate followed by a ½ wave plate contrarotating synchronously.

1.5 The Optical Arrangement

1.5.1 Simultaneous Stokes Parameter Measurement

For case (c) above equation 1.20 then becomes

$$\left.\begin{aligned} I' = \tfrac{1}{2}\{ & I \pm \tfrac{1}{2}Q[\cos 8\psi_1 + \cos 4\psi_1] \\ & \pm \tfrac{1}{2}U[\sin 8\psi_1 - \sin 4\psi_1] \\ & \mp V[\sin 6\psi_1] \qquad \} \end{aligned}\right. \tag{1.22}$$

where angles of the waveplates are referred to the quarter wave plate (1) fast axis. It can be seen that the linear component of the polarisation is modulated equally at the 4th and 8th harmonics of the rotation frequency, while the circular is modulated at the 6th harmonic.

This rapid rate of modulation is advantageous in two ways:-

a) The errors caused by scintillation are much reduced (cf section 1.1.1).

b) Modulation caused by wedge shaped rotating elements, dirt on the rotating components or dichroism from refraction at the element surfaces all appear mostly at once or twice the rotation frequency (Serkowski 1974). As the contribution from these effects is small at the harmonics of interest, their effect is minimised.

Because the circular polarisation is modulated at only twice the rotation frequency where it is more subject to the above effects, the alternative arrangement of a ½ wave plate followed by a ¼ wave plate is inferior.

1.5.2 Linear Polarisation Measurement

Equation 1.18 is appropriate for the measurement of linear polarisation. Only the ½ wave plate is required and the modulation will be at four times the rotation frequency.

1.5.3 Circular Polarisation Measurement

If measurements of the polarisation are taken only at $\psi = \pi/4, 3\pi/4, 5\pi/4, 7\pi/4$ then equation 1.19 reduces to:-

$$I' = \tfrac{1}{2}(I \pm \tfrac{1}{2}Q \mp V) \qquad \psi = \pi/4, 5\pi/4$$

$$I' = \tfrac{1}{2}(I \pm \tfrac{1}{2}Q \pm V) \qquad \psi = 3\pi/4, 7\pi/4 \qquad (1.23)$$

Subtraction of the two gives:-

$$I'(\psi_{3\pi/4} - \psi_{\pi/4}) = I'(\psi_{7\pi/4} - \psi_{5\pi/4}) = V \qquad (1.24)$$

The mechanical arrangement here is complicated by the fact that the quarter wave plate has to be accelerated then decelerated to the next 90° position (section 2.5.2). In addition, in order to reduce linear-to-circular conversion and instrumental circular polarisation it is recommended (Serkowski 1974, Billings 1951) that an asynchronously rotating half wave plate should be placed in front of the quarter wave plate.

1.6 Summary of the Basis for the Design

Consideration of factors causing errors in polarimetry resulted in the conclusion that polarimeters which modulate

the Stokes parameters of the incoming light beam are superior. The optical arrangement required was (at least) one retarder and one analyser, the latter being fixed. A survey of possible retarders resulted in the choice of a rotating superachromatic retarder being chosen as the most superior element. The optical arrangement for the polarimeter, therefore, is essentially two rotating superachromatic retarders followed by a fixed analyser. The retarders (one a ¼ wave plate and the other a ½ wave plate) are to be removable and easily inter-changeable.

REFERENCES

Angel, J.R.P., and Landstreet, J.D., 1970. *Astrophys. J., 162,* L61.

Angel, J.R.P., 1981. Private communication.

Bailey, J. and Hough, J.H., 1982. *Publs. astr. Soc. Pacif., 94,* 618.

Baur, T., Curtis, G.W., Hull, H., and Rush, J., 1974. Planets, Stars and Nebulae Studied with Photopolarimetry, p. 246, ed. Gehrels, T., University of Arizona Press, Tucson, Arizona.

Billings, B.H., 1951. *J. Opt. Soc. Amer., 41,* 966.

Billings, B.H., 1952. *J. Opt. Soc. Amer., 42,* 12.

Chandrasekhar, S., 1950. Radiative Transfer, Oxford University Press, Oxford.

Goldstein, R., 1968. Lazer Focus Magazine, February. Advanced Technology Publications Inc., Massachusetts.

Kemp, J.C., 1969. *J. Opt. Soc. Amer., 59,* 950.

Kemp, J.C., Wolstencroft, R.D. and Swedlund, J.B., 1972. *Astrophys. J., 177,* 177.

Serkowski, K., 1962. *Advances in Astronomy and Astrophysics, 1,* 290.

Serkowski, K., 1973. *Methods of Experimental Physics, 12A,* 361, ed. Carleton, N., Academic Press, New York.

Serkowski, K., 1974. Planets, Stars and Nebulae Studied with Photopolarimetry, p. 135, ed. Gehrels, T., University of Arizona Press, Tucson, Arizona.

Shurcliff, W.A., 1962. Polarised Light. Harvard University Press, Cambridge, Massachusetts.

Title, A.M., 1975. *Appl. Optics, 14,* 229.

Tomaszewski, L., Symonds, G.R. and Landstreet, J.D., 1980.
Publ. astr. Soc. Pacif., 92, 518.

Wolstencroft, R.D., Smith, R.J., Cormack, W.A., and Campbell, J.W., 1983. *Mon. Not. R. astr. Soc., 205,* 23.

CHAPTER 2

THE INSTRUMENT

2.1 The Host Instrument - The U.C.T. Photometer

The polarimeter was designed to be used primarily with the U.C.T. photometer (Warner 1971). The entire instrument would then be called the U.C.T. Polarimeter. It was envisaged that the polarimeter would also be used in combination with the S.A.A.O. radial velocity meter to measure magnetic field strengths (Brown and Landstreet 1981, Borra, Fletcher and Poeckert 1981). Initially it was also intended that the polarimeter could eventually be incorporated into the Reticon Photon Counting System and Image Tube Spectrograph on the Radcliffe telescope, although the space available was extremely limited. Thus, in order to make the polarimeter as instrument independent as possible, it was constructed in a frame containing smaller units. These units were the major cost of the polarimeter. They can be removed and placed at minimal cost in different frames suited to other instruments.

Because of a lack of time the polarimeter was used only with the U.C.T. photometer. This instrument placed a major constraint on the polarimeter, as, although the photometer is a two channel device, the second channel is attached to the offset guider eyepiece to provide a reference of sky transparency. It would have been difficult to modify the first channel to take two photomultiplier tubes so that both ordinary and extraordinary beams from the analyser could be used: this would have required major modifications to the filter box

and a new optical arrangement to mount the two photomultipliers. Consequently the polarimeter had to be a single channel device and the analyser used had to be of a type that blocked one of the two emergent beams (e.g. a Glan Thompson prism), rather than one that split the two beams (e.g. a Wollaston or Foster prism).

This restriction is an important one and, if funds became available, would be worth removing. Serkowski (1974) gives a number of reasons why using both channels is superior - principally a reduction in the errors from photon statistics and a reduced scintillation error.

2.2 The U.C.T. Polarimeter - Implementation

A schematic of the polarimeter is shown in figure 2.1. It consists of three parts:-

a) The optical module

b) The polarimeter controller

c) The reduction program running in the NOVA 3 instrument computer.

Each of these will be considered separately.

Plate 1A shows the instrument on the 1m telescope at S.A.A.O. Plate 1B shows detail of the optical module. Plate 1C shows the controller interfaced to the Nova 3 computer and Plate 1D shows detail of the controller.

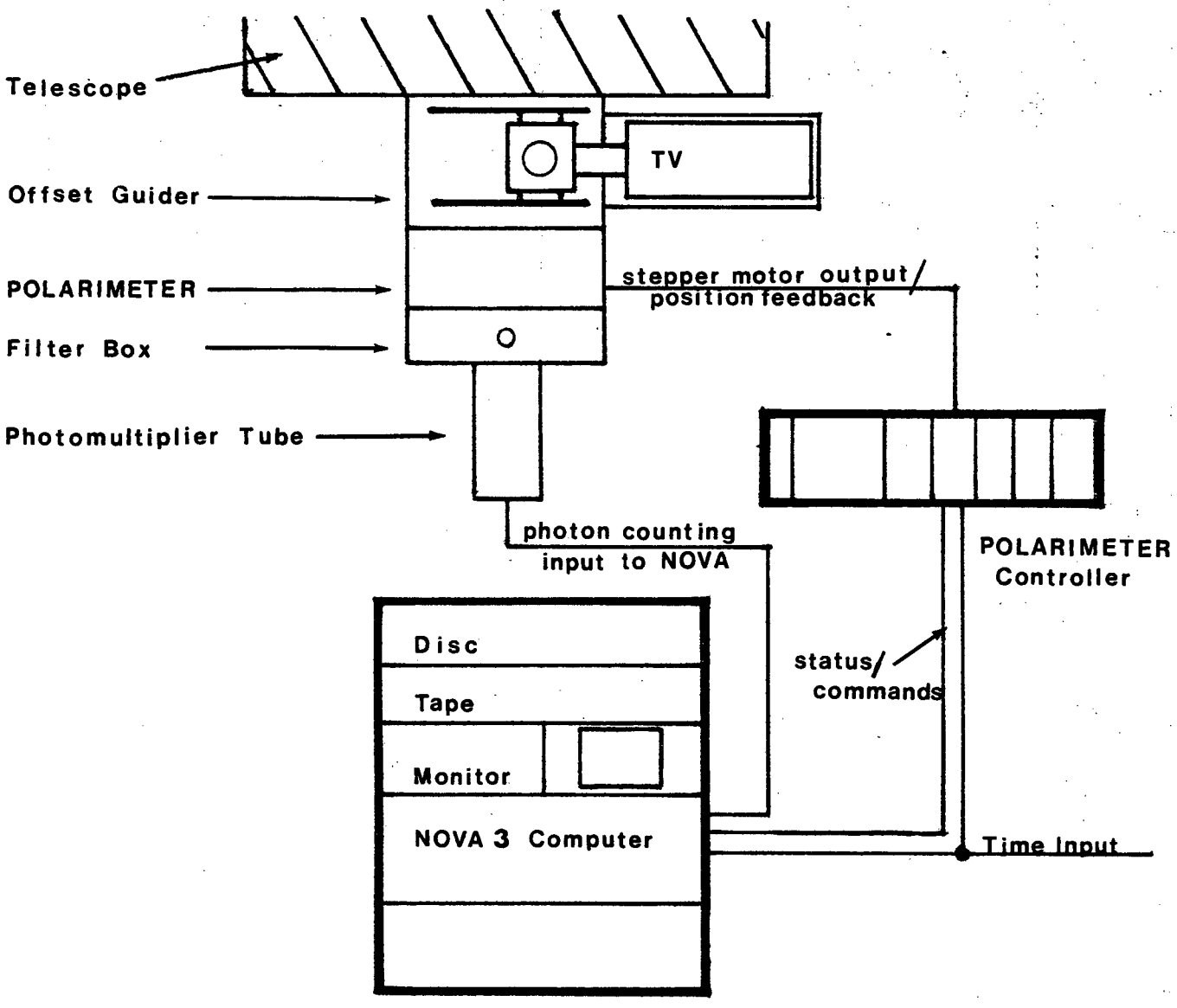

Figure 2.1 Schematic of the Polarimeter

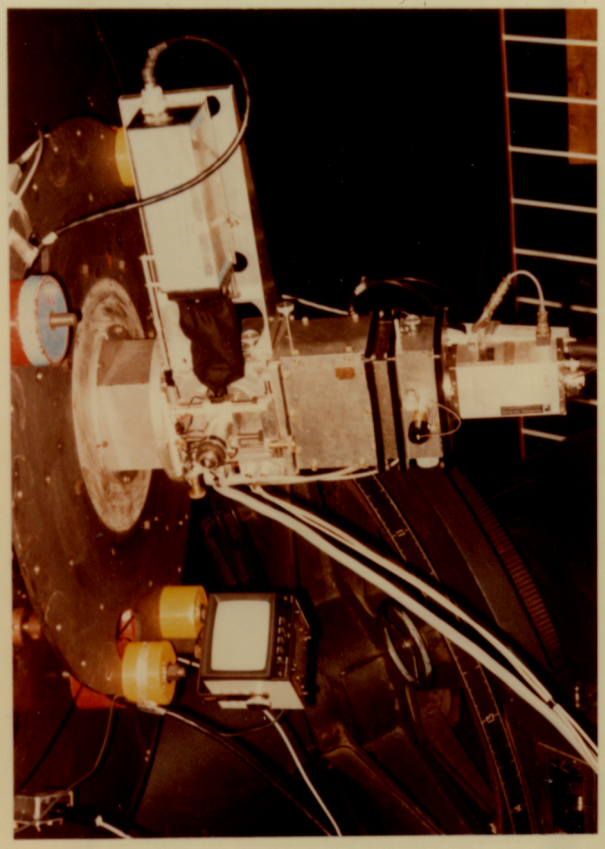

A: The U.C.T. Polarimeter on the 1.9m Telescope

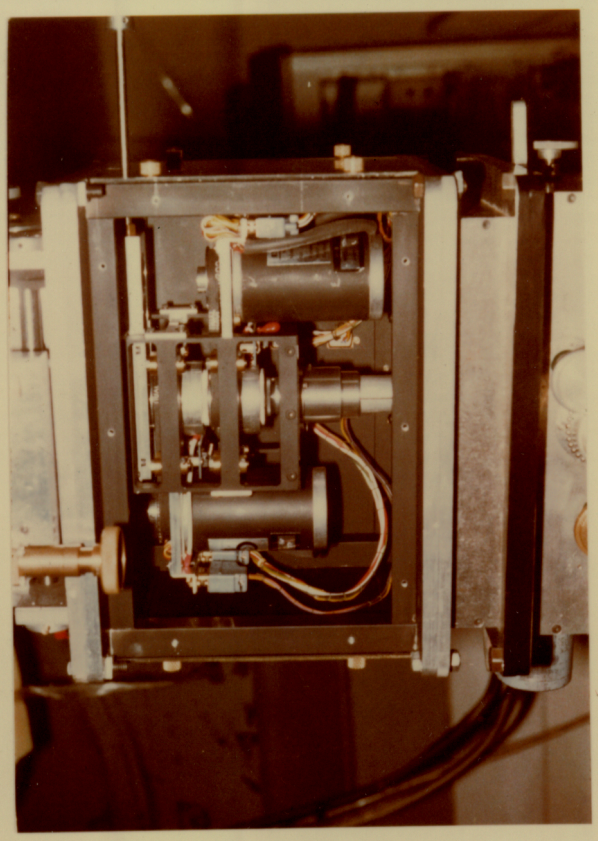

B: Detail of the Optical Module

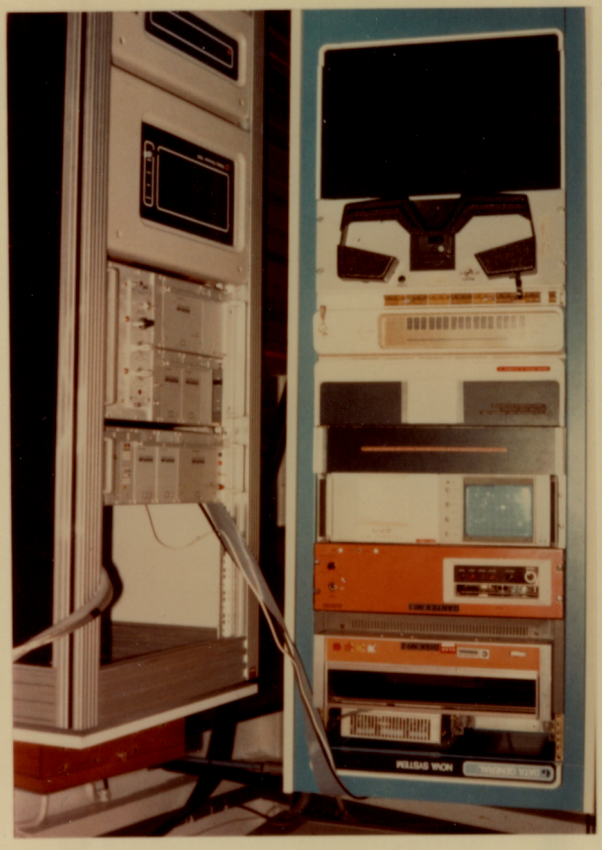

C: The Nova 3 and Polarimeter Controller

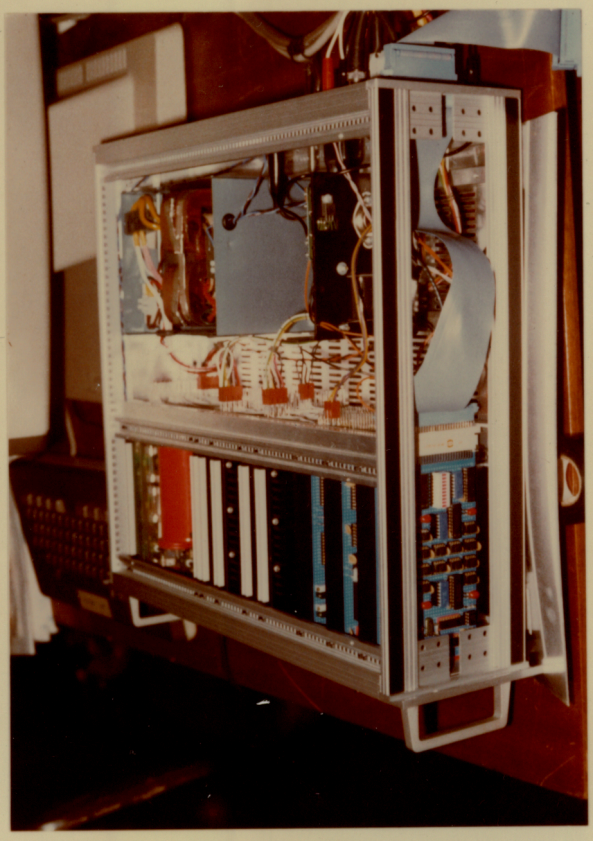

D: Detail of the Controller

PLATE 1

2.3 The Polarimeter Module

Figure 2.2 shows a schematic of the polarimeter optical module. MAE stepper motors model HY200-2240-460B8 (high current and high accuracy options) are used to rotate the waveplates by means of precision toothed belts. The high accuracy option ensures a maximum step error of $0^{\circ}.027$ for the motor stepped in any position, and the high current option ensures superior slewing and accelerating abilities. The motors used have laminated rotors to minimise the heat generated by eddy currents. Tests with motors with unlaminated rotors indicated that they ran too hot at the levels of voltage and current required for adequate performance. Each rotor revolution is broken into 400 steps. The belt drive causes some wander in the rotation of the waveplate. This has been measured over a number of months and at different stages of wear, but has always been found to be less than ¼ step ($0^{\circ}.23$) and typically less than ⅛ step ($0^{\circ}.11$). As the best linear standards have had position angles measured to $0^{\circ}.1$ and the above wanderings are relatively random, this is entirely adequate. Belt life is longer than 2 years.

The position of the waveplate is monitored by an optical sensor detecting two slots 45° apart in the waveplate pulley. Two slots are required to ensure that at least one is detected; as they are unequally spaced, the slots can be distinguished even during rapid accelerations. The outputs from the position pickups are transmitted down to the controller (see next section). There is also an input to the controller which enables it to determine whether the motor is connected.

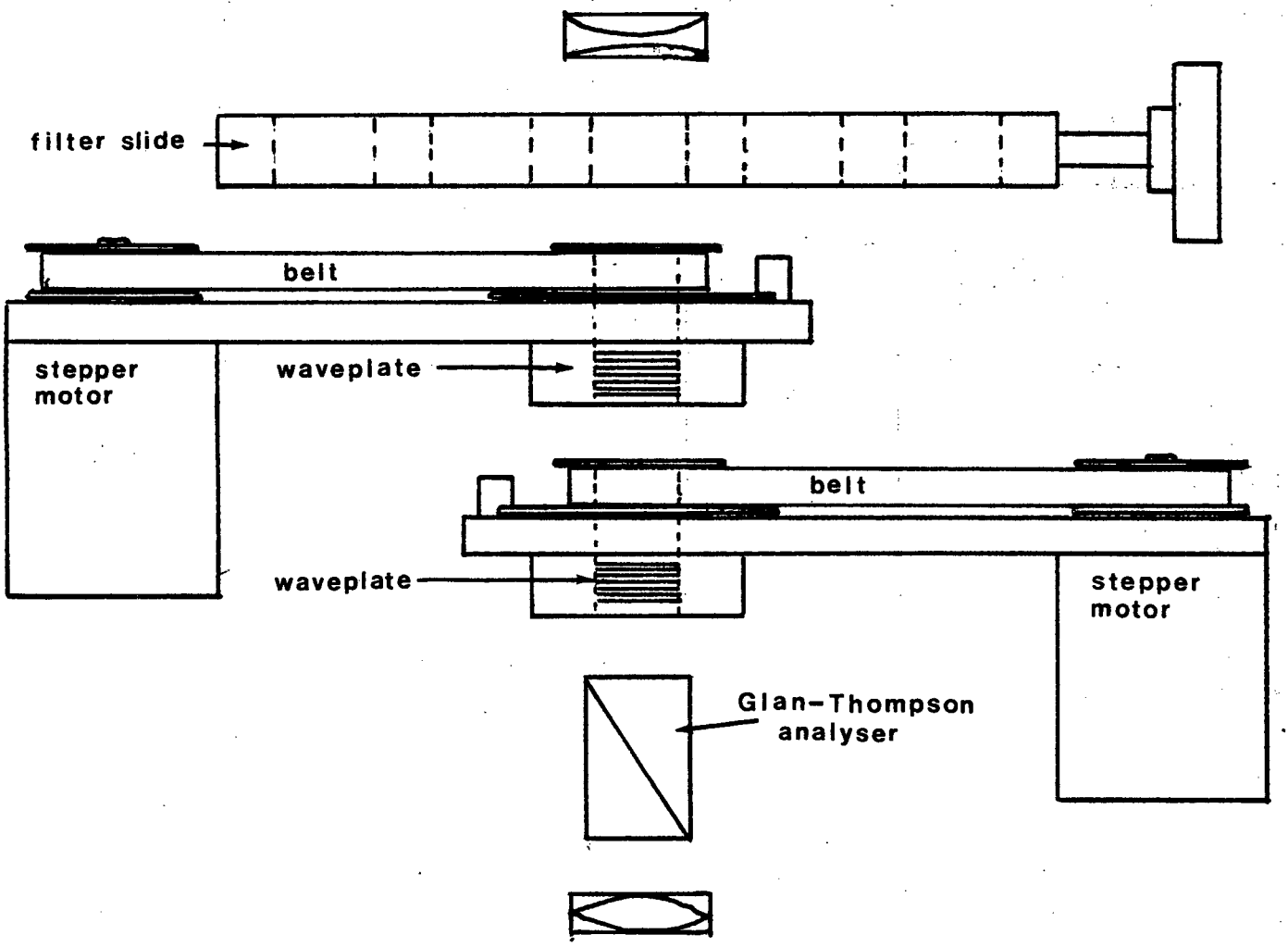

Figure 2.2 Detail of the Optical Module

The filter slide holds the following: two linear polaroids, a linear followed by a ¼ wave plastic retarder to provide a circularly polarised beam, and a Lyot depolariser. A fifth position is left open for observing.

Two suprasil lenses collimate the beam in the polarimeter. The beam width is 3mm for an incident f15 beam or 2.5mm for an f18 beam. The waveplates have a clear diameter of 14mm. The polarimeter module is inserted above any filters or apertures, to avoid problems caused by metallic apertures or filters with residual stress birefringence (Serkowski 1974). The above beamwidth requires that the focus of the photometer be moved down by 4.5cm, necessitating an extension tube for the offset guider eyepiece.

As both waveplate/stepper motor units and the Glan-Thompson analyser can be easily removed from the module, the polarimeter can be converted back to a photometer in only a few minutes (with only a small light loss caused by reflections and absorptions in the suprasil lenses).

The waveplate configurations used are:

a) Linear only - ½ waveplate in lower slot

b) Circular only - ½ wave plate in upper slot
¼ wave plate in lower slot

c) Simultaneous linear - ¼ wave plate in upper slot
and circular ½ wave plate in lower slot

A scheme proposed by Serkowski (1974) to use three apertures to eliminate sky polarisation was not implemented beacuse it causes a doubling of sky brightness.

2.4 The Controller

As rapid modulation rates were required to reduce the effects of scintillation and variable sky transparency, to use the NOVA 3 to output trains of pulses would have been extremely inefficient. It was therefore decided to move this function to an intelligent controller. In any case, external stepper motor drive amplifiers and power supplies were required, so the room left in the cardholder was used by the microprocessor based controller. Figure 2.3 shows a schematic of the unit.

The Digiplan CD10 chopper drive amplifiers provide high performance at reasonable price. They can deliver 4A at 35V with extremely fast switching speeds. Tests on the motors (under load) using exponential ramps produced accelerations of 1250 rev/sec^2 up to 4000 steps/sec. When an external train of pulses is supplied or when allowed to run under an internal (adjustable) oscillator the units generate the pattern of steps required by the motors. Options are provided for forward/reverse rotation, shutting down the drives and for providing short boost currents to increase accelerations.

The CD10 drives need two supply voltages (19V for logic and 35V for the motors) which are supplied by the PM1200 power supply unit (PSU) which in turn requires an external transformer. The transformer was custom wound. The PM1200 and CD10s are produced in a standard "Euromodule" size which makes location in a card frame ("Eurocard" size) very easy.

The intelligence is supplied by a single board microcomputer using a Motorola 6809 microprocessor. Two other

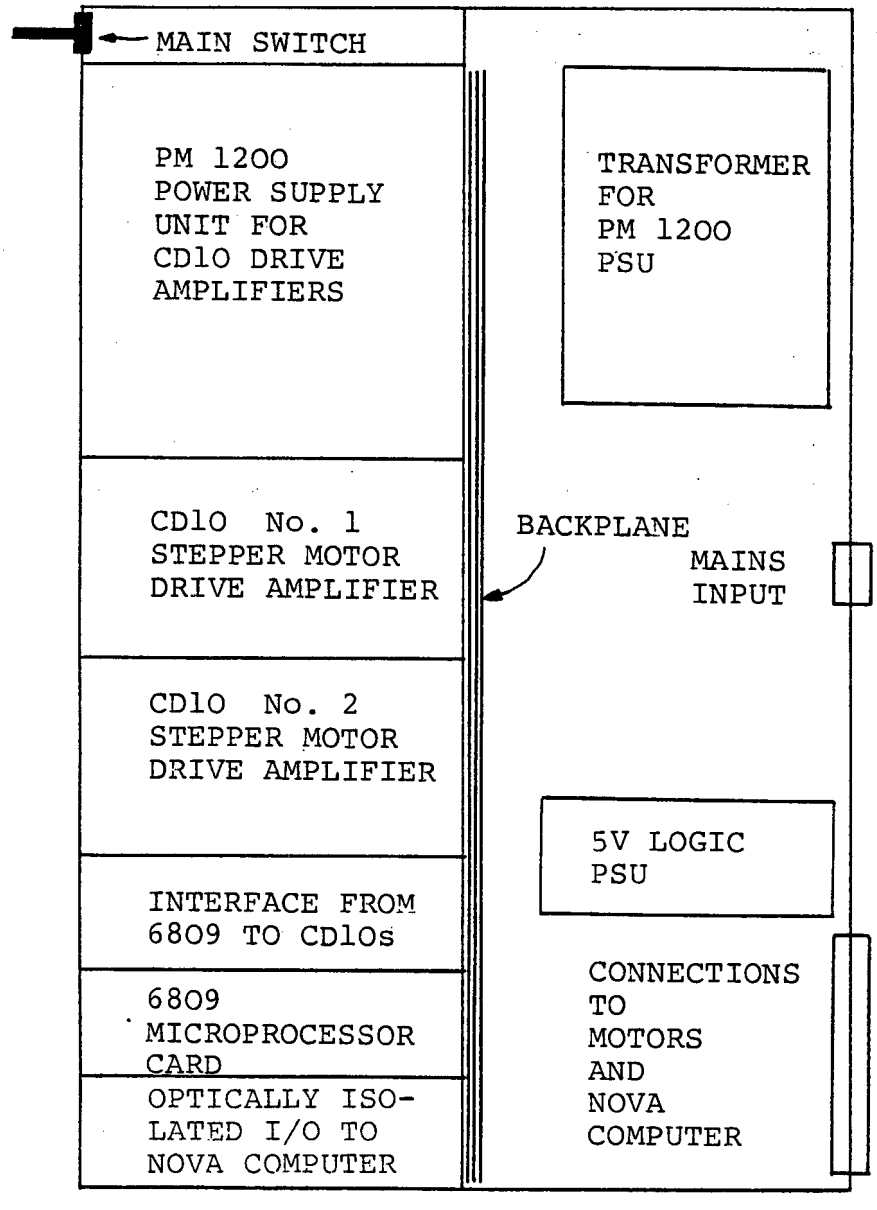

Figure 2.3 Schematic of Polarimeter Controller

circuit boards provide interfaces - one with the NOVA3 and the other with the CD10s. The microcomputer consists principally of 5 chips. These are:-

a) The 6809 microprocessor.

b) Two 6821 parallel interface adapters (PIA's) providing two 8 bit parallel input ports and two 8 bit parallel output ports.

c) A read/write (RAM) memory of 2048 8 bit words.

d) A read only memory (EPROM) also of 2048 8 bit words.

The software for the computer is written in 6809 assembler language. The machine code resides in the EPROM. During program development the EPROM is loaded with the program in an EPROM programmer and then inserted into the microcomputer card. If (as is often the case) the program is found to be unsatisfactory, the EPROM is erased with UV light and reprogrammed. There is a buffered output port from the address and data busses which allows monitoring of the program execution by a logic analyser. This was found to be essential in the program development.

As it is essential that the NOVA knows the position of the waveplates at all times, the controller and NOVA are connected to the same clock pulses (1 khz). Constant speed rotation of the stepper motors is done under interrupt control. Acceleration and deceleration ramps are carefully timed when ending to merge exactly with the interrupts. As most of the polarimeter configurations require output step rates of 4000 steps/sec (circular only 2000 steps/sec), 4 khz interrupts are

generated from the 1 khz on the controller's NOVA I/O card by means of a phase locked loop. Both 4 khz and 1 khz are used as interrupts by the microcomputer and the 4 khz is continually checked against the 1 khz to ensure that it never slips. The cycle time of the 6809 is 1 μs (instruction time typically 4 μs) and as a result the 250 μs interrupts are somewhat closely spaced. Care has been taken to ensure that problems with timing do not occur.

The microcomputer communicates with the NOVA 3 through two 8 bit parallel ports - one in and one out. These are optically isolated from the NOVA so that a failure of the power supply on either computer does not affect the other. To power its half of the optically isolating chips, a 5V supply is connected from the NOVA. The 1 khz interrupt is also optically isolated. There are light emitting diodes (LED's) connected to both input and output ports so that these can be monitored easily. The optically isolating buffers and 4 khz generator are on the NOVA I/O card.

As the voltage levels required by the CD1Os are not TTL compatible, another interface card is used to provide the correct levels. The card also provides monitoring points for the various voltage rails, for the outputs to the stepper motors and for the 1 and 4 khz interrupts and step outputs to the CD1Os. Switches allow manual overriding of the computer inputs (for easy testing) and LED's indicate variously that the motors are running, if any fault conditions exist, whether boost is being applied and whether the motors are in a state such that the data from the polarimeter are valid.

All of the above status information, and more, is available to the NOVA 3 through the parallel port.

In essence, the controller is not specifically for use with a polarimeter: it is a general purpose, intelligent, two-stepper-motor-controller with four inputs from the motors and 8 inputs and 8 outputs to a computer. It is the software residing in the EPROM that makes it a polarimeter controller and this can be changed for a different polarimeter or for a totally different instrument. It has, for instance, provided automatic filter change facilities on the U.C.T. photometer and has been copied almost exactly to provide a controller for the photometer. The goal is to provide identical systems so that each can act as backup for the other.

As the full range of observing situations was encountered and more experience was gained in making polarimetric observations at a site where local expertise was absent, the philosophy of making a controller specific only in the software has enabled updates to be made continuously. Experience over the last two years has shown that this was the best solution.

2.5 The Reduction Program - QUARTZ

The vast assembler program known as QUARTZ resides in the NOVA 3 and has been steadily refined to include all the facilities the astronomer could hope for. It is based on a program called WALTER written for photometry by L.A. Balona. QUARTZ retains all of its underlying structure, including the

disk and magnetic cartridge I/O routines. However, most of the program has been considerably modified. The functions of the program are as follows:-

a) To count the photon events from the photomultiplier and store these in arrays ready for calculation.

b) To provide online calculations for the polarimetry for all possibly configurations of the instrument.

c) To provide online calculations for photometry at the end of each polarimetry integration and also for the high speed photometry (output at a shorter integration time).

d) To store the above data on disk and magnetic tape.

e) To provide displays of all the information required by the astronomer.

f) To monitor the status of the controller and provide the necessary inputs to which the controller should respond.

g) To be self-checking, so that any anomalies can be traced easily and to aid in the further development of the program.

Each of the above will be considered in turn.

2.5.1 Photon Counting

The photon events, amplified by a Products for Research SSR amplifier, are counted by either of two counters on a pulse counting interface in the NOVA 3. The counts are stored

in various arrays on two different timescales - a slower one from 1 to 65500 seconds, used for the polarimetry and photometry, and a faster one from 1/10 sec up to the slower timescale for the high speed photometry. The high speed photometric data are stored sequentially in single precision form in a large array until it is filled, after which storage is reinitialised at the beginning of the array. This allows viewing of sections of the high speed light curve lasting many hours. Slower photometric data are stored in an array of double precision star and sky buffers, each with a different filter number. The counts are also stored in polarimetry buffers, one for star and one for sky, for each filter.

Inspection of equations 1.18 and 1.22-24 indicates that linear only (LO) and simultaneous linear and circular (SLC) polarimetry require that the amplitudes of harmonics be calculated. Circular only (CO) requires the subtraction of two numbers. Two different sets of buffers are therefore used, depending on the configuration of the polarimeter. SLC and LO use 100 (double precision) word buffers and CO uses 2 (double precision) word buffers.

As it is impossible for the exact arrival time of each photon to be known, the time taken for one rotation of the waveplates (in the LO and SLC cases) is split into 100 divisions. The waveplates rotate at 4000 steps/sec or 10 rev/sec so that the duration of each division is 1msec (the interrupt time for the NOVA). The millisecond counts are stored in sequential memory locations 0-99. A buffer is selected on the basis of whether it is star or sky and on its filter number (10-19).

A thorough investigation was made into the optimum number of buffer locations (optimum number of time divisions). The minimum number required to determine the amplitude and phase of a single harmonic is 2, but for 4 harmonics (the 2nd harmonic of the rotation frequency is also fitted) 9 bins are required. Given that this is the minimum number of bins allowed and that the maximum is 100, set by the interrupt time, it was not clear initially which is the optimum number. An investigation by Juritz (private communication) indicated that as long as more than approximately 20 photons were stored in each bin (2000 counts in total) equivalent results would be obtained for any number of bins greater than 9. A total of 100 bins was chosen in order to give the clearest display of the incoming data.

2.5.2 Online Calculations and Observing Procedure

QUARTZ retains that part of the structure from WALTER where a "program" can be written specifying the integration time, whether star or sky and the filter number. Any combination of star and sky observations and filters (including repeats) can be used within a program. At the end of the program the calculations are made for all the filters. This arrangement allows colour equations and extinction corrections to be used for each filter. Dead time corrections are made and non-linear zero point corrections can also be made if desired. These capabilities belonged to WALTER and although many changes have been made for QUARTZ details of the calculations do not belong here.

Calculations are also made on the polarisation buffers at end of the program. The equations used are slightly different from equations 1.18-24 because of some physical constraints:-

a) It is difficult to construct the polarimeter so that the fast axes of the waveplates cross over exactly above the transmission axis of the Glan Thompson analyser in the SLC case.

b) It is difficult to ensure that the cross over takes place at exactly the beginning of an integration.

c) Even if the above was accomplished it is very difficult to ensure that the polarimeter is aligned exactly N-S so that the position angles of the linear polarisation are calculated correctly.

Similar problems occur in the LO and CO cases. The alternative is simple. By observing a standard during twilight, the zero points of the position angles and the circular polarisation can be determined accurately. By ensuring that the optical components can be reassembled in only one way relative to each other, and by starting acceleration ramps and integrations at specific times (e.g. at the beginning of a second), this zero point should be constant from night to night, disturbed only if the instrument is removed from the telescope (point C). This approach has been successful.

Because of the above, it is easier to transform the equations 1.18 and 1.22-24 into Ipθq from IQUV and assume that the analyser can be placed at any angle ϕ to the reference frame. Each configuration needs to be calculated separately.

Simultaneous Linear and Circular (SLC):

Substituting Ipcos2θ for Q, Ipsin2θ for U and Iq for V in the matrix calculations yields

$$I' = \frac{I}{2}\left[\begin{matrix} 1+\tfrac{1}{2}p\cos(8\psi-2\theta+2\phi+\xi)+\tfrac{1}{2}p\cos(4\psi+2\theta+2\phi+\xi) \\ -q\sin(6\psi+2\phi+\xi) \end{matrix}\right] \quad 2.1$$

where ψ is the angle of the fast axis of the upper (¼ waveplate) to the reference frame, ϕ is the angle of the analyser to the reference frame and ξ is some phase shift introduced by an arbitary start time at the beginning of an integration. The fractional circular polarisation q can be found by calculating the amplitude of the 6th harmonic of the rotation frequency. As q is either positive or negative and $(2\phi+\xi)$ is constant, a change of sign of the circular polarisation will be indicated by a 180° phase change of the 6th harmonic. In practice, as the data are noisy, $(2\theta+\xi)$ is obtained by observing the circular polaroid filter and the phase of the 6th harmonic compared with this angle, which then enables the projected amplitude to be calculated.

The linear polarisation is obtained by adding the amplitudes of the 4th and 8th harmonics. Observation of a standard star (or a linear polaroid) of known position angle θ can be compared with the phase of the 4th harmonic which enables the phase zero point to be calculated. In principle this can be obtained from the circular information $(2\theta+\xi)$, but in practice the standard star observation is used. The 8th harmonic could also be used to determine the position angle, but as there are only half as many phase bins per cycle (12½ instead of 25) the 4th harmonic is used alone.

The above amplitudes and phases are obtained from a least squares algorithm. Following the notation of Smart (1958) we expect the number of counts in each of the 100 memory bins, y_r, where r is the bin no. 0-99 to be given by:

$$y_r = A_o + \sum_K \left[A_K \cos\left(\frac{2\pi kr}{n}\right) + B_K \sin\left(\frac{2\pi kr}{n}\right) \right] \qquad 2.2$$

where n = 100 and k = 2,4,6 and 8, because 4th and 8th harmonics are generated by any linear polarisation present in the beam and the 6th harmonic is generated by any circular polarisation. Modulation caused by dirty or wedge shaped waveplates appears mostly at the 2nd harmonic, so it is instructive to derive this amplitude also. After some manipulation (Smart 1958), the coefficients A_K and B_K can be derived as

$$A_o = \frac{1}{n} \sum_r y_r \qquad 2.3$$

$$A_K = \frac{2}{n} \sum_r y_r \cos\frac{2\pi kr}{n} \qquad 2.4$$

$$B_K = \frac{2}{n} \sum_r y_r \sin\frac{2\pi kr}{n} \qquad 2.5$$

Amplitudes and phases are then easily derived as $(A_K^2 + B_K^2)^{\frac{1}{2}}$ and $\tan^{-1} \frac{B_K}{A_K}$.

The uncertainties in the above constants are (Smart 1958)

$$\sigma_{Ao} = \frac{\mu}{\sqrt{n}} \qquad 2.6$$

$$\sigma_{AK} = \sigma_{BK} = \mu\sqrt{\frac{2}{n}} \qquad 2.7$$

where $$\mu = \frac{B_o - nA_o^2 - \frac{n}{2}\sum_K (A_K^2 + B_K^2)}{n-(2k+1)} \qquad 2.8$$

and $$B_o = \sum_r y_r^2$$

These need to be transformed into uncertainties in p, θ and q. After some manipulation it is found that

$$\sigma_p = \frac{\mu}{A_o}\sqrt{\frac{8 + p^2}{n}} \qquad 2.9$$

$$\sigma_\theta = \frac{2\mu}{pA_o}\sqrt{\frac{2}{n}} \qquad 2.10$$

and $$\sigma_q = \frac{\mu}{A_o}\sqrt{\frac{2+q^2}{n}} \qquad 2.11$$

Some corrections are made at various stages in the calculations. Hsu and Breger (1984) indicate that dead time corrections should be made, so these are made to the raw data in the buffers before calculation. As the counts are split over 100 bins, a dead time 100 x larger than the photometric dead time (which is appropriate for total counts) is used. The above paper also indicates that the A_K and B_K coefficients must be scaled by a factor F_B where

$$F_B = \left(\frac{\pi}{n}\right)/\left(\sin\frac{\pi}{n}\right) \qquad 2.12$$

(n number of bins/cycle)

in order to compensate for the fact that the sine curve is constructed from a finite number of "bins". For the 4th harmonic F_B = 1.00264, 6th harmonic F_B = 1.00595 and 8th harmonic F_B = 1.01061.

Although of nearly constant retardance, the waveplates are not perfect over the entire wavelength range. For observations of high accuracy, efficiency factor corrections have to be made as a function of wavelength, and instrumental polarisation

(also a function of wavelength) has to be subtracted. The zero of position angle also varies as a function of wavelength. Corrections on line for all these effects for each filter can be made from a table of corrections.

Finally a correction is made to the circular polarisation. The sky circular polarisation is known to be very small ($\lesssim$0.2%, Wolstencroft, and Kemp 1972, Staude *et al.* 1973) and is normally less than the error resulting from the photon statistics of the sky measurement. As the polarisation buffer containing the last sky measurements is subtracted from the buffer containing the star and sky measurements, this effect can be compensated for afterwards in the following way - unless the correction is disabled, the sky polarisation is assumed to be zero, and an offset (derived from the measured value which is non zero as a result of photon errors, scaled by the ratio of intensities) is applied to the circular polarisation measured for the object.

If desired, a transformation to Stokes parameters may be made by using equations 1.10-13. They are quoted in percent. The errors transform in the following way

$$\sigma_Q = (1 + 7p^2)^{\frac{1}{2}}\sigma_p \qquad 2.13$$

$$\sigma_u = (8 - 7p^2)^{\frac{1}{2}}\sigma_p \qquad 2.14$$

b) Linear Only (LO):

Using only the half wave plate and transforming from IQUV to Ipθq before calculating the meuller matrices, yields

$$I' = \frac{I}{2}[1 + p\cos(4\psi + 2\theta + 2\phi + \xi)] \qquad 2.15$$

Thus in order to simplify computations, exactly the same procedure is followed for calculating p as for the SLC configuration except that the contribution from the eighth harmonic is not included in the calculation. Fits to the 6th harmonic are still produced although these are now meaningless. Errors are also calculated in exactly the same way, although strictly speaking they should be modified to the level of the circular error in the SLC case (eq. 2.11) as the errors in the fit to the 8th harmonic no longer contribute. There is also no difference in the position angle zero point calculation. All of the corrections mentioned above for the SLC case are applied; however if the table of efficiency corrections and instrumental polarisation corrections is required, a different table must be entered.

c) Circular Only (CO):

According to equations 1.23 - 24 a totally different scheme must be followed. It is necessary to slew the waveplates to a given position, after which the integration may begin. This results in a certain amount of "dead time". The slew takes 56 ms and two slews/sec are performed to give one circular polarisation measurement. With this rapid slew, the time wasted is only 11% of the observing time.

Again transforming to $Ip\theta$ and q before calculating the Meuller matrices, an arrangement of a ½ waveplate above a ¼ waveplate eventually yields an intensity

$$I' = \frac{I}{2}\left[1 + \tfrac{1}{2}p\cos(4\psi' + 2\theta + 2\phi) + \tfrac{1}{2}p\cos(4\psi' + 4\psi + 2\theta - 2\phi) + q\sin(2\psi - 2\phi)\right] \qquad 2.16$$

where ψ' is the angle of the fast axis of the ½ waveplate and ψ the angle of the ¼ waveplate. When ψ is not changing (i.e. during

an integration), the average intensity is

$$\langle I' \rangle_{\psi'} = \frac{I}{2}[1 + q \sin (2\psi - 2\phi)] \qquad 2.17$$

If $\psi = \phi + \frac{\pi}{4}$ initially, and 90° slews take place thereafter, then

$$\langle I' \rangle_{\psi'} = \frac{I}{2}[1 + q], \frac{I}{2}[1 - q] \quad \text{alternately.} \qquad 2.18$$

If $\frac{I}{2}[1 + q] = A$ and $\frac{I}{2}[1 - q] = B$ then

$$q = \frac{A - B}{A + B} \qquad 2.19$$

and

$$\sigma_q = \sqrt{\frac{2(A^2 + B^2)}{(A + B)^3}}$$

In this mode the linear coefficients are set to zero on output. Dead times are scaled by the appropriate factor in both photometric and polarimetric calculations, sky corrections as set out in SLC are carried out, if not disabled, and the corrections for efficiency and instrumental polarisations (yet again different) applied, if required.

The SLC and LO calculations take 12 seconds and the CO calculation takes less than 1 second. The floating point calculations are programmed in assembler language using the floating point interpreter. Because of the long reduction time in the two former cases, provision has been made for starting the next integration while the last results are being calculated. If this option is used, a message is output warning the user if an integration time is less than 15 sec, to prevent the computer falling ever more behind. If the option is not used, the warning

may be overridden. No advantage is gained using the option in the CO case.

In addition, provision is made for carrying out reductions during an integration in order for the observer to determine the optimum integration time. These results are not recorded, but displayed on a monitor screen (see 2.5.4).

2.5.3 Storage of Data on Disk and Tape

Routines used to store data are from WALTER. QUARTZ may be run using disk alone, tape alone or both together. Facilities exist for reading large quantities of data from the disk or tape as input and control statements.

An example of the output recorded on disk/cartridge is given in fig. 2.4. Exactly the same data appear on the observer's terminal.

```
10S 015917 +.50424  10   1000 +1.1829 POLR    +133.6
 3521  3988  3447  3901  3495  3958  3429  3880  3360  3799
 3631  4118  3554  4027  3568  4044  3461  3918  3485  3946
11S 015928 +.50436  10   1000 +1.1828 POLR    +133.0
 3450  3905  3552  4025  3485  3947  3567  4043  3374  3816
 3429  3881  3357  3796  3483  3944  3559  4034  3416  3865
12S 015939 +.50449  10   1000 +1.1826 POLR    +134.3
 3553  4025  3478  3937  3532  4000  3373  3813  3508  3972
 3461  3917  3515  3980  3510  3974  3450  3904  3480  3939
0 +.50352 +11.029 +.003  +1.007   +.538+150.287 +43.269   -.366   +.380
1 +.50365 +11.015 +.003   +.576   +.607+159.853 +85.364   -.173   +.429
2 +.50378 +11.011 +.003   +.831   +.536 +75.986 +52.253   -.024   +.379
```

1 2 3

Figure 2.4

Lines labelled (1) are header lines for an integration in each filter. Lines labelled (2) are the final reduction lines for the 3 filters. Lines labelled (3) are the high speed photometry

counts. Fig 2.4 is one polarimetric integration in 3 filters (viz. 10,11,12). No sky integrations were made in this example. The header lines contain the following information (from L to R): filter number, character S or Y for star or sky, SA Standard Time, HJD, filter integration time in seconds, high speed integration time in milliseconds, airmass and sky counts per high speed integration time. The reduction lines contain the following information: filter, HJD of centre of polarimetric integration, intensity and standard error in magnitudes and finally linear polarisation with error, position angle with error and circular polarisation with error in percent and degrees. The high speed lines contain alternately the number of counts in the high speed integration and the corrected counts. Corrections in the high speed data are made for sky and extinction.

2.5.4 Displays

There are 5 principal displays available to provide extensive feedback to the observer at the telescope. These have been found to be essential for obtaining the highest quality data. They are:

a) The high speed light curve. Besides being of interest in its own right this curve is important in assessing the quality of the data;

b) The raw polarisation buffers (100 bin LO, SLC or 2 bin CO). This enables the intensity modulation from the waveplate rotation to be viewed and an estimate of the percentage polarisation to be made, even before the reductions take place;

c) The reduced polarisation and slower photometry curves. Any combination of these may be viewed;

d) An "information" display, including count rates, filter numbers, time gone and time to go during the integrations, SAST, when the run was started, and the last calculated polarisations. Reductions made during an integration have their results displayed here in numerical form. They may also be viewed in display (C) in graphical form above;

e) A display indicating the star to be observed and its RA and Dec. This is useful when a "macroprogram" specifying both the stars to be observed and observing "programs" (see section 2.4.2) is used.

Other displays are also available (see section 2.4.6) for self-checking options.

2.5.5 Controller Interfacing

As the polarimeter controller is relatively intelligent (section 2.3) interfacing with the NOVA is fairly simple. Two 8 bit parallel ports are available. The input port (from the NOVA/QUARTZ point of view) carries the status of the controller. This is broken into three sections:-

a) a "data valid" line;

b) Three "catastrophic error" lines;

c) Four status coded lines (15 status conditions).

The output port carries commands and is split into:

a) Two lines designating the type of observation (LO,CO,SLC and shut down);

b) A synchronise line;

c) A position pickup disable line;

d) Four lines indicating the number of steps in the "gate". A deviation in the waveplate position greater than this number of steps will cause an error message.

QUARTZ provides the error/status messages associated with the various lines. Storage of these messages in the controller would use too much memory space.

During an integration, the data valid line (a) is continually checked. This is especially important in the CO case, to ensure that an integration does not begin while a slew is in progress.

Although the error in the rotation position is generally $<\frac{1}{8}$ step (section 2.3) timing problems within the controller (interrupts occurring at inopportune moments) can result in the position not being read until up to two steps away from the real position zero. This does not cause any problems as any missed steps will always occur as multiples of 8 because of the structure of the stepper motor.

The position sensor has failed once. The instrument has never missed any steps under observing conditions, so a facility has been included to disable the pickups if position sensor failure occurs. Checks that no steps have been lost can then be made by occasionally observing a standard star or polaroid filter.

The synchronise line is used to ensure that ξ (equations 2.1, 2.15) remains constant, and also, in the CO configuration, to ensure that equation 2.18 is valid. A setting up procedure is used to determine the start point of the slews in this latter configuration. The start point has been found to be constant

(as expected) and the set up procedure may be bypassed, if required, by entering the offset of the slew start point from the keyboard.

Catastrophic errors occur when the 4 khz interrupt slips relative to the 1 khz (section 2.4) or when either of the CD10 stepper motor drive units trips out. None of these has occurred.

2.5.6 Self-Checking Facilities

The self-checking facilities were initially included as routines to aid program development but have proved useful in reassuring the observer that the reduction routines are working correctly. The routines are able to generate data (including all of the corrections worked in a reversed direction) in all three configurations (LO,CO,SLC). Displays of the generated data are available. Other facilities include: generation of data from the last calculated polarisation values and a display of the residuals (or the calculated modulation) on the monitor, facilities to print out various buffers, and an option to print out various intermediate stages of the reduction process (in a shambolic but usable format). This last facility is extremely useful in program development.

2.6 QUARTZPLOT - The Analysis Package

Once the reduced data have been recorded at the telescope, further analysis and plotting is necessary. A FORTRAN analysis and plotting package has therefore been developed. This is run on the UCT Sperry Univac computer, and has a wide range of options. These include the following:-

a) Conversion from Ipθq to IQUV and back;

b) Conversion from percentages to polarised flux in magnitudes;

c) Averaging data points;

d) A running average of data points;

e) Plotting the reduced data;

f) Plotting the data folded modulo some period;

g) Plotting the above curve averaged into phase bins;

h) An interface routine to the department's Fourier Analysis package;

i) Editing of bad data points;

j) A least squares fitting routine for determination of angles in oblique rotators (e.g. AM Her class of cataclysmic variables - see chapters 3 - 5);

k) A modelling routine which generates theoretical polarisation curves from the above derived angles and a range of cyclotron models;

l) A linear regression routine (to obtain periods etc.);

m) A routine to roughly determine the magnetic field strength in the AM Her variables from the ratio of linear to circular polarisation.

The program was used to generate the output seen in later chapters.

2.7 Performance Evaluation

The instrument has been in use for two years - enough time for an evaluation to be made under a variety of conditions. However, as most of the use has been for simultaneous linear and circular polarimetry of cataclysmic variables, much less experience has been gained in the use of the linear only and

circular only configurations.

The following factors are required:-

a) SLC linear instrumental polarisation;

b) SLC circular instrumental polarisation;

c) LO linear instrumental polarisation;

d) CO circular instrumental polarisation;

e) SLC linear efficiency factor;

f) SLC circular efficiency factor;

g) SLC position angle variation;

h) LO linear efficiency factor;

i) LO position angle variation;

j) CO circular efficiency factor.

The above are all functions of wavelength.

In addition, the following questions should be addressed:-

a) How good are the estimated errors in each case?

b) How stable is the zero point of the position angle and the circular zero from night to night?

Although tests were carried out during commissioning at the end of 1982, the instrument has had many refinements since then. In particular, the CO configuration was implemented only recently. The instrument has been used almost entirely in white light on objects where photon statistical errors were the major source of error by an order of magnitude or more. Consequently most of the performance tests were done on nights which were non-photometric and claims made for the instrument may be somewhat conservative.

The linear standard stars used were those listed in Serkowski (1974) and later refined by Hsu and Breger (1982).

The linearly unpolarised standards used were also those of Serkowski (1974). No good set of circular standards exists. Calibration was therefore performed on a piece of circular polaroid. The circular instrumental measurements were taken while observing the linear standards (which were assumed to have zero circular polarisation).

2.7.1 Simultaneous Linear and Circular

Examples of data used for determining the linear efficiency factor are shown in Table 2.1. The standards are taken from the list given by Hsu and Breger (1982). The zero point of the position angle was taken from the o Sco observation. This determined the position angle of the transmission axis of the end polaroid (usually used for setting the zero point) as $158^{\circ}.3$ in V. Unfortunately measurements made in the band centred at 7500Å in the standards are not directly comparable with the UCT Pol I_C band measurements. It is evident that the efficiency factors are close to 1.00, vindicating the choice of superachromatic retarders for very wideband observations. The deviation of the position angle is also relatively small. All of the wideband observations shown in subsequent chapters were therefore left uncorrected for efficiency or deviation of position angle, although facilities exist for these corrections to be applied at the telescope if they are ever required.

The linear instrumental polarisation was determined during the commissioning run in conditions of bright moonlight. The broad band (S20) instrumental polarisation was measured under those conditions to be $0.073 \pm 0.02\%$ at 29°. The star used was E Ind with polarisation $0.006 \pm 0.008\%$. As the sky brightness

Table 2.1

Star	Filter	Polarisation (%)		Position Angle (Deg)		Efficiency	Position Angle Deviation (Deg)
		Standard	UCT Pol	Standard	UCT Pol	(P_{OBS}/P_{STD})	($\theta_{OBS}-\theta_{STD}$)
O Sco	V	4.18±0.02	4.174±0.019	32.0±0.1	32.4 ±0.2	0.999	0.0 (ref)
	B	3.50±0.01	3.276±0.018	32.0±0.2	36.2 ±0.3	0.936	3.8
	I_C [0.75]	4.42±0.02	4.212±0.010	32.1±0.2	30.4 ±0.2	0.953	-2.1
CD $-33^{\circ}12361$	V	7.31±0.04	7.247±0.018	20.4±0.1	21.5 ±0.1	0.991	0.6
	B	6.97±0.03	6.918±0.039	20.1±0.1	23.0 ±0.2	0.993	3.3
	I_C [0.75]	6.53±0.03	6.013±0.050	21.3±0.1	19.3 ±0.2	0.921	-2.4

was 0.3% of the star and was 38% polarised, the instrument at polarisation quoted above is bound to be a very conservative upper limit. From the close agreement in the linear polarisation standards, a value of $\lesssim$0.03% is indicated.

Circular efficiency factors were measured with the aid of a circular polaroid. The percentage polarisation measured for this filter in the V band was +98.047$\pm$0.052%. It is likely that the real polarisation is within 1% of this, so the calculated circular polarisations are expected to be within 1% of their true values in this band. As the circular polaroid was made from a linear polaroid followed by a ¼ wave plastic retarder optimised for the V band, the dependence of the circular efficiency on λ was not determined. As expected measurements of this filter through other bandpasses showed considerable linear polarisation.

The circular instrumental polarisation was found to be very small, as detailed below:-

V filter : 0.017 $\pm$ 0.005%

B : 0.011 $\pm$ 0.019%

I : 0.015 $\pm$ 0.019%

These measurements were made at the same time as those for the linear efficiency and are the average circular values measured for a number of stars.

2.7.2 Circular Only

Measurements through the same circular polaroid described above were made with the polarimeter configured in the circular only mode. It was reassuring to find that the results were in agreement with the SLC case.

The V band polarisation of the circular polaroid was found to be +98.173 ± 0.028% which differs negligibly from the measurement taken in the SLC configuration (98.047 ± 0.052%). The CO V band instrumental polarisation was found to be -0.001 ± 0.071%. This latter measurement has a fairly large error because it was taken in poor conditions.

2.6.3 Linear Only

Only limited calibration of the LO configuration has been possible. The linear polaroid was measured as 98.3% in V indicating that the efficiency is close to 1.00, but more accurate tests on standard stars are required. The instrumental linear polarisation was not determined. As the LO optical arrangement is optimal for a linear polarimeter (section 1.5.2, Serkowski 1974) it is likely that this configuration will perform extremely well.

A simple (although relatively expensive) improvement can be made by using two ½ wave plates, one of which is fixed. If the wave plates are identical, this removes any wavelength-dependent deviation of the position angle. The fixed ½ wave plate could be located in the filter slide without requiring any other modifications.

2.7.4 The Quality of the Calculated Errors

A detailed investigation into the accuracy of the error calculations was carried out for the circular polarisation in the CO and SLC configurations, using both bright and faint stars. A number of measurements were taken and the scatter compared with the calculated error on each measurement.

a) SLC: Calculated errors for a measurement of low circular polarisation and a photon error of 0.002 magnitude averaged 0.159%. The scatter in the points indicated that the error should have been 0.162%. On a fainter star with photon errors of 0.010 magnitude errors on measurements of small circular polarisation averaged 1.276% while the scatter gave an error of 1.275%. However the agreement was not as good on sources of almost 100% polarisation. Comparison between the calculated errors and the scatter indicated that the former were overestimated by a factor of 3. This is likely to be the result of assumptions, made in the statistical calculations for the uncertainties, breaking down when the number of photons in some bins is very small (as a result of the strong modulation of the intensity during a wave-plate rotation).

Although this analysis was carried out for the circular polarisation, the errors in the linear polarisation are connected through the factor μ (equation 2.8), and the above conclusion therefore also applies to the linear polarisation error calculations in the SLC and LO cases.

b) CO: The same effect, although slightly more pronounced, was found for this configuration. In non-photometric conditions, which affect the CO measurements (modulated at 1 hz) more than the SLC measurements (modulated at 60 hz), the scatter on a source of low polarisation was found to be slightly greater than the calculated error (by a factor $\sim$1.4). It is likely that this discrepancy would be eliminated in photometric conditions. However, for sources almost 100% polarised, the uncertainties were again overestimated, by factors ranging from $\sim$4 for bright sources to $\sim$10 for faint sources.

2.7.5 Stability of the Zero Points

The zero points are extremely stable. This conclusion was established by repeatedly restarting the motors between measurements of the two polaroids (circular and linear). It was found that the SLC linear zero point repeated to $\sigma_m = 0^{\circ}.12$ and the circular repeated to $\sigma_m = 0^{\circ}.07$. This scatter can be accounted for by the measurement error from photon statistics. The linear zero point will change every time the instrument is removed from the telescope. The LO zero point was, as expected, the same as the SLC linear zero, and similarly repeatable. Placing the ½ wave plate into the upper slot in the polarimeter instead of the lower one in this configuration has the effect of making the position angles run backwards. The CO zero point (i.e. the offset to the point at which the slews must start) is always 257 steps ($231^{\circ}.3$).

2.8 Summary

It has been found that the instrument is capable of the highest quality polarisation measurements in SLC, CO and probably in LO configurations. This is a result of:-

a) The high polarisation efficiency factors over a wide wavelength range;

b) The low instrumental polarisations;

c) The ability to provide precisions at the level expected from photon statistic errors.

In addition a great deal of flexibility and feedback through QUARTZ allows the observer to make the best use of observing time, and the use of a separate and intelligent controller makes more efficient use of the instrument computer and

provides for a measure of flexibility in the polarimeter design.

Some improvements could be made. These include:-

a) Using a Wollaston or Foster beam splitter instead of the Glan Thompson analyser. This would prevent half of the light being wasted but would require two detectors.

b) Using a second ½ wave plate in the filter slide to ensure that the linear only measurements of position angle are independent of wavelength.

c) Some refinements to QUARTZ.

Further possibilities include the use of a CCD detector to obtain imaging and high quantum efficiencies, adaptation as a "magnetometer" where circular polarisation measurements of spectral line wings are made to determine the magnetic field, and spectropolarimetry using a spectrograph or scanner. As the heart of the polarimeter - the analyser and rotating retarders - have been built as small units this will hopefully make possible the adaptation required for other instruments.

Finally, had more time been available, adaptation of the instrument to measure infra-red polarisations (Bailey and Hough 1982) would have been extremely desirable, especially in the field of research continued in this thesis. If simultaneous optical/IR observations were not required, adaptation to measure IR polarisations could be made relatively easily.

REFERENCES

Bailey, J. and Hough, J.H., 1982. *Publ. astr. Soc. Pacif., 94,* 618.

Borra, E.F., Fletcher, J.M. and Poeckert, R., 1981. *Astrophys. J., 247,* 569.

Brown, D.N., and Landstreet, J.D., 1981. *Astrophys. J., 246,* 899.

Hsu, J-C. and Breger, M., 1982. *Astrophys. J., 262,* 732.

Juritz, J.M., 1982. Private communication.

Serkowski, K., 1974 in Planets, Stars and Nebulae studied with Photopolarimetry, p. 135, ed. Gehrels, T., University of Arizona Press, Tucson, Arizona.

Smart, W.M., 1958. Combination of Observations, Cambridge University Press.

Staude, J., Wolf, K. and Schmidt, Th., 1973. *I.A.U. Symp., 52,* 139.

Warner, B., 1971. *I.A.U. Coll. 15,* 144.

Wolstencroft, R.D. and Kemp, J.C., 1972. *Astrophys. J., 177,* L137.

CHAPTER 3

OBSERVATIONS OF EF ERI

3.1 Introduction

The optical counterpart of the X-ray source 2A0311-227 was first identified by Griffiths *et al.* (1979) and Williams (Hiltner 1979) as a star whose spectrum closely resembles those of the AM Her class of cataclysmic variables. The circular polarization discovered by Tapia (1979) confirmed the star's membership. Spectroscopic, photometric and X-ray observations have established an orbital period of 81 minutes and quasi-periodic variations on a time scale of 6 minutes have been reported (Patterson, Williams and Hiltner 1981) in the optical and X-ray bands.

In this chapter the first simultaneous linear and circular polarimetry and high speed photometry of the star (now renamed EF Eri) are reported.

3.2 Observations

All observations were made with the U.C.T. Polarimeter on the 1.9 and 1.0m reflectors at the Sutherland site of the South African Astronomical Observatory. A cooled RCA 31034A photomultiplier with a crown glass Fabry lens was used throughout. Integration times ranged from 5 sec to 2 sec for the high speed photometry data and from 120 sec to 20 sec for the polarimetry. Observations were made in white light (i.e. the full response of the RCA 31034A/Fabry combination, 360nm - 920nm) to maximize the count rate, except for runs

S3219 and S3220 which were taken through filters - a broadband blue (BG18), a broadband red (GG495) and a Cousins I filter (RG9): Blue, Red, I, respectively. The log of observations is given in Table 3.1. Sky background and extinction corrections to the data were made online. Frequest sky readings were taken to ensure that variations in the polarised background were accounted for. If the moon was rising or setting, sky readings were taken at least every 3 minutes.

Examples of the light curves and polarisation data obtained are shown in Figures 3 to 6. All data are phased according to the ephemeris

$$\text{HJD } 2444131.6751+0.056265967E$$
$$\pm 0.000000057$$

obtained from 14 linear polarisation peaks which define $\phi = 0.0$. The above epoch is that given by Bailey, Hough and Axon (1980).

This ephemeris agrees to within the errors with that derived by Tapia (private communication) from 25 peaks spanning 5 years:

$$\text{HJD } 2443894.68240+0.0562660082E$$
$$\pm .00009 \pm .0000000046$$

and also that quoted by Bailey *et al.* (1982) based on a narrow minimum in the infra-red light curve.

3.2.1 The White Light Data

Figures 3.1, 2 and 3 show the range of behaviour observed in the star. On the basis of the circular polarisation variations during the orbit, the runs listed in Table 3.1 can be classed, as a first approximation, as type 1 or type 2.

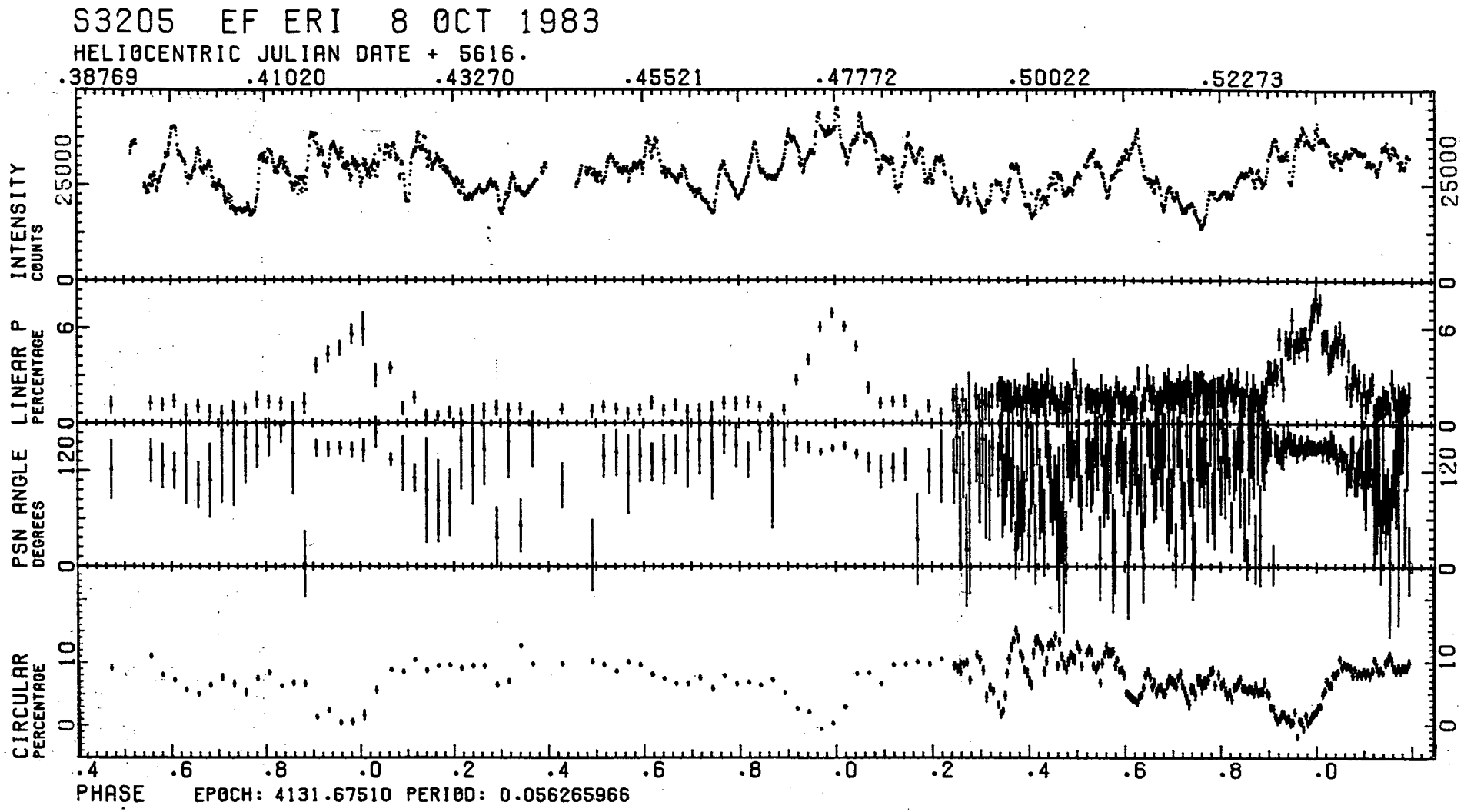

Figure 3.1 Intensity and polarisation data for run S3205. Each intensity point is a 5 second integration and each polarisation point 120 seconds or 20 seconds.

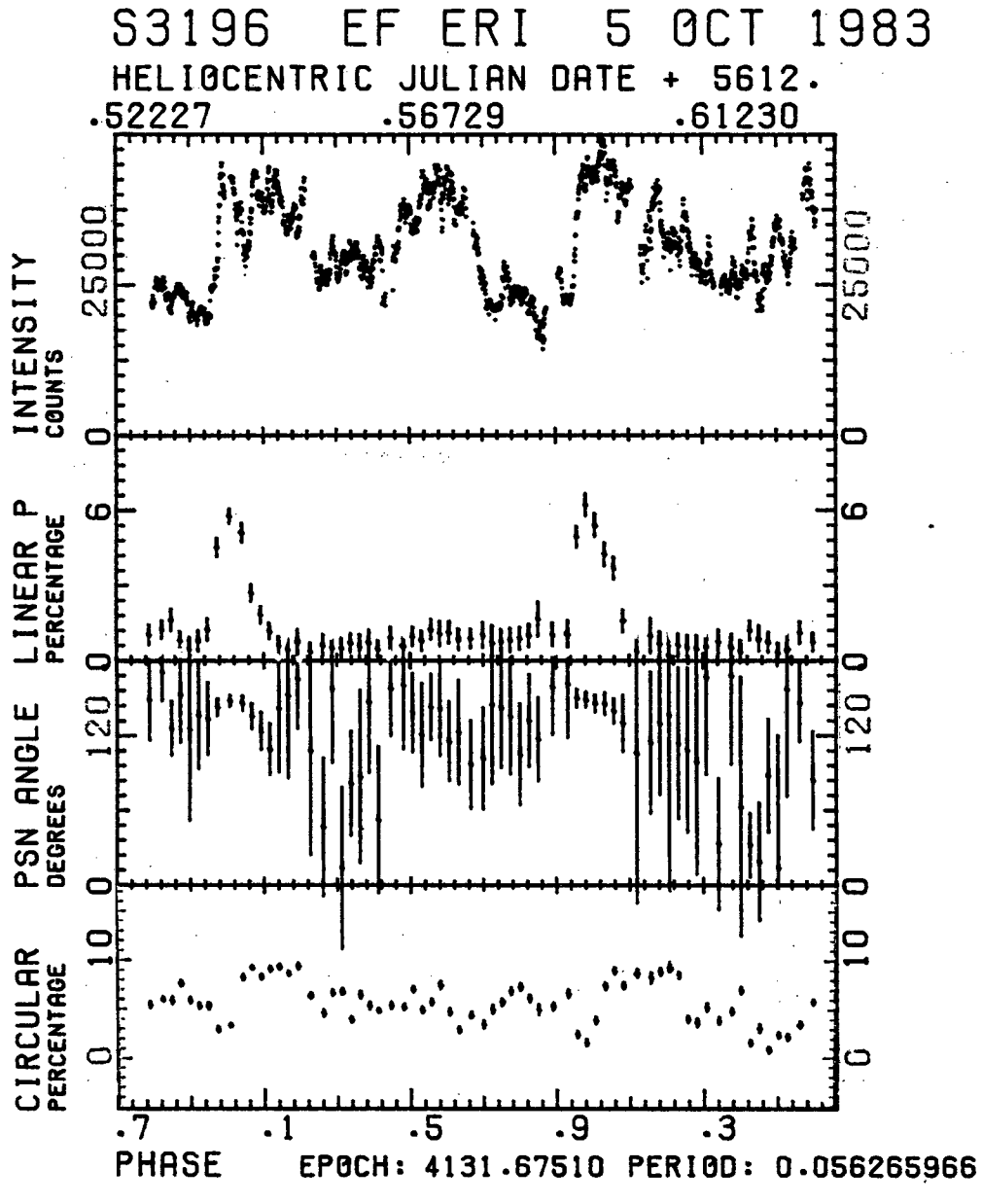

Figure 3.2 Intensity and polarisation data for run S3916. Each intensity point is a 5 second integration and each polarisation point 120 seconds.

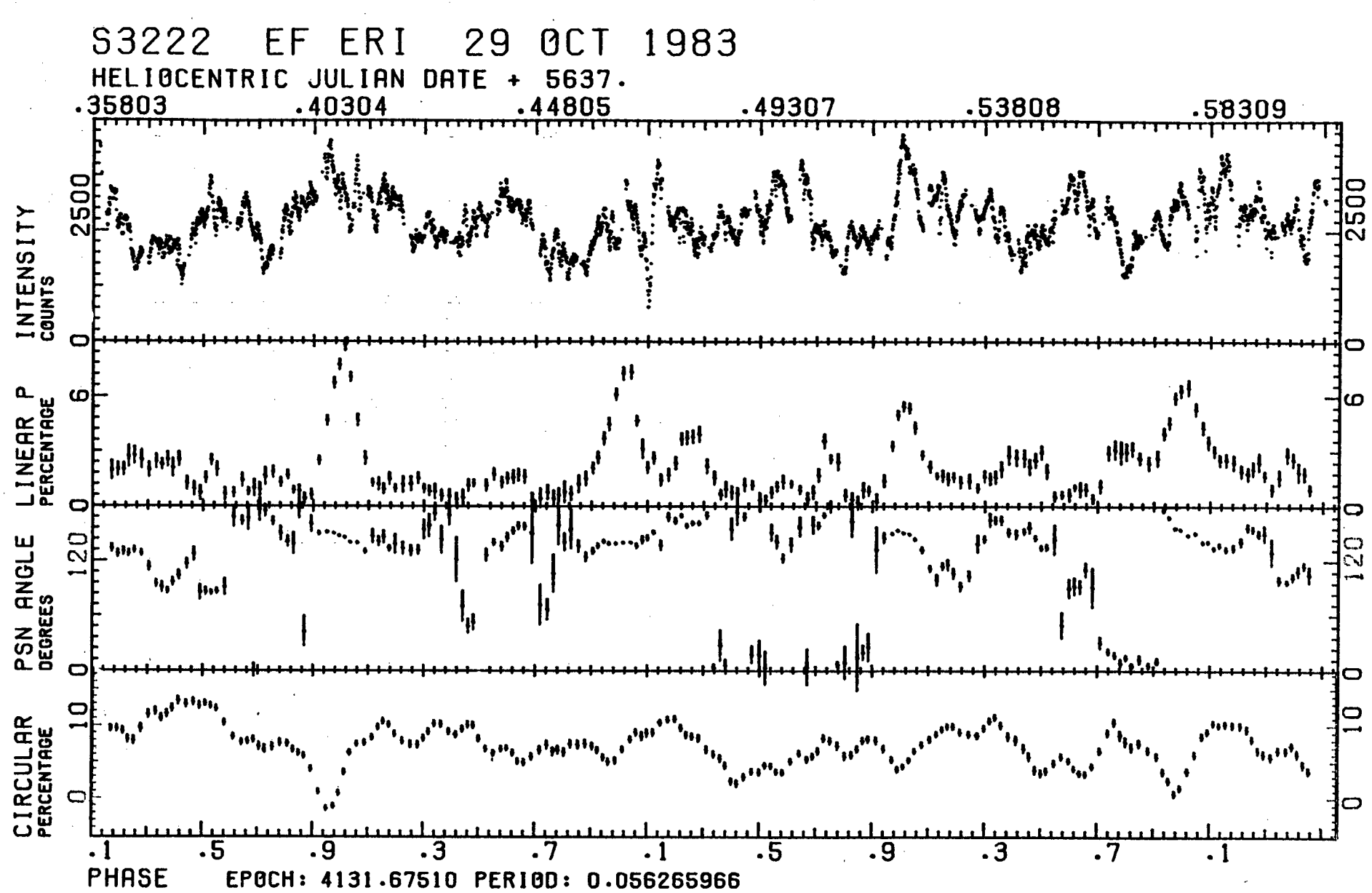

Figure 3.3 Intensity and polarisation data for run S3222. Each intensity point is a 6 second integration and each polarisation point 90 seconds. The polarisation data have been running averaged three at a time.

Table 3.1 Observations of 2A0311-227 = EF Eri

Run Number	Date	$JD_{\odot}$ start 2445000+	ΔT(Pol) (sec)	ΔT(Phot) (sec)	Duration (cycles)	Telescope (m)	Filter	Type
S3181	4 Sep 83	581.5255	120	5	1½	1.9	None	1
S3183	5 Sep 83	582.5204	120	5	2	1.9	None	1
S3196	5 Oct 83	612.5260	120	5	2	1.9	None	2
S3205	8 Oct 83	616.3905	120,20	5	2½	1.9	None	1
S3214	25 Oct 83	633.3774	30	2	4	1.0	None	2
S3219	27 Oct 83	635.3889	40,120	5,10	1,1	1.0	Red, Blue	
S3220	29 Oct 83	636.5594	120	10	1	1.0	I	
S3222	29 Oct 83	637.3581	30	2	4½	1.0	None	1,2
S3224	30 Oct 83	638.3693	30	2	4	1.0	None	2

Figure 3.1 shows a type 1 run, figure 3.2 a type 2 run. The principal difference is found at ϕ = 0.5 where the circular polarisation is at a maximum in type 1 runs (approximately 12% in white light), but considerably less or even at a minimum in type 2 runs. The morphology of type 2 orbital variations however, is less constant from orbit to orbit than that of type 1. Other differences are also evident - the type 1 intensity curves are double humped with a primary maximum at ϕ = 0 but the type 2 curves show more random behaviour; the linear polarisation peaks are more symmetrical in the type 1 runs but type 2 peaks are asymmetric or doubled. Finally, the type 2 position angle data show somewhat greater variation during an orbit than do those of type 1.

Run S3222 (Figure 3.3) shows that the star can change from the type 1 state to the type 2 state within one orbital period. Until $JD_{\odot}$ 5637.42 the polarisation and intensity data are type 1. However, the next circular polarisation minimum at ϕ = 0 is much shallower and half an orbit later the circular polarisation has dropped to only 3 percent. Linear peaks become doubled. These are the first published polarisation data showing such a transition. Such data for EF Eri are in any case scarce; the only sources are Bailey, Hough and Axon (1980) and Bailey *et al.* (1982). These show type 1 curves. Description of the circular polarisation in Tapia (1979) and schematics of data by Tapia communicated in Allen, Ward and Wright (1981) and Chanmugam and Dulk (1981) show type 2 curves with (sometimes) doubled linear peaks.

All of the photometric data have been searched for periodicities. No strictly periodic variations besides those at the orbital period and half period were found. In some runs, notably S3205 (Figure 3.1), there is flaring on a time-scale of 6 minutes. This has been reported elsewhere at both optical and X-ray wavelengths (Patterson, Williams and Hiltner 1981) and in the circularly polarised flux by Tapia in the above paper. However, S3205 does not show any circular polarisation variations convincingly correlated with the flares.

3.2.2 The Filtered Data

Figure 3.4 indicates that there is a maximum circular polarisation in the red band with less in the blue and I bands. This result is consistent with the more comprehensive investigations in Bailey *et al.* (1982) which show that the polarisation peaks at 550nm. There is no evidence for a linear polarisation peak in the blue and the circular polarisation varies between 3 and 7 percent. At ϕ = 0.43 there is a dip in both the red and I curves. The phases of the dips identify them with the infra-red minima reported by Bailey *et al.* (1982) and optical minima reported by Watson, Mayo and King (1980). The red band data show the system to be in a type 2 state. The state during the blue and I runs is unknown.

3.3 Modelling the Average Behaviour

In order to derive the average behaviour of the star each of the white light runs was folded and binned into 15 phase bins (Figure 3.5). As a first step in modelling the

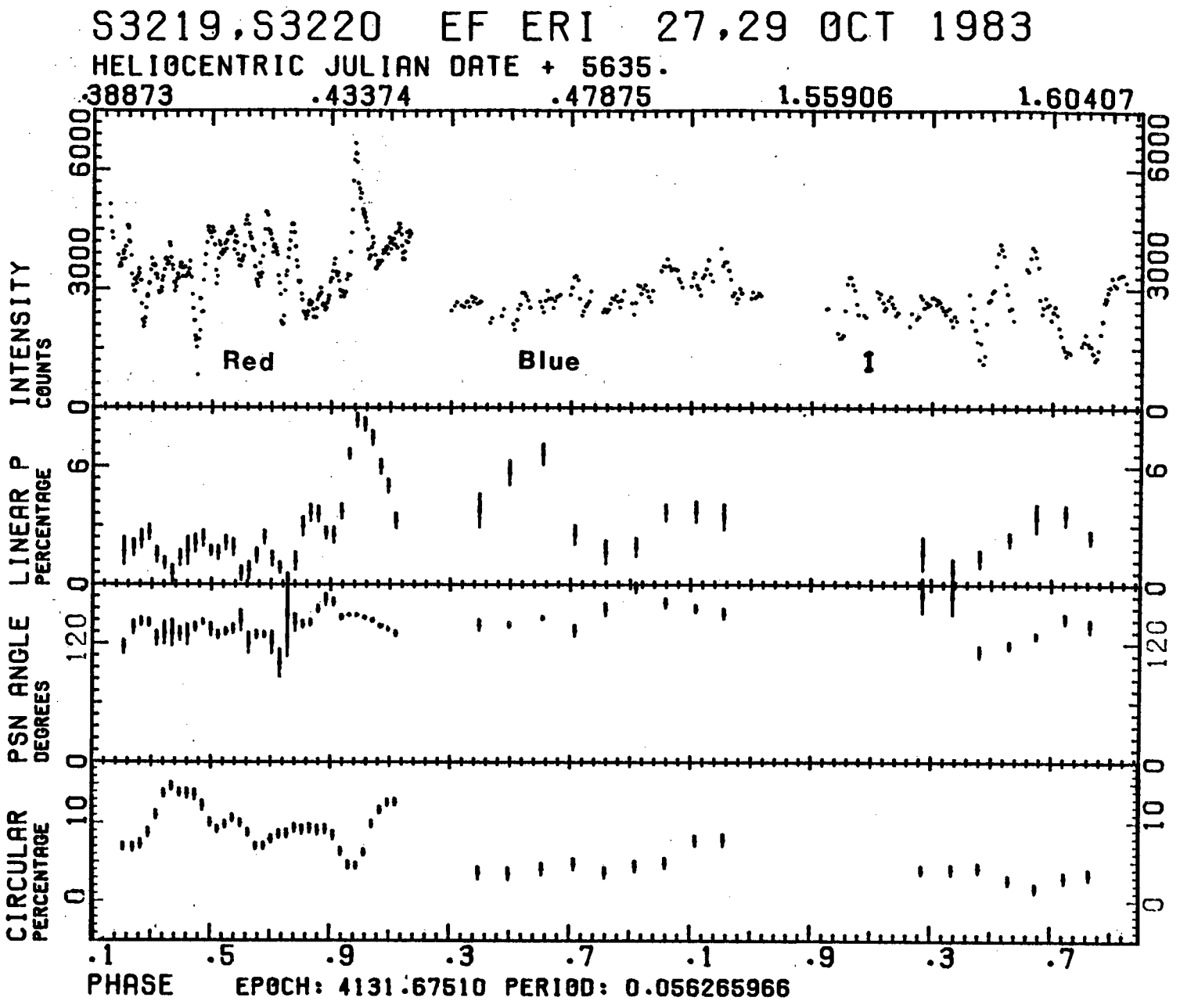

Figure 3.4 Intensity and polarisation data for runs S3219, S3220 in Red, Blue and I_C filters. Various integration times have been used.

star a centred dipole magnetic field was assumed for the primary whose rotation was synchronised, and radial accretion at one pole only considered. A further initial assumption was that the fraction of the surface over which accretion takes place is small ($\lesssim 0.01$). In such a model the projected angle, θ, of the column against the sky background is given by

$$\tan\theta = \frac{\sin\beta\sin\phi}{\sin\beta\cos i\cos\phi+\sin i\cos\beta}$$

where i is the angle between the rotation axis of the primary and line of sight (inclination) and β is the magnetic co-latitude of the accretion column on the surface of the primary. ϕ is orbital phase. The formula differs from the one by Brainerd and Lamb (1983) only in that $\phi = 0$ is defined as the instant when the accretion column is in the plane of the rotation axis and line of sight but on the far, not near, side of the primary, which is in keeping with the phase convention used so far. Because the linearly polarised component of the cyclotron emission from the accretion column is parallel to the magnetic field for regions in the column with $KT \lesssim 20$keV (Brainerd and Lamb 1983), θ is also the measured linear polarisation position angle measured from some mean value. It is then possible to compute a set of curves for θ over an orbit and select the best i and β by a least squares fit. The above authors also emphasise that, where possible, it is important to use the entire position angle curve.

A solution was made for each of the folded runs. Figure 3.5 shows the best fit for run S3205 (solid line).

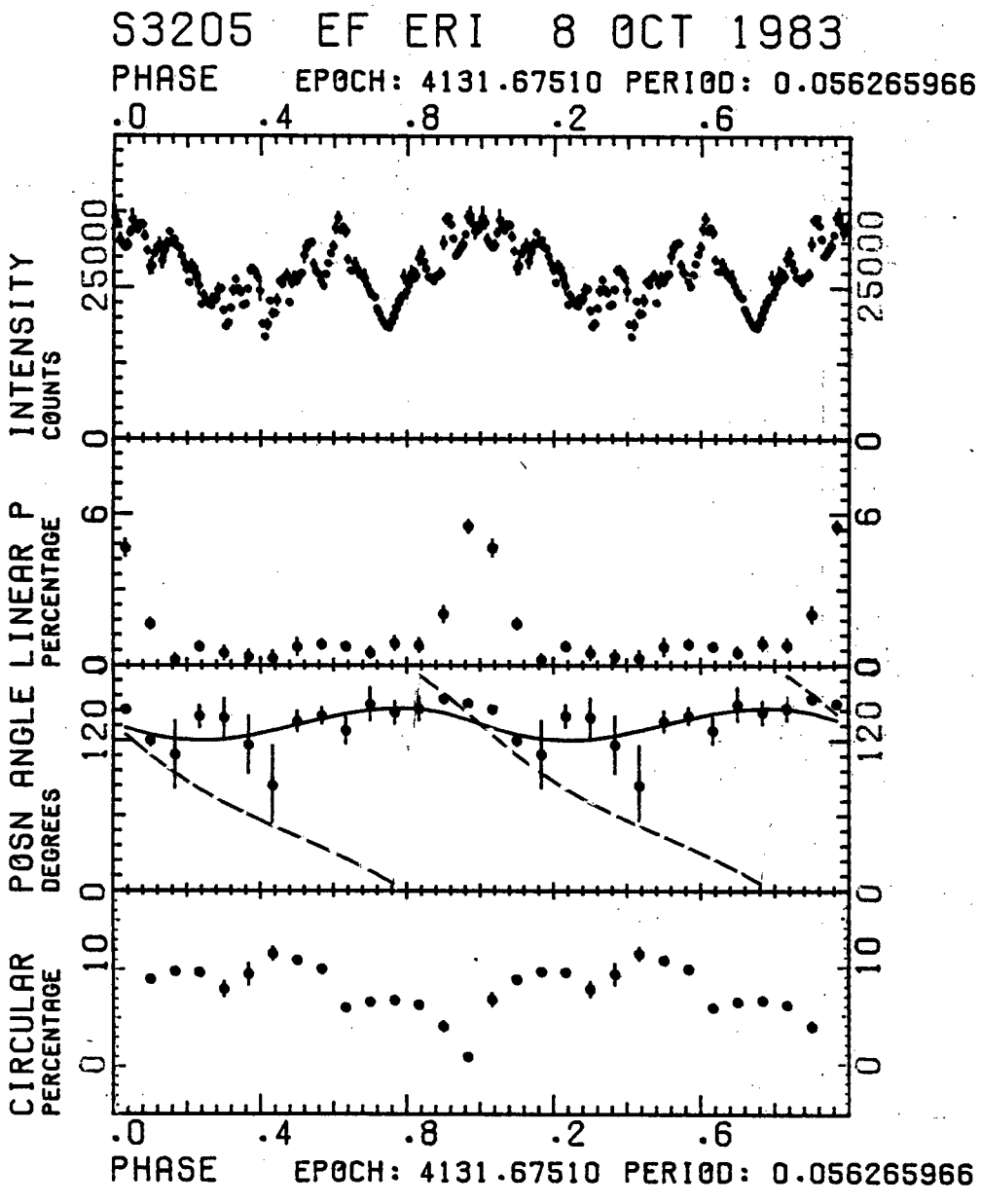

Figure 3.5 Phase-folded intensity and polarisation data for run S3205. The best fit to the position angle data for the inclination i and magnetic colatitude β is shown (solid line). The dotted line shows the variation expected for $i=\beta=45^{\circ}$.

This indicates that $\beta \lesssim 15^{\circ}$, a result common to all the folded runs. As β is small, i is not strongly constrained. However, the fact that the circular polarisation drops to approximately zero, at least in the type 1 runs, and that there is a strong linear polarisation peak at $\phi = 0$, indicates that $i + \beta \simeq 90^{\circ}$, or $i \simeq 75^{\circ}$. Where the circular polarisation does not drop to zero (type 2 runs) at $\phi = 0$, β must be smaller in the simple model adopted.

As $(i + \beta) \simeq 90^{\circ}$ at the linear polarisation peak, the method of Meggit and Wickramasinghe (1982) can be used as a check. This yields values of $65^{\circ}<i<85^{\circ}$, depending on what value of $\frac{d\theta}{d\phi}$ is adopted. The slope of the position angle in Figures 3.1 and 3.2 is almost zero at $\phi = 0$, and then follows a decreasing trend 0.08 of a cycle later. It is not obvious what slope should be used. Another constraint can be placed on i from the absence of an X-ray eclipse (see Patterson, Williams and Hiltner 1981). Assuming an unevolved secondary, the period of the system implies a secondary mass of 0.15 $M_{\odot}$ (Warner 1976). Imamura (1984) finds a primary mass of 1 $M_{\odot}$ from the X-ray spectrum. A wider range of primary masses from 1.4 $M_{\odot}$ to 0.5 $M_{\odot}$ results in a mass ratio $\frac{M_s}{M_p}$ of $0.1 \lesssim q \lesssim 0.3$. For the above ratios Horne (1983, Figure 5) implies $i \lesssim 80^{\circ}$ ($q=0.1$), $i \lesssim 75^{\circ}$ ($q=0.3$).

In conclusion the best values which can be derived from the data are:

$$0^{\circ}<\beta<15^{\circ},\ 65^{\circ}<i<75^{\circ}$$

These values disagree with the usually adopted inclinations and magnetic colatitudes ($i = \beta = 45^{\circ}$). The dotted

curve drawn on top of the position angle data in Figure 3.5 shows this clearly.

Attempts by Imamura (1984) to model the X-ray light curve assuming the standard $i = \beta = 45^{\circ}$ were also not successful. The absence of a hard X-ray eclipse implies $|\beta - i| > 11^{\circ}$, lending further support to the above derived values for i and β.

As $\cos^2\beta + \cos^2 i \simeq 1$ the case made by Brainerd and Lamb (1983) that the discovery of AM Her objects is greatly influenced by observational selection effects is strengthened.

Some of the consequences of the simple model with $\beta \lesssim 15^{\circ}$ are:-

a) Because both magnetic poles are almost perpendicular to the orbital plane there is little preference for accretion at either pole (Schneider and Young 1980). Although Bailey *et al.* (1983) report that flickering in the visual and infrared bands is correlated, implying accretion at one pole only, no simultaneous polarisation data were obtained. It is possible that type 1 curves are the result of single pole accretion but that type 2, because of their greater variety, are the result of double pole accretion.

b) The accretion stream must move out of the orbital plane before falling to the surface of the white dwarf. At some phase, approximately $\phi = 0.5$, the stream must pass across the line of sight to the accretion column. Depending on the exact nature and curvature of the accretion stream (see Liebert and Stockman 1983) the point of intersection of the line of sight with the stream could be at a considerable distance from the primary, or it could be closer to the accretion column in

a region where there is considerable curvature of the stream. In either case $i \simeq 70^{\circ}$ ensures that there can be enough material in the line of sight to cause the infra-red minimum (Bailey *et al.* 1982, Allen, Ward and Wright 1981, this paper), Hα to change from emission to absorption (Verbunt *et al.*, 1981, Allen, Ward and Wright 1981), and the minimum in the X-ray intensity (Patterson, Williams and Hiltner 1981, White 1982).

3.4 Modelling the Polarisations

The angle α between the line of sight and the column is given in terms of the simple model used so far by:

$$\cos\alpha = \cos i\cos\beta - \sin i\sin\beta\cos\phi.$$

This equation together with the results of calculations (including the effects of collisions) made by Barrett and Chanmugam (1983), (1984) for a homogeneous plasma slab with kT = 1 keV, $B = 3\times10^{7}$G and $\Lambda=10^{8}$ allow circular and linear polarisation curves to be synthesized. Figure 3.6 shows the synthesized curves for $i=75^{\circ}$, $\beta=15^{\circ}$ and cyclotron harmonics 4 to 9 superimposed on the folded data for run S3205. The general shape of the synthesized curve harmonics 6 and 7 show fairly good agreement with the observed data. It should be noted that the synthesized polarisations have been diluted by half. This was necessary despite the overall reduction in the percentage polarisations found by Barrett and Chanmugam (1983), (1984) when collisions were included. Consequently no calculations were made for the higher temperature regime (kT≃20keV) investigated by Meggitt and Wickramasinghe (1982)

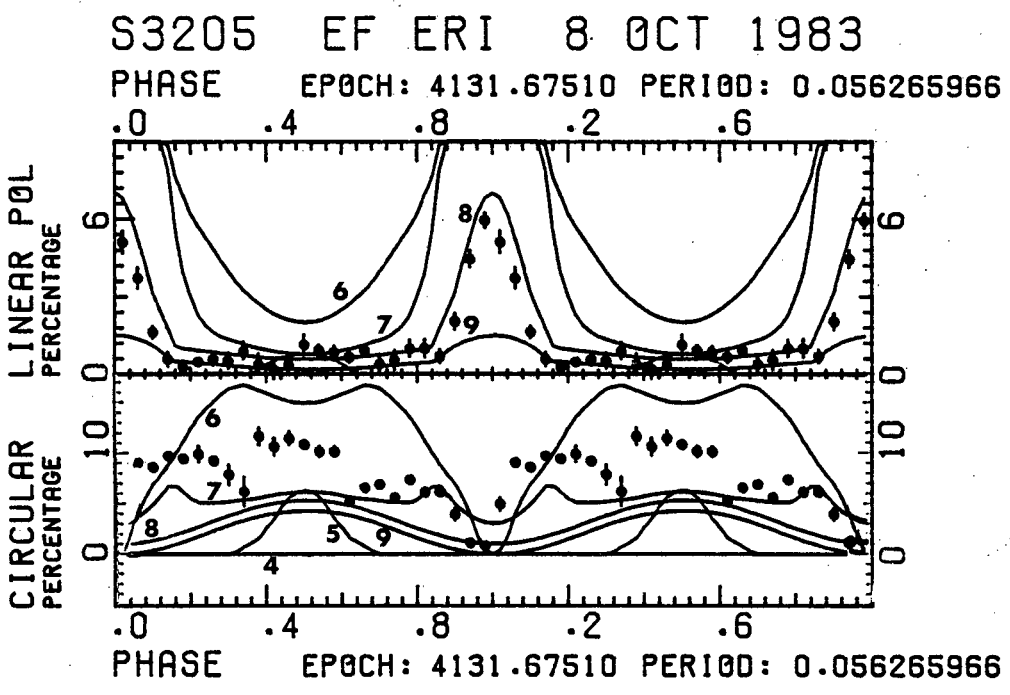

Figure 3.6 The synthesized average polarisation curves for i=75°, β=15° and cyclotron harmonics 4 to 9 superimposed on the data for S3205. The harmonics are calculated using kT=1keV, B=3×10^{7}G and Λ=10^8.

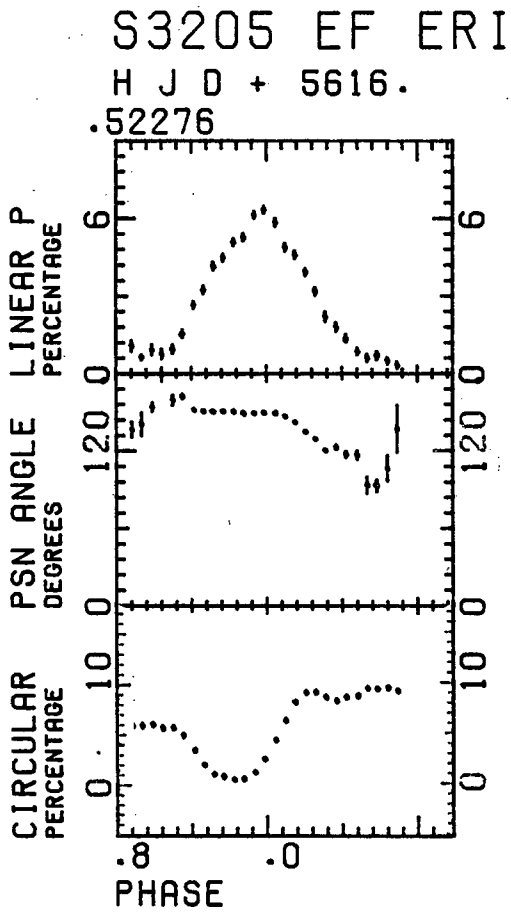

Figure 3.7 Filtered version of the last linear polarisation peak of run S3205. The original 20 second points were averaged 3 at a time and the resultant points running averaged 3 at a time.

for the collisionless case where even higher percentage polarisations were found.

A similar analysis has been carried out by Bailey *et al.* (1982) using earlier calculations by Chanmugam and Dulk (1981) for circular polarisation only. Synthesis of the polarisation curves using $i = \beta = 45^{\circ}$ with the later calculations show poorer agreement in the overall shape for a type 1 curve.

3.5 Details and Cycle to Cycle Variations

So far the average behaviour for the polarisation has been modelled by assuming a centred dipole, with accretion over only a small area at one pole. There are some characteristics of the data that such a model has difficulty in explaining.

3.5.1 The Shape of the Position Angle Curve during Linear Polarisation Peaks

Figure 3.7 shows a filtered version of the last linear polarisation peak of run S3205 (Figure 3.1). The data show the constant then decreasing trend of the position angle with the sharp "knee" at $\phi = 0.08$ mentioned earlier. The position angle is extremely well determined during the linear polarisation peak and there is no question as to the reality of this structure. The same shape appears in the two previous cycles at $\phi = 0$ (Figure 3.1) and for all type 1 runs. It exists in approximately half of the type 2 runs. Interestingly a very similar structure is found in the data

provided by Tapia for AM Her in Brainerd and Lamb (1983, Figure 3). No simple single or double accretion column model based on a centred dipole can explain the observations if radial accretion is assumed. However, if β is small, the column must be curved towards the orbital plane. Just after $\phi = 0.5$, the curved part of the column would come into view from behind the part closest to the white dwarf, causing the position angle to decrease rapidly. With more analysis, it may be possible to deduce the detailed shape of the column from the position angle data.

3.5.2 The Phasing of the Linear Polarisation Peaks

The simple model predicts that the centre of the linear polarisation peak should be contemporaneous with the centre of the circular polarisation minimum. Although this is generally the case,some peaks are delayed, notably during run S3222 (Figure 3.3) where a delay of 0.05 of a cycle occurs for the first two peaks. This also requires some curvature of the accretion column and possibly a different location for the production of circularly and linearly polarised light.

3.5.3 Eclipse-like Features in S3196

Besides showing type 2 behaviour, S3196 (Figure 3.2) also has steeply rising linear polarisation peaks coinciding with extremely rapid rises in intensity (more than doubled in 70 seconds). The intensity data show an extended secondary minimum from $\phi = 0.8$ to $\phi = 0.95$. These data are consistent with an interpretation where the accretion column is beyond

the limb of the primary (i.e. $i+\beta>90^{o}$). However, the circular polarisation minima are relatively shallow and remain positive, in contradiction to the above explanation which requires a negative excursion at this phase. No satisfactory explanation has yet been found.

3.5.4 Derivation of β from the Position Angle Data

The problem of explaining the change in polarisation curves from type 1 to 2 remains. Accretion onto both poles is a possible explanation: especially if β is small, i is large and the shock front is situated well above the surface of the white dwarf primary. An alternative explanation is that conditions in the accretion column change, so that the harmonic dominant in a particular wavelength region changes. As the maximum level of polarisation is $\simeq$15 percent it may be possible that only small changes in the accretion rate, masked by the flickering, could suffice, especially if the column is strongly curved. However, the circular polarisation should then tend to be correlated with the flickering, which is not seen to be the case. Certainly run S3222 (Figure 3.3) shows no systematic increase or decrease in accretion rate when the circular polarisation changed from type 1 to type 2.

A second alternative explanation in terms of the simple model requires that the area over which accretion takes place is enlarged, with more accretion taking place in some parts of the accretion region than in other parts (Kuijper and Pringle 1982). In order to test this hypothesis a β was calculated in each run for every position angle point where there

was significant linear polarisation. No value of i could be found which resulted in β being even approximately constant, which, despite the noise in the data, gives some credence to the hypothesis. However, the position angle at $\phi = 0.0$ departs from 145^{o} in only two of the twenty white light cycles, which indicates that variations in longitude of the accretion region are infrequent. Of course, large variations in β prompt the question whether it is valid to average the polarisation curves into phase bins as in section 5. However, most of the early type 1 runs taken on the 1.9m (e.g. Figure 3.1) indicate that, for them at least, the variation of the position angle (which is relatively well determined in the low time resolution data as a result of decreased photon noise) during an orbital cycle is small, which in turn indicates that β itself is small, and that averaging is a meaningful procedure.

3.5.5 Narrow Dips and Flickering

As mentioned earlier there is no correlation between intensity variations of the sort seen at $JD_{\odot}$ 5616.47 (Figure 3.1) and changes in percentage polarisation. This is confirmed by inspection of the 20 sec time resolution data where changes in percentage polarisation and intensity take place independently.

There are two large circular polarisation dips at $\phi = 0.37$ and $\phi = 0.65$ in the last cycle of S3205 (Figure 3.1). The former is followed by a rapid increase in polarisation from 2 percent to 15 percent in 140 sec followed by a decline nearly as rapid and is not correlated with intensity variations. The latter is roughly contemporaneous with a bright flare. Other

type 1 orbits have been searched for similar behaviour. Although none was found at exactly the same phase there is a tendency for large amplitude variations in the circular polarisation to occur at approximately the same phases, suggesting that the effects are observed for only a limited range of viewing angles to the axis of the cyclotron emitting region.

3.6 Conclusions

While some of the basic characteristics of the star are in agreement with the standard single accretion column model, many details of the intensity and polarisation curves remain unexplained. Some progress can be made by assuming curvature in the column, a larger area of accretion, or accretion at two poles. Each of these possibilities needs to be investigated more fully. An analysis of the correlation between the flickering in the optical and infrared for both type 1 and 2 polarisation curves would settle the question of accretion at two poles while careful modelling of the accretion column (including curvature) from position angle data would lead to a greater understanding of the structure of the cyclotron emitting region. This may enable linear and circular polarisation curves to be synthesised from the position angle data.

It is clear from this study that a larger inclination and smaller magnetic colatitude are required for EF Eri than have been assumed so far. This conclusion is supported by the X-ray modelling done by Imamura (1984). It is important to calculate whether the curved funnel could provide the correct wavelength dependence for the X-ray absorption feature.

Finally, it is clear from this study and from other work that the morphology of the polarisation and intensity curves of AM Her stars is variable even on long time scales. Observations over longer periods will be important in unravelling the details of these systems.

REFERENCES

Allen, D.A., Ward, M.J., & Wright, A.E., 1981. *Mon. Not. R. astr. Soc., 195,* 155.

Bailey, J., Hough, J.H. & Axon, D.J., 1980. *Nature, 285,* 306.

Bailey, J., Hough, J.H., Axon, D.J., Gatley, I., Lee, T.J., Szkody, P., Stokes, G. & Berriman, G., 1982. *Mon. Not. R. astr. Soc., 199,* 801.

Bailey, J., Hough, J.H., Gatley, I. & Axon, D.J., 1983. *Nature, 301,* 223.

Barrett, P.E. & Chanmugam, G., 1983. *Proc. I.A.U. Coll. 72,* p. 217, eds. Livio, M. & Shaviv, G., D. Reidel Publishing Company.

Barrett, P.E. & Chanmugam, G., 1984. *Astrophys. J., 278,* 298.

Brainerd, T.J. & Lamb, D.Q., 1983. Preprint.

Chanmugam, G. & Dulk, G.A., 1981. *Astrophys. J., 244,* 569.

Griffiths, R.E., Ward, M.J., Blades, J.C., Wilson, A.S., Chaisson, L. & Johnston, M.D., 1979. *Astrophys. J., 232,* L27.

Hiltner, W.A., 1979. *I.A.U. Circ.* No. 3324.

Horne, K., 1983. Ph.D. Thesis, California Institute of Technology, Pasadena, California.

Hsu, J. & Breger, M., 1982. *Astrophys. J., 262,* 732.

Imamura, J.I., 1984. Preprint.

Kuijpers, J. & Pringle, J.E., 1982. *Astr. Astrophys., 114,* L4.

Liebert, J. & Stockman, H.S., 1983. Preprint.

Meggitt, S.M.A. & Wickramasinghe, D.T., 1982. *Mon. Not. R. astr. Soc., 198,* 71.

Patterson, J., Williams, G. & Hiltner, W.A., 1981. *Astrophys. J., 245,* 618.

Schneider, D.P. & Young, P., 1980. *Astrophys. J., 240,* 871.

Serkowski, K., 1974. Planets, Stars and Nebulae Studied with Photopolarimetry, p. 135, ed. Gehrels, T., University of Arizona, Tucson.

Shurcliff, W.A., 1962. Polarised Light, Harvard University Press, Cambridge, Mass.

Tapia, S., 1979. *I.A.U. Circ.,* No. 3327.

Tinbergen, J., 1973. *Astr. Astrophys., 23,* 25.

Verbunt, F., van den Heuvel, E.P.J., van der Linden, Th. J., Brand, J., van Leeuwen, F. & van Paradijs, J., 1980. *Astr. Astrophys., 86,* L10.

Warner, B., 1971. *I.A.U. Colloq. No. 15,* p. 144, Bamberg.

Warner, B., 1976. *I.A.U. Symp. 73,* p. 85, ed. Eggleton, P., Mitton, S. & Whelan, J.

Watson, M.G., Mayo, S. K. & King, A.R., 1980. *Mon. Not. R. astr. Soc., 192,* 689.

White, N.E., 1981. *Astrophys. J., 244,* L85.

CHAPTER 4

OBSERVATIONS OF E1405-451

4.1 Introduction

The X-ray source E1405-451 was first discovered in the HEAO-1 soft x-ray survey (Jensen *et al.* 1982) and identified optically by Mason *et al.* (1982) with a 15th magnitude star whose properties resembled those of the AM Her class of cataclysmic variables. Membership of the class was confirmed by Tapia (1982) from the existence of strong circular polarisation. Quasiperiodic oscillations at roughly 2 sec were reported by Mason *et al.* (1982) and further investigated by Middleditch (1982) and Mason *et al.* (1983). IUE observations by Nousek and Pravdo (1983) indicated the presence of a magnetically confined wind. Circular polarisation in the optical and IR has been reported by Bailey *et al.* (1983) and linear polarisation by Visvanathan and Tuohy (1983).

This chapter makes use of photometric observations by J.W. Menzies, South African Astronomical Observatory, and polarimetric observations by S. Tapia, Steward Observatory.

4.2 Observations

All observations were made at the Sutherland site of the S.A.A.O. except for those taken before July 1982 which were made at the Catalina station of Steward Observatory. A full log of the observations is provided in Table 4.1. The instruments used to gather the polarisation data were the "Minipol"

Table 4.1

Run Serial No.	*Date (UT)*	*Duration (Cycles)*	*Telescope (m)*	*Type of Obs.*	*Passband*	*Observer*	*Instrument*
1	23 Feb 82	0.5	1.55	CP	Red	ST	Minipol
2	20 Mar 82	1.0	1.55	CP	Red	ST	Minipol
3	23 Nov 82	0.5	1.55	LP	White	ST	Minipol
4	17 Apr 82	1.0	1.55	LP	Red	ST	Minipol
5	20 Apr 82	1.5	1.55	CP,LP	Red	ST	Minipol
6	14 May 82	0.7	1.55	CP,LP	Red	ST	Minipol
7	13 Jul 82	1.0	1.0	LP	Red	ST	Minipol
8	17 Jul 82	1.0	1.0	LP	Red	ST	Minipol
9	18 Jul 82	1.0	1.0	LP	Red	ST	Minipol
10	24 Jul 82	1.0	1.9	LP	Blue	ST	Minipol
11	26 Jul 82	1.0	1.9	CP	U	ST	Minipol
12	6 Aug 82	1.5	1.0	Phot	UBVRI	JM	StAP
13	2 Feb 83	0.8	1.0	Phot	BVI	JM	StAP
14	4 Feb 83	1.1	1.0	Phot	BVI	JM	StAP
15	5 Feb 83	1.0	1.0	Phot	BVI	JM	StAP
16	6 Feb 83	1.2	1.0	Phot	UBV	JM	StAP
17	6 Apr 83	2.7	1.9	SLC	White	MC	UCT Pol
18	7 Apr 83	1.0	1.9	SLC	White	MC	UCT Pol
19	9 Apr 83	1.5	1.9	SLC	White	MC	UCT Pol
20	10 Apr 83	3.1	1.9	SLC	White	MC	UCT Pol
21	11 Apr 83	3.7	1.9	SLC	White	MC	UCT Pol
22	12 Apr 83	3.2	1.0	SLC	White	MC	UCT Pol
23	13 Apr 83	1.0	1.0	SLC	Blue, Red	MC	UCT Pol
24	14 Apr 83	0.2	1.0	SLC	Blue, Red	MC	UCT Pol
25	18 Apr 83	1.4	1.9	Phot	UBVI	JM	RPP
26	18 Apr 83	1.0	1.0	HSP	White	MC	UCT Phot
27	18 Apr 83	1.0	1.0	SLC	Blue, Red	MC	UCT Pol
28	16 Jul 83	1.5	1.0	Phot	UBVRI	JM	StAP
29	16 Jul 83	1.0	1.9	SLC,HSP	White	MC	UCT Pol
30	17 Jul 83	1.4	1.0	Phot	UBVRI	JM	StAP
31	17 Jul 83	2.0	1.9	SLC,HSP	White	MC	UCT Pol
32	3 Aug 83	1.0	0.75	HSP	White	MC	UCT Phot
33	7 Aug 83	1.0	0.75	HSP	White	MC	UCT Phot
34	8 Aug 83	1.0	0.75	HSP	White	MC	UCT Phot
35	24 Apr 84	2.0	1.9	SLC,HSP	White	MC	UCT Pol
36	25 Apr 84	1.4	1.0	Phot	UBVRI	JM	StAP
37	28 Apr 84	1.7	1.0	Phot	UBVRI	JM	StAP
38	28 Apr 84	2.2	1.9	SLC,HSP	Blue, Red	MC	UCT Pol
39	29 Apr 84	1.3	1.9	SLC,HSP	White	MC	UCT Pol
40	29 May 84	1.2	0.75	SLC,HSP	White	MC	UCT Pol
41	30 May 84	3.1	0.75	SLC,HSP	White	MC	UCT Pol
42	31 May 84	2.0	0.75	HSP	White, Blue	MC	UCT Phot
43	1 Jun 84	1.0	0.75	HSP	Red	MC	UCT Phot
44	2 Jun 84	1.2	0.75	SLC,HSP	White	MC	UCT Pol
45	27 Jun 84	2.0	1.9	SLC,HSP	White	MC	UCT Pol
46	17 Aug 84	1.1	1.0	SLC,HSP	White	MC	UCT Pol
47	18 Aug 84	2.0	1.0	LP,HSP	White	MC	UCT Pol
48	20 Aug 84	0.5	1.0	CP,HSP	White	MC	UCT Pol

(Frecker and Serkowski 1976) and the U.C.T. Polarimeter (Chapter 2). The St. Andrews Photometer and Radcliffe People's Photometer (Glass, 1982) were used for the multicolour photometry. Altogether there are 48 runs covering approximately 75 orbits. On one or two occasions simultaneous multicolour photometry and white light polarimetry were obtained. The type of observation is denoted by the abbreviations CP for circular polarimetry, LP for linear polarimetry, Phot for multicolour photometry, SLC for simultaneous linear and circular polarimetry and HSP for high speed photometry. The pass bands are denoted by white (3500Å - 9200Å), red (5500Å - 9200Å) blue (3500Å - 5500Å) or by U,B,V,R_C,I_C where standard passbands were used.

4.2.1 The Ephemeris

We follow the convention of Mason *et al.* (1983) where phase zero is taken as the centre of a narrow dip at the minimum of the light curve. The dip is not often present in our data but it is more or less centrally placed in the minimum so the centres of the minima are also at phase zero. At this time there is a minimum in the circular polarisation data (Bailey *et al.* 1983 and see later). Forty seven minima available from our data listed in Table 4.2 and three times of minima published by Bailey *et al.* (1983) were used for linear regression of 50 points, yielding the following ephemeris:

$$T_{min} = \text{HJD } 2445048.9423476 \pm 45 + N \times 0.070497235 \pm 56$$

An O-C diagram is presented in figure 4.1. It can be seen that there are groups of points lying either above or below

Table 4.2

CYCLE NO	HJD	O-C(DAYS)	O-C(MIN)	O-C(PHASE)
0	5048.94283	.00048	.695	.007
395	5076.78585	-.00291	-4.184	-.041
396	5076.85807	-.00118	-1.703	-.017
423	5078.76160	-.00108	-1.553	-.015
439	5079.88941	-.00122	-1.763	-.017
809	5105.97390	-.00071	-1.024	-.010
810	5106.04520	.00009	.132	.001
811	5106.11330	-.00231	-3.320	-.033
1637	5164.34513	-.00119	-1.716	-.017
1694	5168.36361	-.00105	-1.518	-.015
1707	5169.28146	.00033	.477	.005
1793	5175.34461	.00072	1.036	.010
1977	5188.31413	-.00125	-1.803	-.018
4562	5370.55128	.00054	.784	.008
5427	5431.53088	.00004	.052	.001
5428	5431.60244	.00110	1.582	.016
5469	5434.49071	-.00102	-1.466	-.014
5470	5434.56385	.00162	2.340	.023
5483	5435.47819	-.00050	-.719	-.007
5484	5435.54967	.00048	.696	.007
5485	5435.62004	.00036	.513	.005
5497	5436.46548	-.00017	-.246	-.002
5498	5436.53604	-.00011	-.155	-.002
5499	5436.60768	.00103	1.490	.015
5511	5437.45383	.00122	1.754	.017
5512	5437.52465	.00154	2.219	.022
5513	5437.59416	.00055	.797	.008
5514	5437.66394	-.00016	-.236	-.002
5597	5443.51701	.00164	2.355	.023
6856	5532.27456	.00317	4.560	.045
6857	5532.34356	.00167	2.404	.024
6871	5533.33284	.00399	5.742	.057
6857	5532.34364	.00175	2.519	.025
6870	5533.26134	.00299	4.299	.042
6871	5533.33119	.00234	3.366	.033
10874	5815.52791	-.00138	-1.981	-.020
10874	5815.52993	.00064	.928	.009
10929	5819.40526	-.00137	-1.978	-.019
10930	5819.47751	.00038	.546	.005
10931	5819.54925	.00162	2.336	.023
10944	5820.46271	-.00138	-1.990	-.020
11370	5850.49421	-.00170	-2.454	-.024
11381	5851.27004	-.00134	-1.935	-.019
11382	5851.34095	-.00093	-1.341	-.013
11383	5851.41028	-.00210	-3.022	-.030
11423	5854.23000	-.00227	-3.266	-.032
11424	5854.29977	-.00300	-4.313	-.042
11778	5879.25809	-.00070	-1.003	-.010
11779	5879.32909	-.00019	-.279	-.003
12502	5930.29972	.00094	1.347	.013

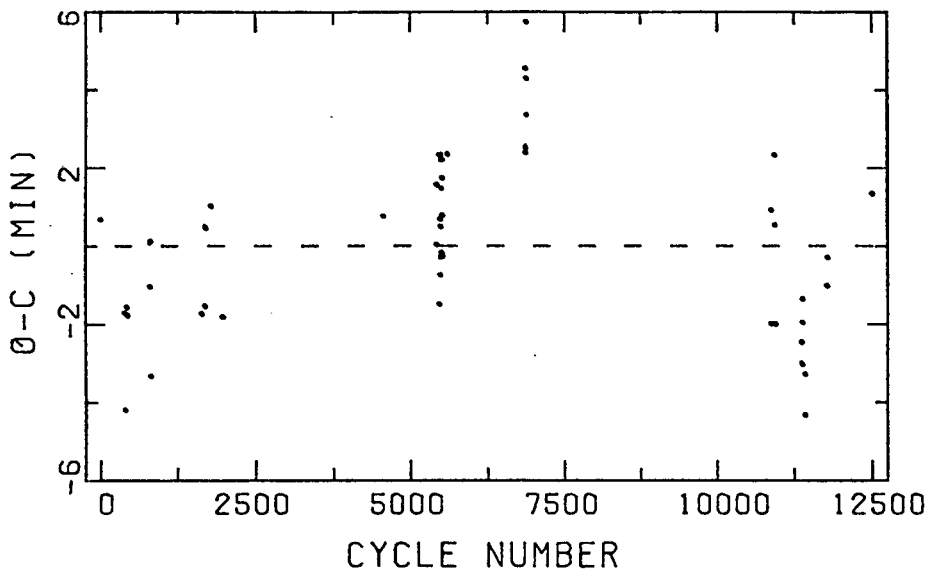

Figure 4.1 Residuals (O-C) in minutes for 50 times of minima plotted against cycle number

the best fit line. Minima from runs made in July 1973 (cycle numbers 6856 to 6871) were approximately 3.8 minutes late - a 7σ deviation from the mean. These minima were determined from observations made by different observers. Minima determined during May/June 1984 were an average of 2.7 minutes early (6σ). While it is true that a parabolic fit would reduce the residuals it is not clear if this is the correct approach (Pringle 1975). The variations appear not to conform to any trend but rather appear erratic.

4.2.2 The Light Curve - Photometry

Figure 4.2, 4.3, and 4.4 show examples of the intensity and polarisation data for 1982, 83 and 84. The intensity is strongly modulated at the orbital period. There is a deep U-shaped minimum defining phase zero which occurs at roughly the same time in all bands followed by an increase in the intensity and flickering activity. The shape of the maximum is either double-humped (figure 4.3) or a rounded sawtooth (figure 4.4). The shape of the modulation is similar in all 5 passbands but the V and R_C bands are modulated most strongly. Figure 5 shows the wavelength dependence of the maxima and minima of the light curves for runs 12, 25, 30 and 37, and the low state during March 1983 reported by Maraschi *et al.* (1984) when there was little or no modulation present over an orbit (their Table 4). As the system was in a high state on 16 February 1983 (the light curve published in figure 4A of Maraschi *et al.* (1984) from spectroscopic observations is in agreement with our run 16 taken 10 days earlier) and again on 18 April 83 (run 25), the low state lasted less than 2 months.

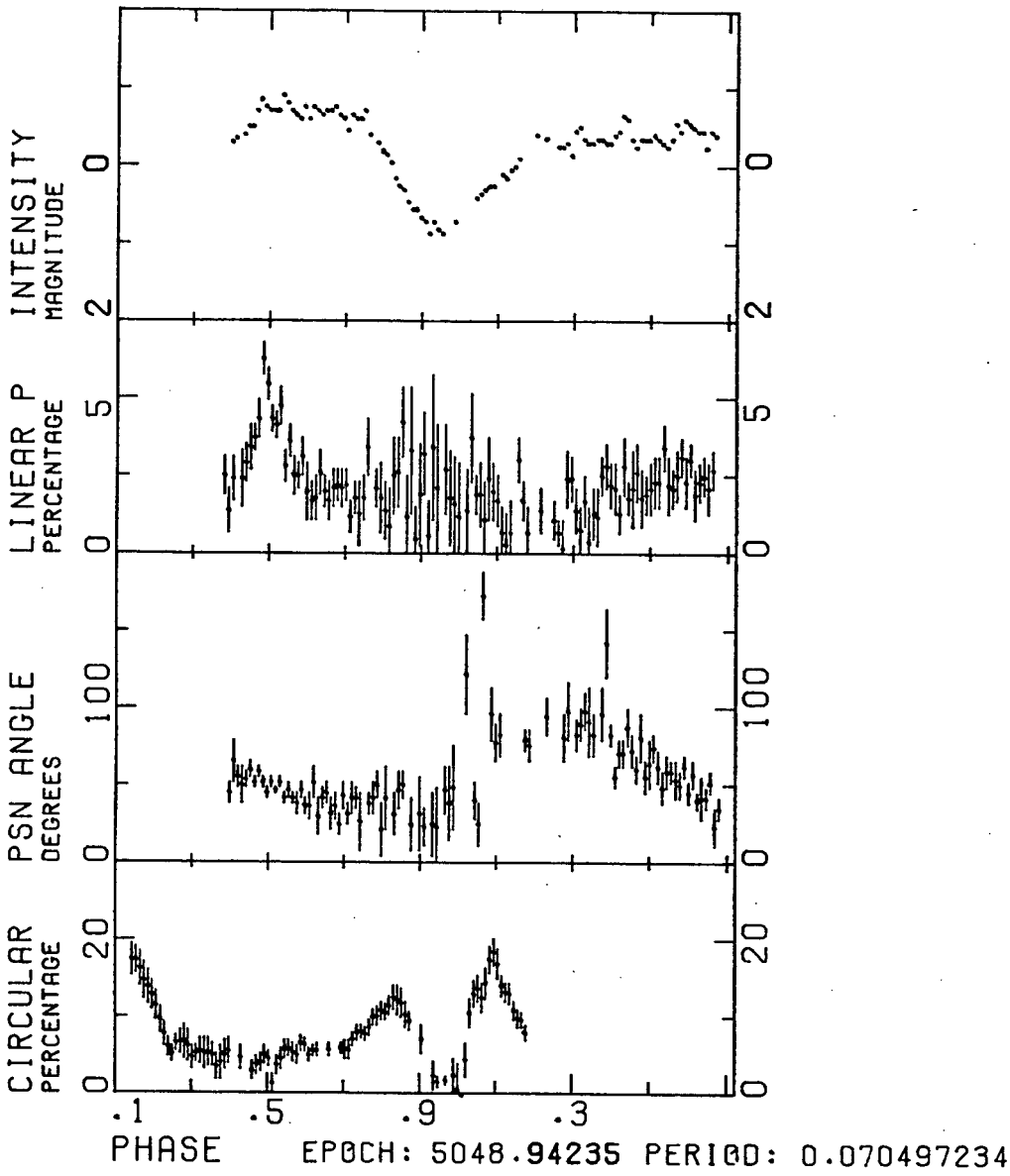

Figure 4.2 1982 - An example of red band data. The linear polarisations and intensities were taken on 18 July and the circular polarisations on 20 March (Runs 2 and 9).

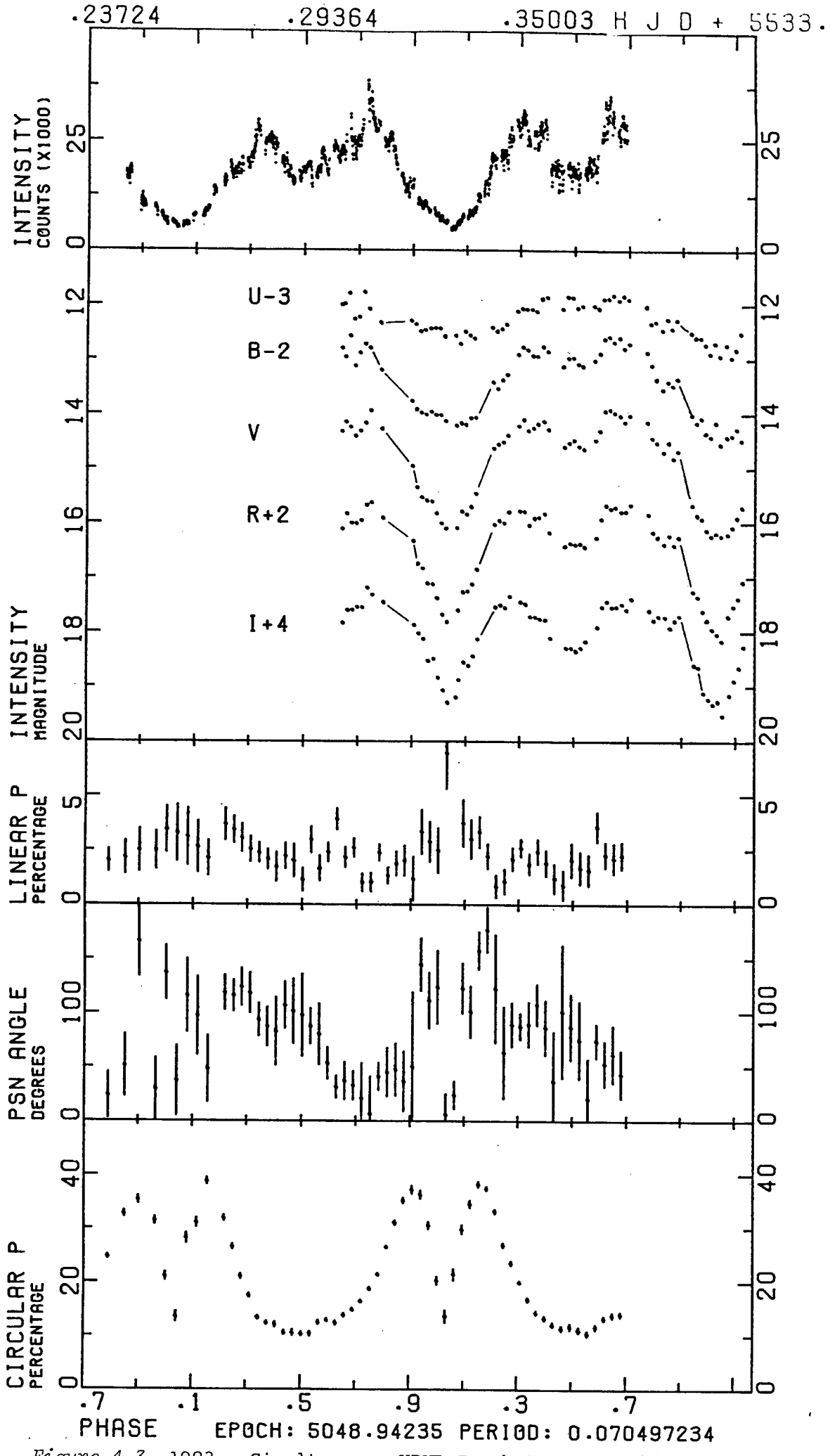

Figure 4.3 1983 - Simultaneous UBVR$_C$I$_C$ photometry, white light high speed photometry, and linear and circular polarimetry on 17th July (Runs 30 and 31). Offsets of -3, -2, 2 and 4 magnitudes have been added to the U,B,R$_C$, and I$_C$ intensities respectively.

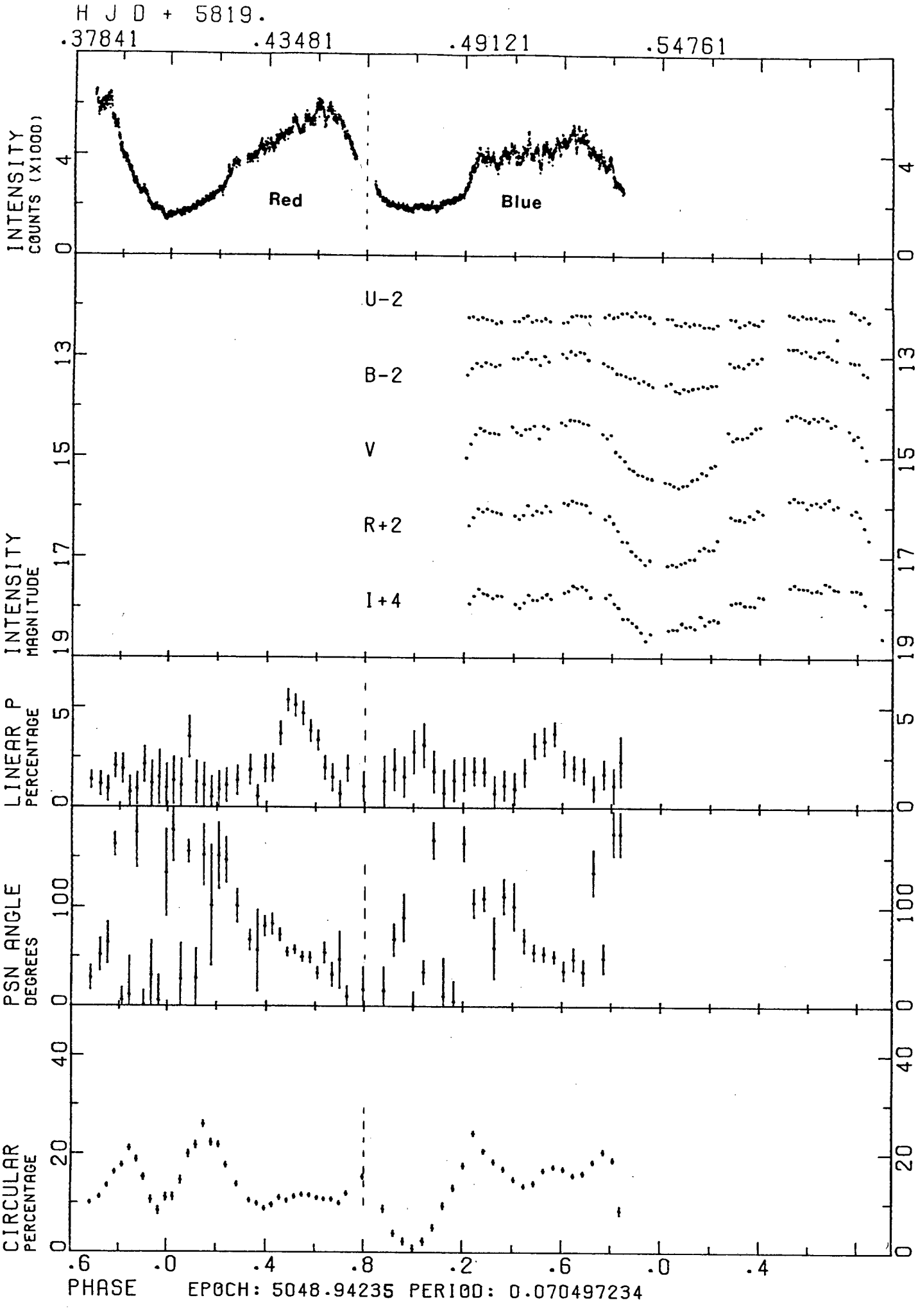

Figure 4.4 1984 - Simultaneous $UBVR_CI_C$ photometry and one orbit of red and one of blue high speed photometry and polarimetry on 28 April (Runs 37 and 38). Offsets of -2, -2, 2, and 4 magnitudes have been added to the U,B,R_C, and I_C intensities respectively.

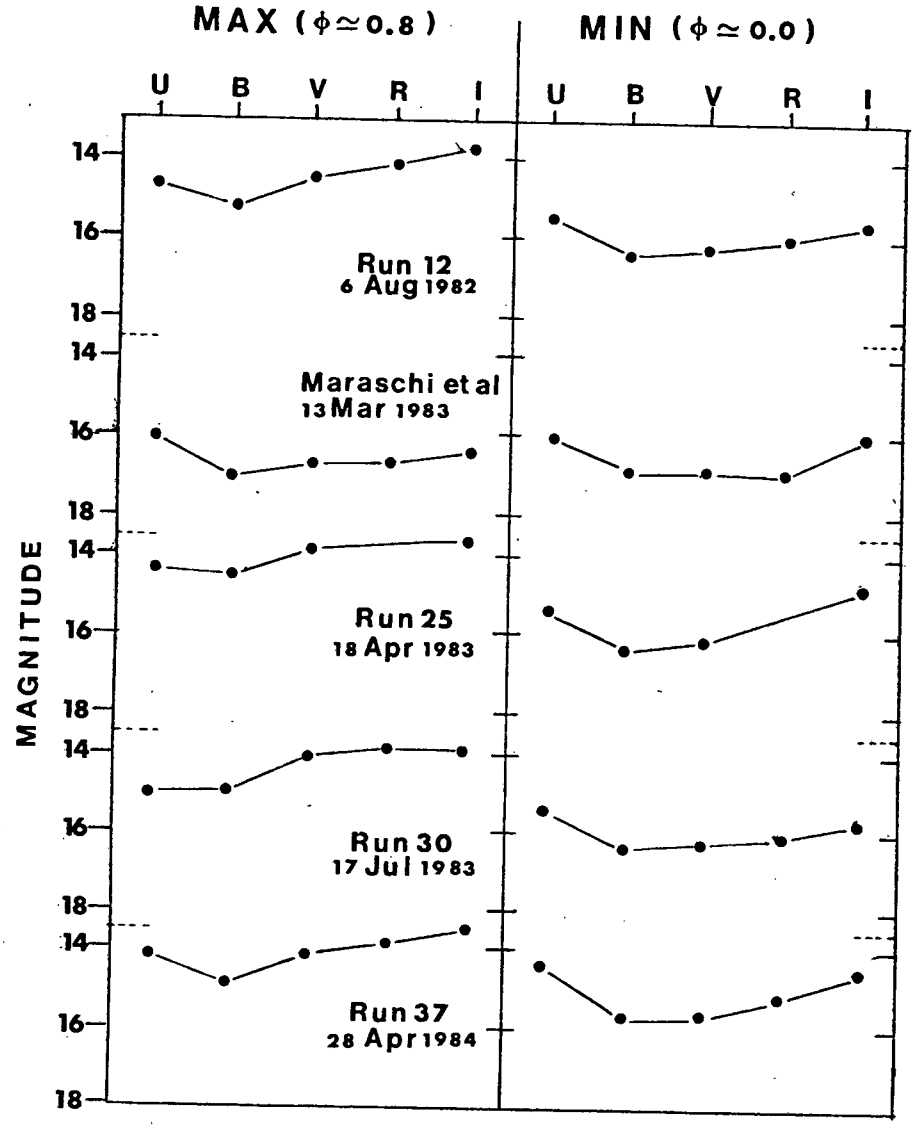

Figure 4.5 The wavelength dependence of the light curve at ϕ=0.8 and ϕ=0.0 for runs 12,25,30,37 and the minimum reported by Maraschi *et al.* (1984).

From the U band observations of Mason *et al.* (1983) and the V band observations of Bailey *et al.* (1983) it can be ascertained that the system was in high states at those times, similar to runs 12, 25 and 37 (figures 4.4 and 4.5). The deep U band minimum observed by Mason *et al.* (1983) is visible in only the first of our U band photometry (run 12, 6 August 1982) and since then seems to have disappeared, although the system has been at a comparable brightness.

4.2.3 The Light Curve - Polarimetry

The general shape of the orbital modulation of the circular polarisation is that reported by Tapia (1982) and Bailey *et al.* (1983), viz. approximately sinusoidal with a deep minimum cut into the peak of the circular polarisation at phase zero (figures 4.2, 4.3, and 4.4). The maximum circular polarisation varies from less than 20 percent in March 1982 (figure 4.2) to 40 percent in July 1983 (figure 4.3). The width and depth of the minimum at phase zero also varies considerably, with both wavelength and time. The dependence upon wavelength for high state data is shown in figure 4.6 and the variation over time for white light or V band data is shown in figure 4.7. The shape of the circular polarisation curve is very similar in the blue and the red except for the wider minimum at ϕ=0 (figure 4.4) in the blue. It is also similar to the curve published for PG1550+191 by Liebert *et al.* (1982) (where the circular polarisation is always negative). Peak values of polarisation drop sharply to the UV (run 11) and to the IR (Bailey *et al.* 1983).

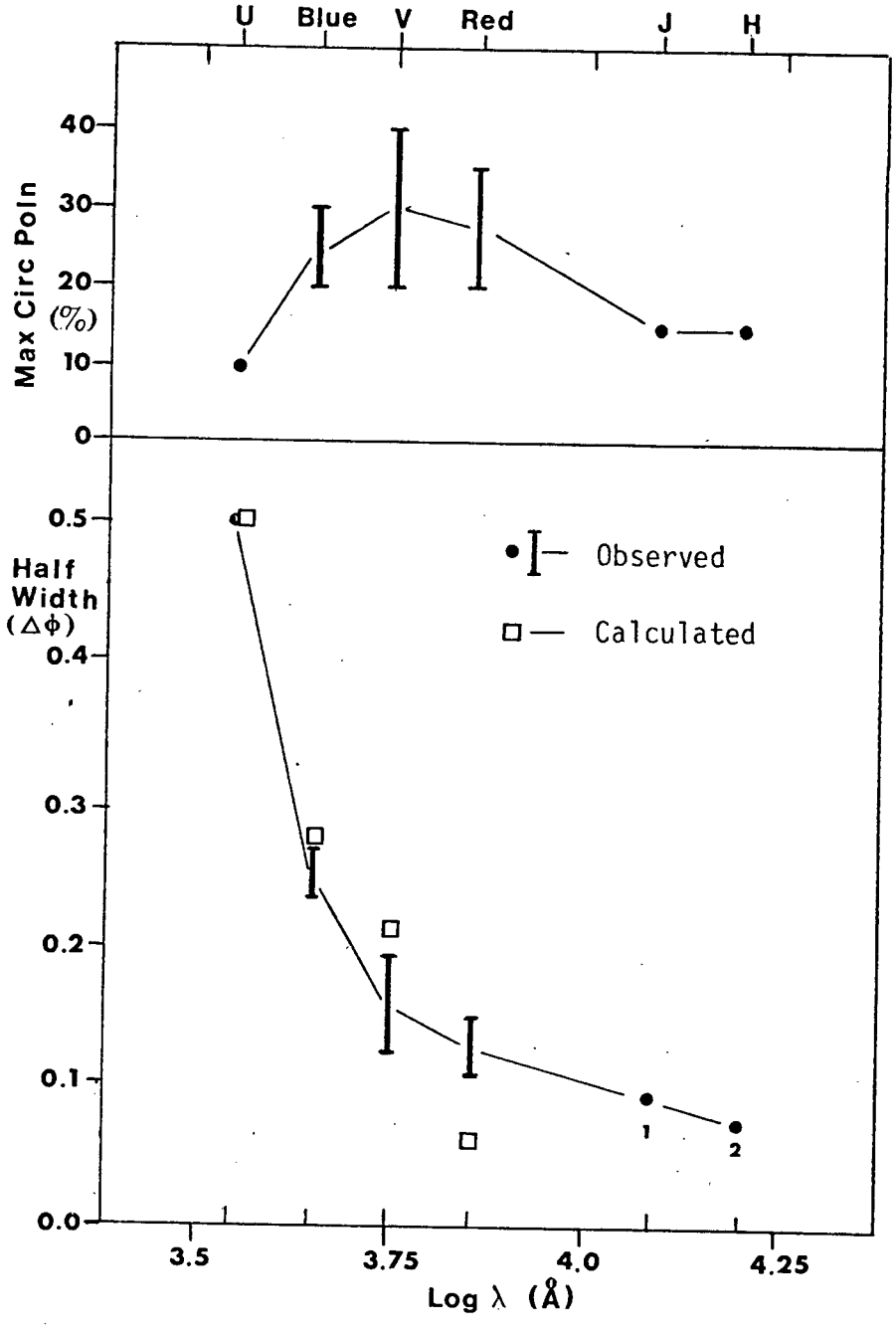

Figure 4.6 The dependence of the maximum circular polarisation and width of the minimum at ϕ=0 upon wavelength for high state data. Points 1 and 2 are from Bailey *et al.* (1983).

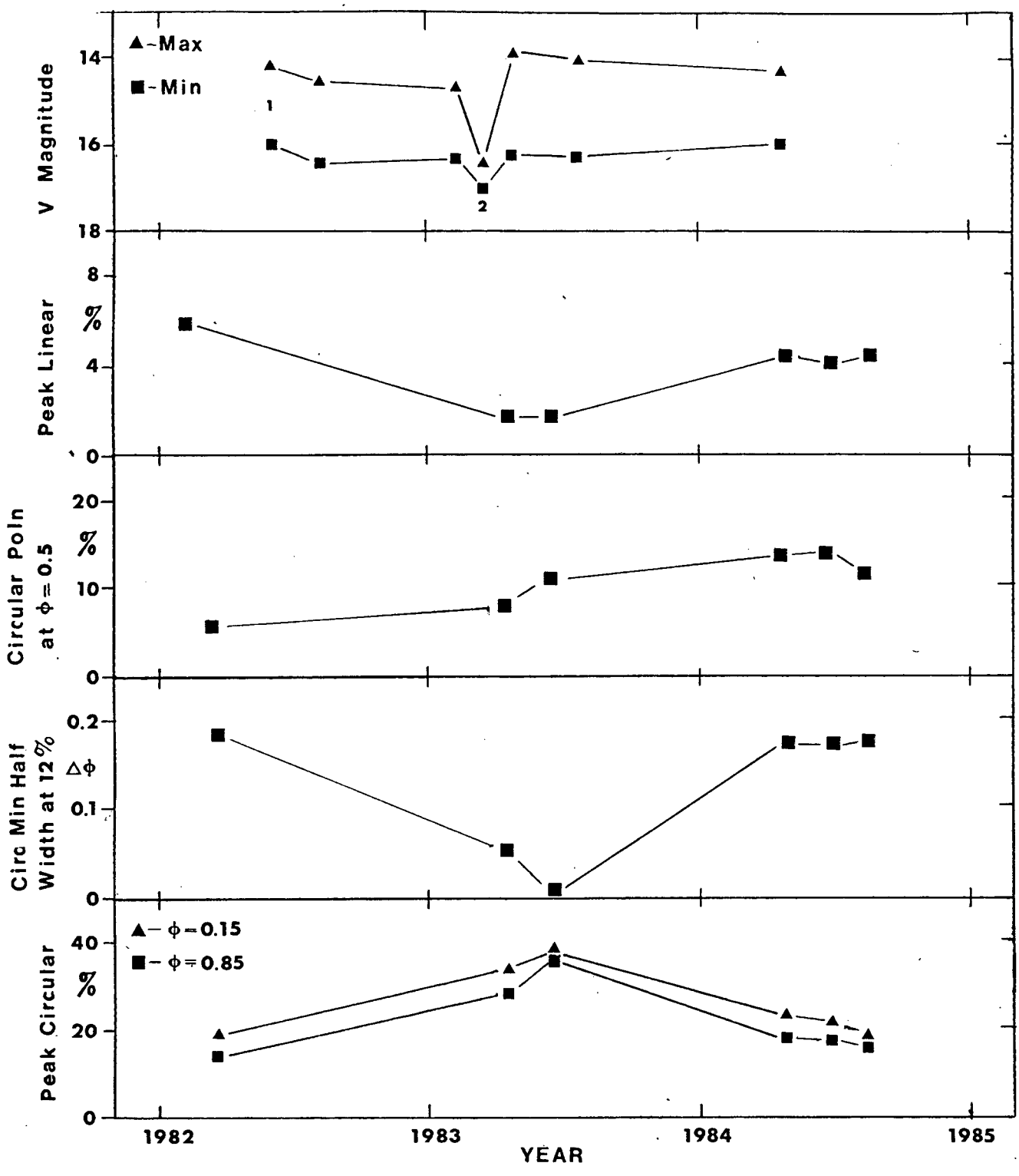

Figure 4.7 The variation of the maximum values attained by the circular polarisation, the width of the circular polarisation minimum at ϕ=0, the maximum linear polarisation and the V band magnitudes as a function of time. Points 1 and 2 are from Bailey *et al.* (1983) and Maraschi *et al.* (1984) respectively.

Early measurements of linear polarisation have led to some incorrect conclusions about the geometry of the system. Initial reports by Tapia (1982) stated that a linear polarisation peak existed at phase zero (i.e. during the minimum of the light curve and of the circular polarisation). Observations by Visvanathan and Tuohy (1983) tended to confirm this description, but it is clear from our extensive observations that the effects of increased photon statistic errors during the minimum of the light curve have been underestimated. As it is the square root of the sum of the squares of the Stokes parameters Q and U, the linear polarisation will be increased by an increase in photon errors. We have averaged many orbits of the data and found the linear polarisation at phase zero to be a minimum (see figures 4.8 and 4.9) and less than 1 percent. However, fairly strong linear polarisation peaks are observed at $\phi \simeq 0.55$ (examples are shown in figures 4.2 and 4.4) at which phase the the photon errors are considerably reduced. These peaks reach 6 percent and are roughly the same height in the red and the blue. Their visibility is variable on a time scale of months and is strongly anti-correlated with the peak values of the circular polarisation (figure 4.7). During 1983 the linear peak was invisible in individual runs but on averaging 10 orbits (runs 20,21,22, figure 4.8) a double peak can be seen with maxima of approximately 1.8 ± 0.3 percent at $\phi = 0.3$ and 0.6. The occurrence of the double peaked maxima appears to be linked with the double peaked structure of the light curve. When the light curve is sawtooth-shaped the linear polarisation maximum at $\phi = 0.3$ is diminished (although not entirely absent)

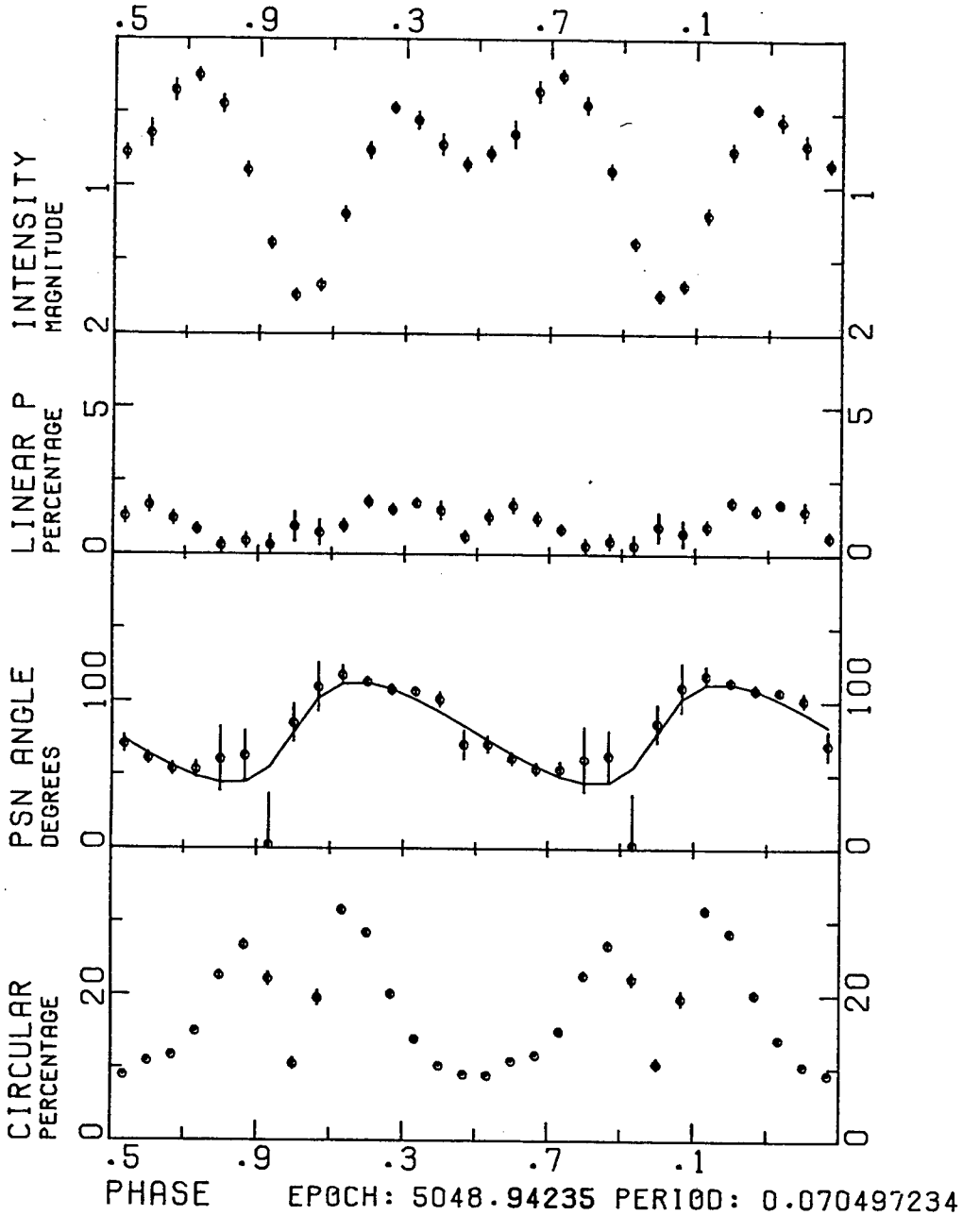

Figure 4.8 The average intensity and polarisation curves for runs 20,21,22 with the best fit for i,β superimposed on the position angles.

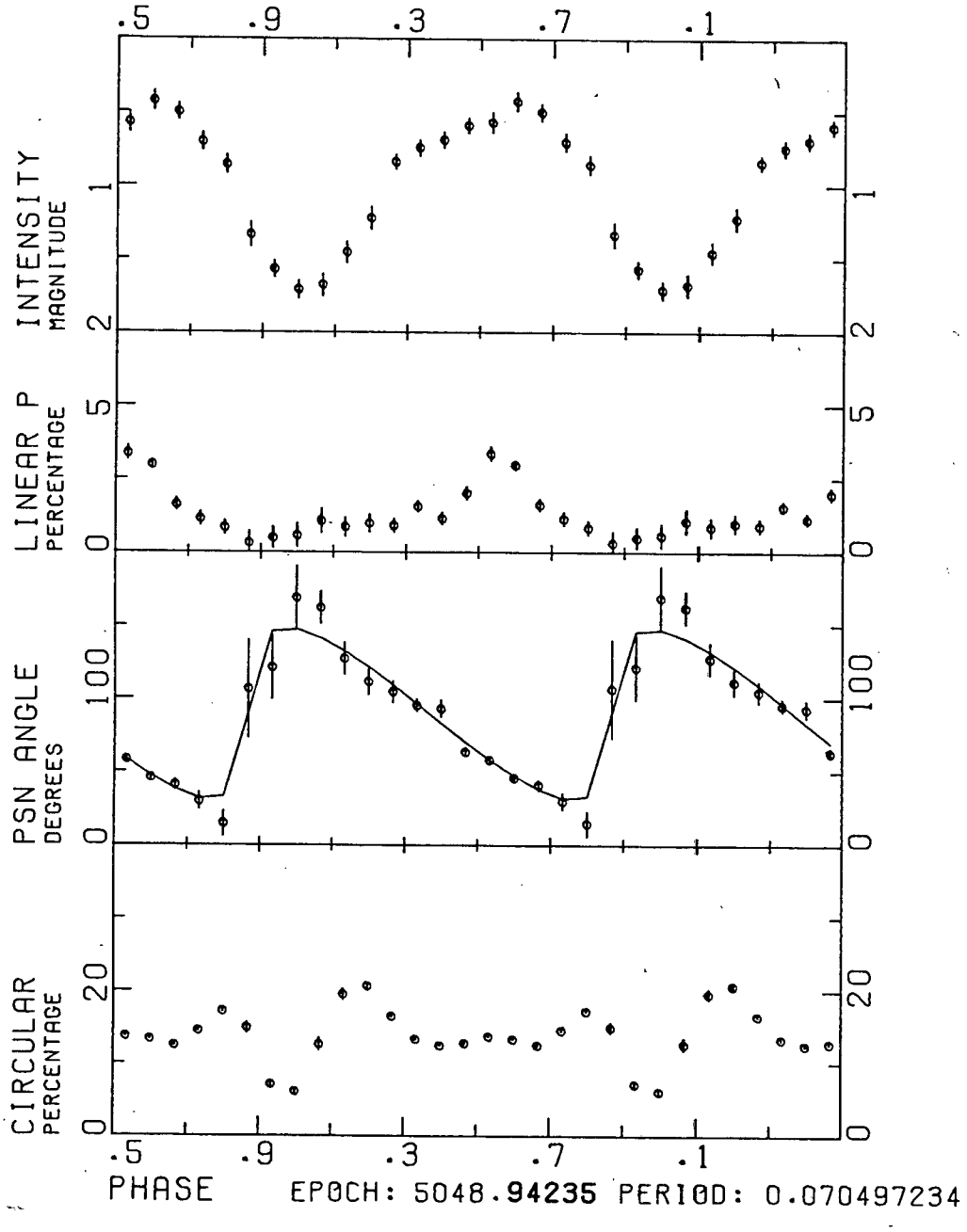

Figure 4.9 The average light curve and polarisation for runs 35,38,39 with the best fit for i,β superimposed on the position angles.

and that at ϕ=0.6 enhanced to the 6 percent values reported above (figure 4.9).

While superposition of many orbits of linear polarisation data reduces the photon errors and allows the detection of very low levels of polarisation in the average behaviour, this procedure does not rule out the existence of occasional peaks in the linear polarisation at ϕ=0.

The position angle of the linear polarisation can be seen to decrease during the bright part of the orbit in individual observations (figures 4.2, 4.3 and 4.4) but its behaviour during the faint part is only evident when a number of runs are averaged. A wave-shaped variation is then apparent with a steep rise during the minimum and a slow decline during the maximum (figures 4.8, 4.9).

4.3 The Orientation of the System

4.3.1 General Considerations

From the averaged intensity and polarisation data (figures 4.8, 4.9) it is clear that, near phase zero, we are closest to looking down on top of the accretion column resulting in very large values of circular polarisation, while at ϕ=0.5 the accretion column is closest to perpendicular to the line of sight. The circular polarisation never changes sign, so the accretion column is always visible on one hemisphere of the white dwarf primary. The linear polarisation peak at $\phi \simeq 0.5$ indicates that the accretion column is near the limb of the primary at this phase. Thus, if we adopt the simplest model of radial accretion over a small fraction of the surface

of the primary, the centre of which is at angle β to the rotation axis (referred to below as the magnetic colatitude), and if we observe the system at an inclination of i (Brainerd and Lamb 1983), then $i + \beta \leq 90^{\circ}$. If we assume that at phase zero we are looking down approximately on top of the accretion column then $i \simeq \beta$.

Corroborative evidence for this view is provided by the light curve, which shows that the system is brighter when the accretion column is seen perpendicular to the line of sight, by the position angle curve, which has its most rapid change when the column passes closest to the line of sight, and by the sharp minimum in the circular polarisation caused by self absorption in the column (Barrett and Chanmugam 1984) or the presence of an unpolarised background (Wickramasinghe and Meggitt 1984). The most model-independent data available for determining the orientation of the column are the position angles. These were therefore analysed in more detail.

4.3.2 Evidence for Changes in the Position of the Accretion Column

The position angles, averaged in phase bins, show variations from week to week which, with the variations in linear and circular polarisation already discussed, suggest that the accretion column moves in latitude. Least squares fits of the position angles to a model similar to that of Brainerd and Lamb (1983) were used to determine i and β for various groups of runs. Initially the data were binned in phase and the standard deviation of the mean found for each phase bin. After

weighting each bin by the inverse of the standard deviation, the square of the residuals (summing over phase) was calculated for each (i,β) pair in the grid. The (i,β) pair corresponding to the lowest residual defined the best fit.

Variations in β were evident from this analysis but problems arose in assigning confidence levels to the error contours in the (i,β) plane. In order to avoid any assumptions about the distribution of the position angles and estimated errors, a Bootstrap technique (Efron 1979) was used to calculate the error contours. This selects random sets of linear polarisations from the observed data. The above procedure was then followed, except that the best fit was found by means of a Newton-Raphson technique. The points plotted in figure 4.10 represent the best fits for the two groups of averaged data shown in figures 4.8 and 4.9. By joining the points around the perimeter of the set of solutions an overlap of approximately 10 in 600 exists - i.e. the non-parametric bootstrap confidence level at which the two groups of observations are different is approximately 98%. The parametric 99% confidence levels, assuming normally distributed errors in the real data, are also shown and are in fairly good agreement with the bootstrap data. The $i + \beta = 90^{\circ}$ line and $i + \beta = 40^{\circ}$ lines in figure 4.10 indicate the limits $i + \beta \lesssim 90^{\circ}$ deduced from the circular polarisation and $i + \beta \gtrsim 40^{\circ}$ deduced from the existence of some linear polarisation (see Wickramasinghe and Meggitt, 1984). If we take a value of the inclination midway between these two lines and centred in the distribution of calculated points then

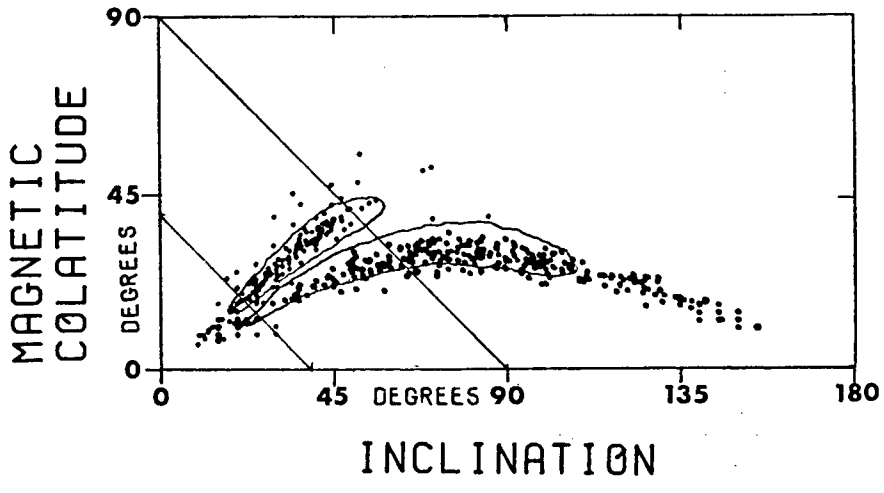

Figure 4.10 Loci of the bootstrap-generated best fits for the two sets of run shown in figures 9 and 10 with 99% confidence level contours derived with the assumption that the errors are distributed normally. The $i+\beta=90^{o}$ and $i+\beta=40^{o}$ lines are also drawn.

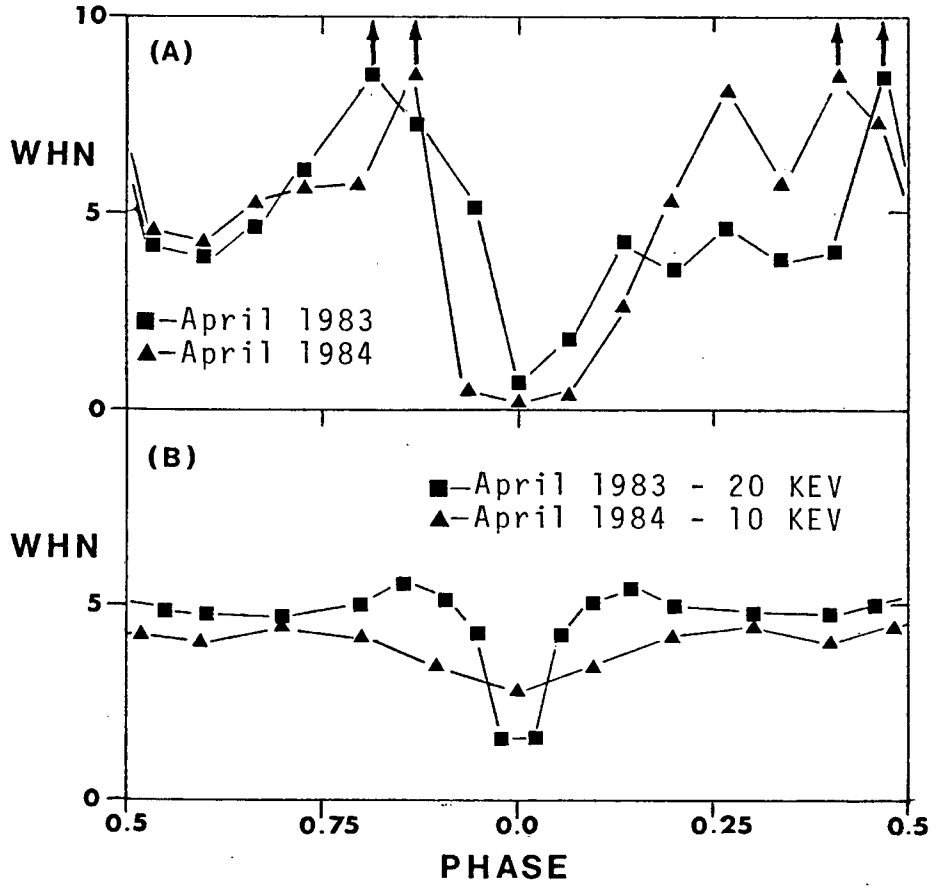

Figure 4.11 The flux weighted harmonic number (WHN) for the April 1983 and 1984 observations (A) and from the shock front calculations of MW (B) using the values of i and β appropriate in each case.

$$i \simeq 38^{\circ} \pm 10^{\circ}$$

and

$$\beta(20,21,22) = 20^{\circ} \qquad \beta(35,38,39) = 32^{\circ}$$

for the two groups of observations, where ( ) refer to the run numbers of Table 4.1.

As it is fairly well constrained in each set, it is convenient to express β in terms of i:-

$$\beta(20,21,22) = 4^{\circ} + 0.42i$$

$$\beta(35,38,39) = 0.84i$$

for the region $i = 45^{\circ} \pm 20^{\circ}$. Other less well constrained results are:

$\beta(29,31) \simeq 3^{\circ} + 1.1i$ $\quad (i = 38^{\circ} \Rightarrow \beta \simeq 45^{\circ})$

$\beta(40,41,44) \simeq 7^{\circ} + 0.26i$ $\quad (i = 38^{\circ} \Rightarrow \beta \simeq 17^{\circ})$

$\beta(45,46,47) \simeq 7^{\circ} + 0.28i$ $\quad (i = 38^{\circ} \Rightarrow \beta \simeq 18^{\circ})$

The mean β for the above 5 sets is $\sim 27^{\circ}$, if i is 38°.

It can therefore be stated that, at a very high confidence level, there are variations in the colatitude of the accretion column of the order of 10° to 15°. The variations are not, however, confined to shifts in latitude. The differences in arrival time of the minima seen in the O-C diagram (figure 4.1) imply variations in the longitude of the accretion column of the order of 10° to 15° (3 minutes of time). At the latitude of the accretion column, this corresponds to roughly half of the distance on the white dwarf surface compared with the latitude shifts. There is no correlation between the deviations in latitude and longitude.

4.3.3 Consequences of the Modelling

The calculated curves for the appropriate (i,β) values, (38,20) and (38,32) are shown superimposed on the position angle data in figures 4.8 and 4.9. The closeness of the fits indicates that the simple model used in the above analysis (Brainerd and Lamb 1983) is consistent with the observations. It can be seen, however (figure 4.10), that the contours of constant error are crescent shaped regions in the i,β plane (at least for this system) and constrain β more closely than i. It is also found above that the parametric 99% confidence levels assuming a normal distribution of the position angles and their errors is for the most part acceptable although the bootstrap calculation is superior.

At phase zero the angle between the accretion column and the line of sight is less than 20^{o}. This supports the proposal by Nousek and Pravdo (1983) that the P Cygni profiles seen in IUE spectra of E1405-451 are caused by a magnetically confined wind directed toward the earth.

4.4 Comparison with Cyclotron Emission Calculations

The i and β deduced from the phase-averaged data determines the angle at which the accretion column is viewed. Then a comparison can be made with theoretical calculations of the linear and circular polarisation. Two competing models exist. That of Barrett and Chanmugam (1984) uses low temperature cyclotron emission regions (0.2 keV to 1 keV) but that of Wickramasinghe and Meggitt (1984) applies to higher temperature emission regions (5-40 keV). While both groups of authors have calculated

the cyclotron emission from a homogeneous slab with different temperatures and size parameters ($\Lambda = \omega_p^2 L/\omega_c c$ where ω_p is the plasma frequency, ω_c the cyclotron frequency and L the path length through the source), Wickramasinghe and Meggitt (1984 hereafter WM) have also presented calculations for cyclotron emission from the preheated region above the shock front, taking the temperature structure into account.

4.4.1 The Ratio of Linear to Circular Polarisation

Calculations by Barrett and Chanmugam (1984 - hereafter BC) and Meggitt and Wickramasinghe (1982) show that the ratio of linear to circular polarisation (Q/V) is independent of optical depth:

$$\frac{Q}{V} = \frac{\sin^2\alpha}{2(\omega/\omega_c)\cos\alpha} .$$

Here α is the angle between the line of sight and the accretion column and $\omega_c = eB/mc$ is the cyclotron frequency, so (ω/ω_c) is the harmonic number. This relationship applies, however, only for the emission from a single harmonic in a constant temperature homogeneous slab. When more than one harmonic is emitted, the final linear and circular polarisations are flux weighted means of all the harmonies present in the passband, and ω/ω_c depends on α and therefore on phase.

It has been found in VV Puppis (see Chapter 5) that the weighted harmonic number (WHN) varies between 3.6 and 7.8 during the bright phase of the orbit. For this range of harmonic numbers to be in the white light bandpass the magnetic field must be between $\sim$30MG (otherwise the lower harmonics

would be at longer wavelengths than those visible in the bandpass) and ∿38MG (otherwise the higher harmonics would be at shorter wavelengths than those visible in the bandpass). The polar field in VV Puppis is known to be ∿32MG (Wickramasinghe and Meggitt 1982). It is therefore evident that the magnetic field strength can be roughly estimated (at least to within a factor of 2) from the WHN and filter bandpasses. As the field strength is not known for E1405-451 this method was used to provide an estimate.

The weighted harmonic number was calculated for the two sets of white light data in figures 4.8 and 4.9 with α given by values of i and β determined for each set and is shown in figure 4.11A. Over most of the orbit the WHN lies between 3 and 7, except at phase 0, where it drops to zero. By analogy with the WHN for VV Puppis this indicates that the field strength of E1405-451 is probably 30-35MG. A field of 20MG is almost certainly too low as the WHN would lie in the range 6 to 15.

There is evidence, discussed more fully below, that a shock front model for the cyclotron emitting region provides a much superior fit to the data than the constant temperature models. We are unsure of the validity of the $Q/V - \omega/\omega_c$ relation in the shock front models. We therefore show in figure 4.11B the WHN plotted against phase for T_s = 20 keV and geometry deduced for the April 1983 runs, and T_s = 10 keV for the April 1984 geometry from the shock front calculations of WM. These authors assumed a magnetic field of 30MG. The agreement in WHN with phase is extremely encouraging, and supports our

estimates of a field strength of ∿30MG in the cyclotron emitting region.

4.4.2 Tests of the Cyclotron Calculations

If it is accepted that the magnetic field is approximately 30MG, it is possible to calculate the cyclotron harmonics in each filter bandpass. As i and β for the April 1983 and April 1984 runs are well determined, it is a simple task to calculate the predicted fluxes and linear and circular polarisations over an orbit using the models of BC and WM. The calculated polarisations were weighted by the fluxes emitted at each harmonic. It was necessary to assume an additional unpolarised flux broken into two components - one constant and the other varying in phase with the polarised flux.

There are a number of degrees of freedom in the above calculations. These are:

(i) The choice of emission models, i.e. whether constant temperature or shock front, and what values of temperature and Λ.

(ii) The harmonics to be included in each filter bandpass (dependent on the adopted bandpasses and the magnetic field strength) and how to weight them.

(iii) The orientation of the system, i.e what effect do uncertainties in i and β have on the calculated curves.

(iv) The two background components. These are ascribed to the fluxes from each of the stellar photospheres, the emission from the spectral line emitting regions and

the Raleigh-Jeans tail of the blackbody flux from the accretion shock (Bailey *et al.*, 1983, WM).

No attempt was made to explore the entire parameter space, partly because of the lack of a complete grid of models. It was found that the shock front models of WM are superior to both their own constant temperature models and those of BC. Figure 4.12 shows the April 1983 folded data with the best fits to the following models (with $i = 37^{\circ}$ and $\beta = 20^{\circ}$):

(i) Shock front T_s = 20 keV (WM)

(ii) Constant temperature T = 40 keV
$\Lambda = 10^4$ (WM)

(iii) Constant temperature T = 20 keV
$\Lambda = 10^5$ (WM)

(iv) Constant temperature T = 10 keV
$\Lambda = 10^6$ (WM)

(v) Constant temperature T = 1 keV
$\Lambda = 10^8$ (BC)

(vi) Constant temperature T = 0.2 keV
$\Lambda = 10^8$ (BC)

Harmonics 3 to 7 were used for the white light bandpass.

It is clear that the 20 keV shock front model is by far superior to the constant temperature models and provides an exceedingly close fit to the observations in spite of the coarseness of the grid provided by WM. The fit was found to be best for the above values of i and β along the $\beta = 4^{\circ} + 0.42i$ relation determined earlier. Fits using $i = 34^{\circ}$ and 42° with the appropriate β were much poorer. A constant background of 3% of the peak flux plus a varying background of 50% of the polarised flux at each harmonic at a particular phase, were

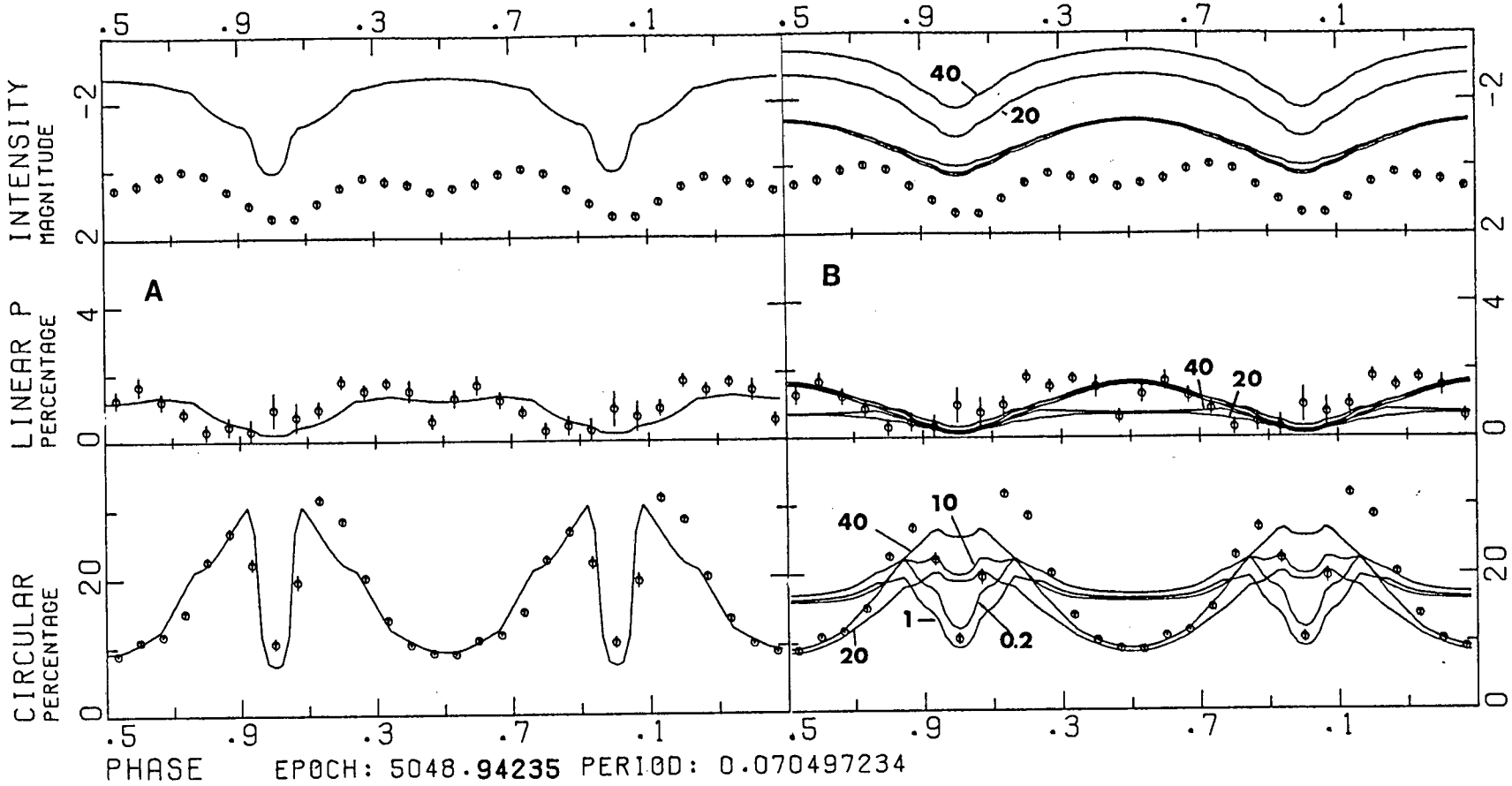

Figure 4.12 Phase-folded April 1983 data with the best fits for one shock front (A) and five constant temperature (B) models with different temperatures and size parameters (see text).

required. Thus the variable component of the flux was 2/3 polarised. The closeness of the fits in white light to the flux and polarisations is encouraging, and indicates that the cyclotron emission calculations for the shock front models are realistic. They lend support to the assumptions of those models - in particular a flat coin-shaped emission region and a preheated shock precursor where the polarised radiation is principally produced (WM).

The data taken during April 1984 (figures 4.4, 4.9) are not symmetric about phase zero, especially the linear polarisation and flux curves. A poorer fit was therefore expected from the models, which are all symmetric. Figure 4.13 shows the fits for 10 keV and 20 keV shock front models. It can be seen that, despite the asymmetry, the 10 keV calculation provides a good fit to the data. As the field was expected not to have changed the same harmonics as figure 4.12 were used. Again $i \simeq 37^{o}$ with the appropriate β provided the best fit. In order to explain the asymmetry various tilts of the accretion column from the radial direction were included in the calculations for α. Although asymmetries in the height of the circular polarisation maxima and in the linear polarisation could be produced in this way phase shifts in the polarisation curves considerably larger than those observed (from the O-C diagram figure 4.1) are also introduced. In addition, the deduced tilts are in opposite directions for the linear and circular curves. Therefore the asymmetries do not appear to result from non-radial accretion.

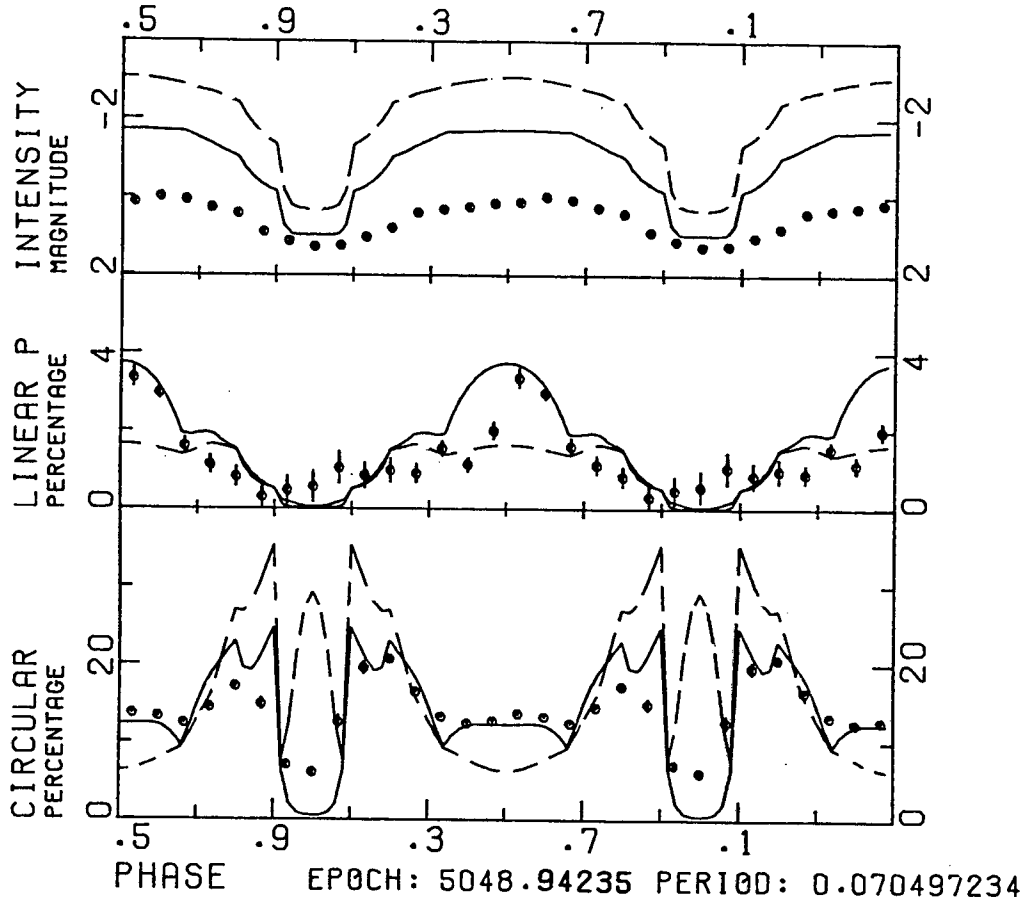

Figure 4.13 Phase-folded April 1984 data with 10 keV (solid line) and 20 keV (dashed line) shock front model fits.

The asymmetries might be explained if the shock front has a temperature that varies with longitude such that the following part has a higher shock temperature than the leading part. Then between ϕ=0 and 0.5 a higher shock temperature would be observed than between ϕ=0.5 and 1.0. The shock front calculations by WM are only for temperatures of 10 keV and 20 keV, but we may understand the asymmetry if we assume that the polarised radiation is produced at a temperature closer to 20 keV for $0<\phi<0.5$ and at a temperature closer to 10 keV for $0.5<\phi<1.0$. The observed linear polarisation peak at ϕ=0.55, and the lower circular polarisation peak at ϕ=0.8 can then be simultaneously produced.

Some structure in the shock front in longitude might occur if one of the poles of the magnetic field does not point directly at the secondary. Evidence that there is a misalignment of some 90° is provided by Maraschi *et al.* (1984) from the phasing of the spectral emission line peaks.

The system was at a comparable brightness during the April 1983 and April 1984 sets of runs, except at phase zero, where the 1983 runs were fainter. It is therefore unlikely that the mass transfer rate was very different in the two cases. Thus the reason that the 20 keV calculations provide a better fit to the April 1983 data, while the 10 keV calculations provide a better fit to the April 1984 data is more likely to be that both the areal structure of the shock front and the viewing angle were different at these two times.

4.4.3 Fits to the Multicolour Data

Figures 4.12 and 4.13 indicate that the shock front calculations of WM fit the white light data satisfactorily. Consequently the calculations were extended to compare with the observations made through filters. A magnetic field strength of 30MG was assumed and only those harmonics present in the various bandpasses were included. Strictly the calculated flux should be convolved with the filter response functions, but the simplified procedure is adequate for present purposes. The calculations show that the circular polarisation in the blue at $\phi \simeq 0.5$ is higher than in the red and the U band circular polarisation is low, as we find in run 11, and that the width of the circular polarisation minimum at $\phi \simeq 0$ is wider in the blue than in the red. The calculated widths are shown plotted as open squares in figure 4.6. It is also found that the U band flux should be modulated least over an orbit, in agreement with our observations. However it is difficult to achieve agreement in detail, principally because the constant background we have used should be wavelength dependent, and the transmission functions of the filters are not taken into account. The former effect will be especially strong in the U band calculations, where the contribution of the unpolarised Balmer continuum is considerable.

4.5 The High Speed Photometry

Intensity data were recorded into 200 millisecond bins in runs 26, 32, 33, 34, 41 and 42. The log power spectrum of

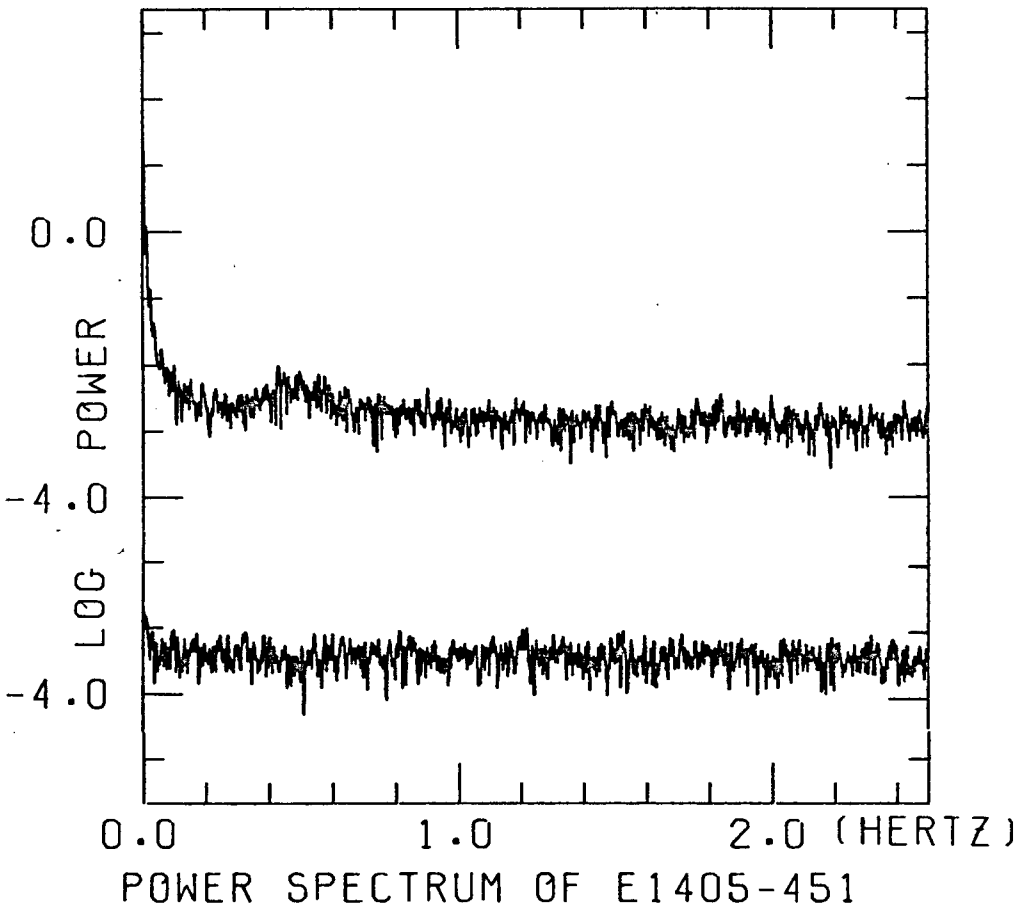

Figure 4.14 Log power spectrum of E1405-451 showing quasiperiodic oscillations at approximately 2 sec, and the power spectrum of a control star for comparison.

run 26 shows enhanced power at approximately 2 sec (figure 4.14), confirming the report of Mason *et al.* (1983) and Middleditch (1982). For comparison, the power spectrum of a run on a slightly brighter, constant star, taken immediately before run 26, is shown below the E1405-451 power spectrum. Both spectra have been smoothed by a 9-point running average.

The remainder of the runs were taken with the intention of investigating the variation with colour and around the orbit, of the excess power at high frequencies. Unfortunately, the observations, made on the 0.75m telescope, are swamped by scintillation noise at the frequencies of interest. The white light data taken during the bright phase of run 42 does show the power enhancement visible in figure 4.14, although the noise level is higher.

4.6 Conclusions

We have accumulated a large amount of data for E1405-451, which has enabled us to provide an improved orbital ephemeris and to present examples of multicolour photometry, high speed photometry and linear and circular polarimetry. The variations of intensity and polarisation with time and their dependence on wavelength at particular phases enabled us to:

(1) Analyse the position angles to find the inclination of the system and the magnetic colatitude, which produced evidence that the colatitude is variable.

(2) Analyse the O-C residuals in the phase zero timings which produce evidence for variations in longitude of the accretion column.

(3) Use model calculations by Wickramasinghe and Meggitt (1984) and Barrett and Chanmugam (1984) to derive an estimate of the magnetic field in the accretion region of ∿30MG.

(4) Compare the various theoretical calculations by WM and BC with the conclusion that the shock front models of WM provide excellent fits to the observations.

(5) Discount non-radial accretion as the cause of the asymmetry in the intensity and polarisation curves. Instead we propose that temperature gradients with longitude in the shock front could cause the observed effects.

(6) Confirm the 1-3 second quasi-periodic oscillations found by Mason *et al.* (1982).

REFERENCES

Bailey, J., Axon, D.J., Hough, J.H., Watts, D.J., Giles, A.B. and Greenhill, J.G., 1983. *Mon. Not. R. astr. Soc., 205*, 1P.

Barrett, P.E., and Chanmugam, G., 1984. *Astrophys. J., 278*, 298.

Brainerd, T.J., and Lamb, D.Q., 1983. Preprint.

Cropper, M.S., 1984. *Mon. Not. R. astr. Soc.*, in press.

Cropper, M.S. and Warner, B., 1984. In preparation.

Efron, B., 1979. *Ann. Stat., 7*, 1.

Frecker, J.E., and Serkowski, K., 1976. *Appl. Optics, 15*, 605.

Glass, I.S., 1982. S.A.A.O. Facilities Manual.

Jensen, K.A., Nousek, J.A. and Nugent, J.J., 1982. *Astrophys. J., 261*, 625.

Liebert, J., Stockman, H.S., Williams, R.E., Tapia, S., Green, R.F., Rautenkranz, D., and Ferguson, D.H., 1982. *Astrophys. J., 256*, 594.

Maraschi, L., Treves, A., Tanzi, E.G., Mouchet, M., Lauberts, A., Motch, C., Bonnet-Bidaud, J.M. and Phillips, M.M., 1984. Preprint.

Mason, K.O., Middleditch, J., Cordova, F.A., Jensen, K.A., Reichert, G., Murdin, P.G., Clark, D. and Bowyer, S., 1983. *Astrophys. J., 264*, 575.

Middleditch, J., 1982. *Astrophys. J., 257*, L71.

Meggitt, S.M.A. and Wickramasinghe, D.T., 1982. *Mon. Not. R. astr. Soc., 198*, 71.

Nousek, J.A., and Pravdo, S.H., 1983. *Astrophys. J., 266*, L39.

Pringle, J.E., 1975. *Mon. Not. R. astr. Soc., 170,* 633.

Tapia, S., 1982. *I.A.U. Circ.* No. 3685.

Visvanathan, N., and Tuohy, I., 1983. *Astrophys. J., 275,* 709.

Wickramasinghe, D.T. and Meggitt, S.M.A., 1982, *Mon. Not. R. astr. Soc., 198,* 975.

Wickramasinghe, D.T. and Meggitt, S.M.A., 1984. Preprint.

CHAPTER 5

OBSERVATIONS OF OTHER AM HER STARS

5.1 Introduction

There are ten AM Her stars known. Of these, two (AM Her itself and AN UMa) are too far north to be visible from Sutherland and two have been discussed in some detail in chapters 3 and 4. The remaining 6 (in order of increasing Right Ascension) are:-

1) HO139-68
2) VV Puppis
3) CW 1103+254
4) E1114+182
5) PG1550+191
6) E2003+225

No observations of CW1103+254 were made because its time of visibility coincides with that of VV Puppis and E1405-451 and its declination is inconveniently far north. E1114+182 has been in a faint state since its discovery by Biermann *et al.* (1982) and, at a magnitude fainter than 19, has been beyond the reach of even the 1.9m telescope at Sutherland.

Observations of the remaining four objects in the above list are presented and briefly discussed in this chapter.

5.2 VV Puppis

This star was discovered by van Gent (1931) as a variable with a period of 100 minutes. Early spectroscopic and photometric investigations include those by Herbig (1960),

Walker (1965) and Warner and Nather (1972) (hereafter WN) but it was not until the discovery of strong linear and circular polarisation by Tapia (1977) that the nature of the unusual light curve as that of an AM Her star was appreciated. Polarimetric studies by Liebert *et al.* (1978) and Liebert and Stockman (1979) produced evidence for accretion at both poles and placed limits on the size of the accretion region. Broad features in the spectrum of VV Puppis were interpreted by Visvanathan and Wickramasinghe (1979) as emission features from cyclotron radiation and a magnetic field of 31 MG was deduced, an order of magnitude lower than had been calculated (assuming the fundamental frequency of the cyclotron radiation) until then. The star was recently detected as a strong X-ray source (Patterson *et al.* 1984).

5.2.1 The Observations

Our observations were made at the Sutherland site of the S.A.A.O. in April 1983 and February 1984. They are listed in table 5.1. All observations were made with the U.C.T. Polarimeter. No filters were used with the RCA 31034A photomultiplier but a crown glass fabry lens restricted the UV response with a resultant passband of 3500Å to 9200Å.

As is customary with VV Puppis, Walker's (1965) ephemeris was used to phase the data. This is:

Maximum light = $JD_{\odot}$2427889.6474 + 0.0697468256E

As noted by Patterson *et al.* (1984), recent maxima have been occurring ∿0.03 cycles earlier than predicted.

An example of the light and polarisation curves is shown in fig. 5.1. Most of the February 1984 data set was

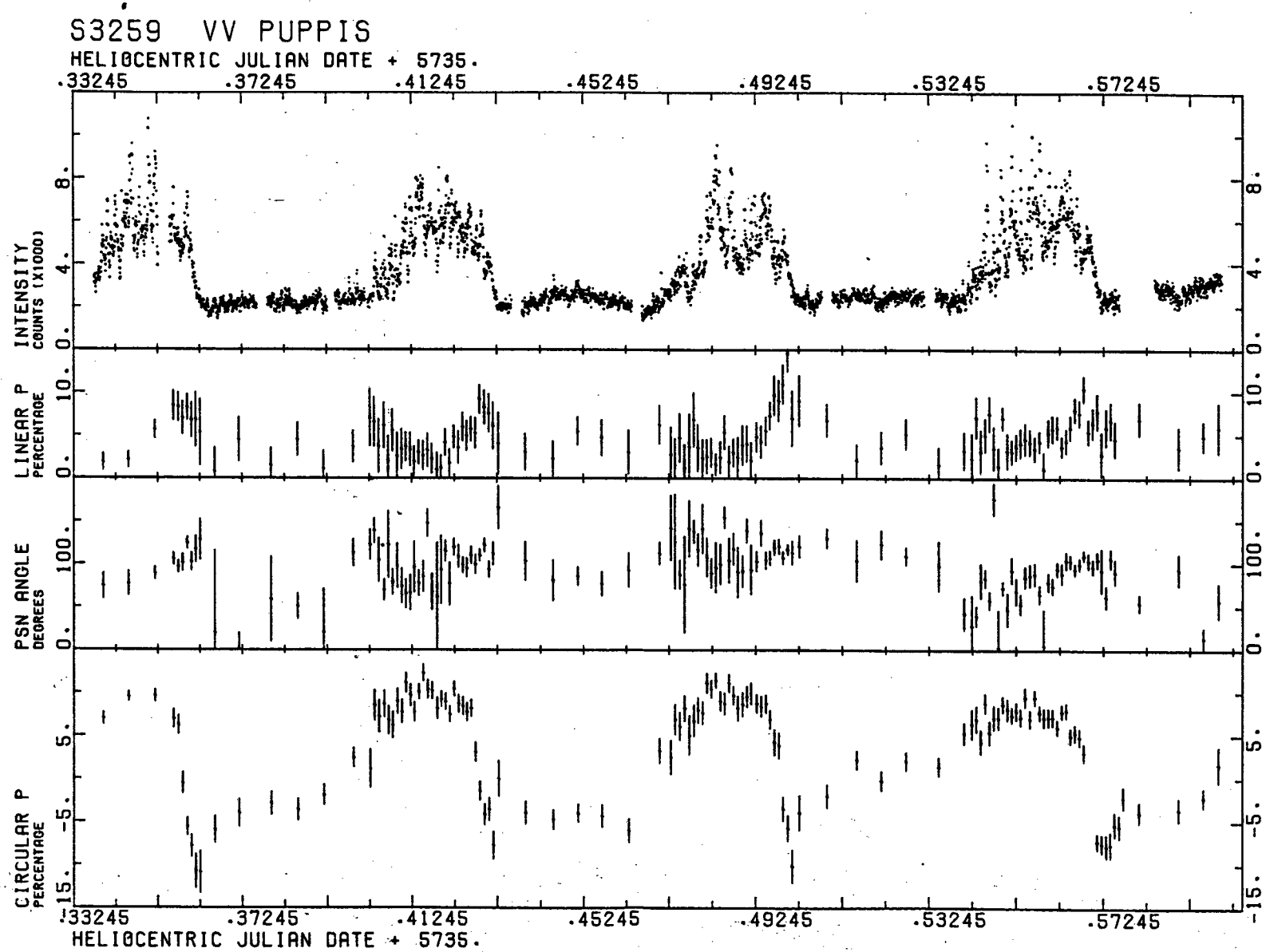

Figure 5.1 Run S3259 taken on 4 February 1984. Polarisation data (originally taken at 120 or 20 seconds) have been averaged 3 at a time,

phase folded and is shown in fig. 5.2.

The light curve is strongly modulated at the orbital period. The star is bright for approximately 40 percent of its orbital cycle and faint for the rest of the cycle. The rise to maximum light at phase 0.8 is much more gradual than the abrupt drop to minimum light at $\phi \sim 0.18$. At this phase there is also a strong linear polarisation peak rising to $\sim$9 percent. There is linear polarisation present during the entire bright part of the orbit and a second, lower, linear polarisation peak is evident at phase 0.7 in the phase folded data (fig. 5.2). The position angle generally increases during the bright phase but not in the simple way expected from radial accretion at one pole only (chapter 4 and Brainerd and Lamb 1983). It also appears to have a slightly double humped shape. The circular polarisation rises from a value of $\sim$-3 percent during the faint part of the orbit to $\sim$8 percent during the bright part. The decrease in polarisation at the end of the bright phase is more rapid than the increase at the beginning of the bright phase and is followed by a short dip lasting 0.05 of an orbit at $\phi \sim 0.16$. It passes through zero at ϕ = 0.11 during April 1983 and ϕ = 0.14 during April 1984. The increase in circular polarisation at the beginning of the bright phase takes place at ϕ = 0.71 during both 1983 and 1984 observations.

During February 1984 the light curves were characterised by extremely large and rapid flares in brightness. Flares of up to 3 times the mean bright phase intensity were observed in run S3258. Similar flaring, although not so

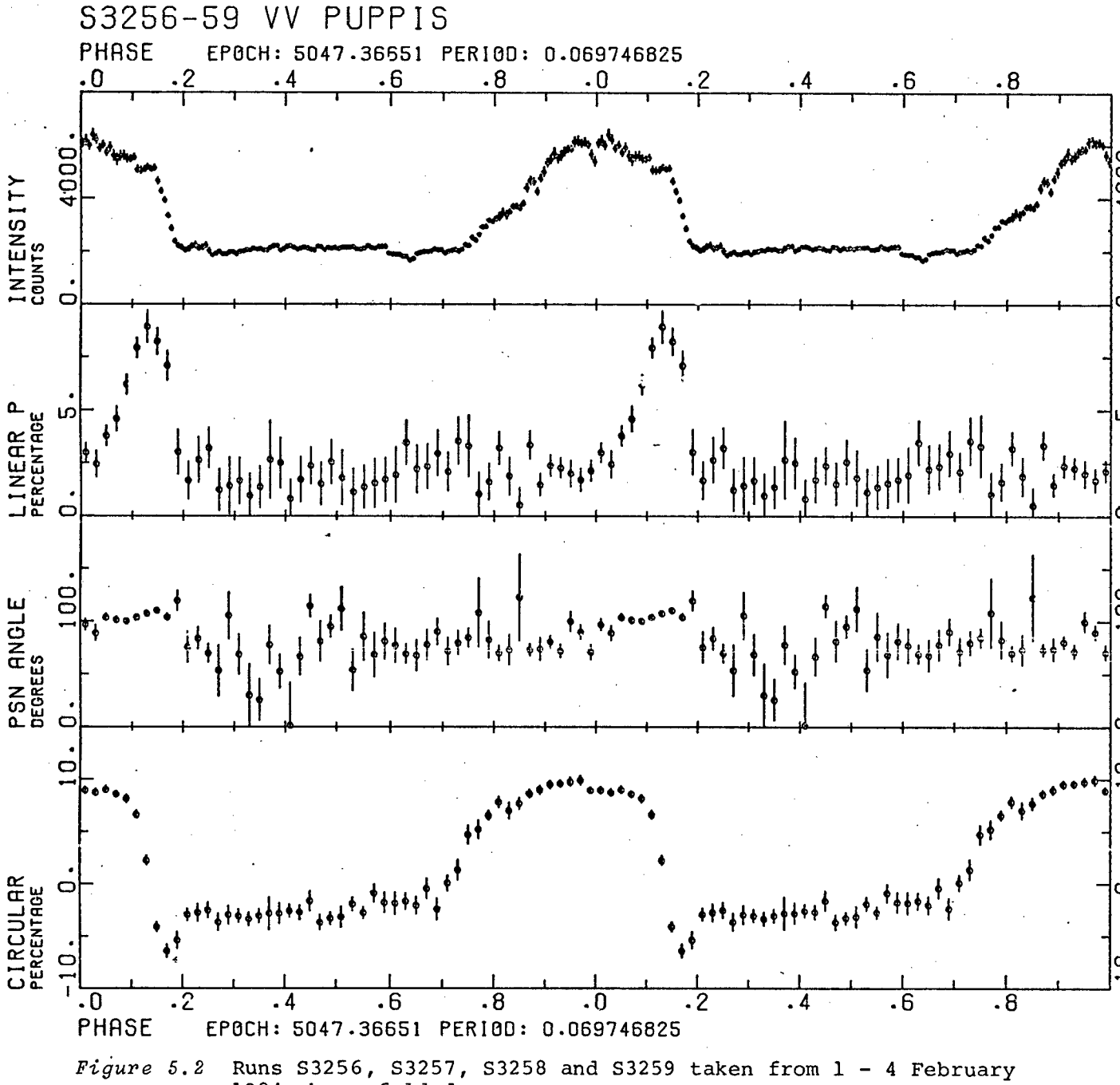

Figure 5.2 Runs S3256, S3257, S3258 and S3259 taken from 1 - 4 February 1984 phase folded.

extreme, was observed by WN. By good fortune the last orbit of run S3259 (fig. 5.1) was observed simultaneously with EXOSAT (Osborne *et al.* 1984 - fig. 1). Flaring activity in the soft X-ray and optical was highly correlated. Of the 11 strong flares observed in the optical, 8 had X-ray counterparts with the 8 strongest X-ray flares. The time resolution of the X-ray curve is $\sim$1 min and it is plotted on a fairly small scale, but there is no evidence for a delay between the X-ray and optical optical flares greater than the X-ray integration time (60 seconds).

Data presented by Liebert and Stockman (1979) indicate that the circular polarisation is stronger in the blue (3200-5600Å) than the red (5600-8600Å). This is shown in greater detail in the spectropolarimetry of Wickramasinghe *et al.* (1984). The white light circular polarisation curves published by Liebert *et al.* (1978) and Liebert and Stockman (1979) were taken during different brightness states. These also show transitions from positive to negative polarisations at ϕ = 0.11 and ϕ = 0.14; for the bright state (1979) data, the transition from negative to positive occurs at ϕ = 0.70, but the corresponding faint state transition takes place much later, at $\phi \sim 0.81$. Linear polarisation data taken by Bailey (1978) also during the faint state shows peaks at $\phi \sim 0.15$ (9 percent) and $\phi \sim 0.73$ (6 percent), when transformed from the Stokes Parameters Q and U to p and θ. Another peak is also evident in his data at $\phi \sim 0.53$ for which there is no counterpart in the phase folded data in fig. 5.2.

5.2.2 The System Geometry

It is fortunate that the accretion column is eclipsed by the primary in VV Puppis, as the eclipse duration provides a strong constraint on the inclination i and magnetic colatitude β. Visvanathan and Wickramasinghe (1981) have shown that

$$\cot i = \cos\pi\gamma\tan\beta$$

where γ is the fraction of the orbit for which an eclipse of the column takes place. This assumes a pointlike accretion column. As both the height and extent of the accretion column is known ($h \sim 0.01\ R_{WD}$, $f \sim 10^{-4}$), it is necessary to modify the expression. The shape of the accretion column is assumed to be cylindrical, of height h (in units of R_{WD}) and with base subtending a semiangle δ at the centre of the white dwarf. The fraction f of the surface over which accretion takes place is related to this angle by

$$f = \tfrac{1}{2}(1 - \cos\delta)$$

For $f = 10^{-3} \Rightarrow \delta = 3^{\circ}.6$. The perimeter of the base of the column is parametrised in terms of a variable t (the angle from the north point) yielding the following expression for the marginal visibility determined by $\pi \leq t \leq 2\pi$ of any point on the perimeter:

$$\cos i = \tan(\beta-\delta\cos t)\cos\left(\pi\gamma-\frac{\delta\sin t}{\sin(\beta-\delta\cos t)}\right)$$

$$+\ \frac{\cos(\pi/2+\cos^{-1}(1/(1+h))}{\sin i\cos(\beta-\delta\cos t)}$$

The equation is solved iteratively for i with γ,β,δ,h and t as input parameters. For t in the above range there are two values of t which give the same i, except for a singlar value corresponding to first contact. For the geometry of VV Puppis this corresponds to the maximum i for $\pi \leq t \leq 2\pi$.

An observed set of γ, δ and h yields a curve in the (i,β) plane. This can be superimposed on the 99% confidence region in the plane obtained from analysis of the position angle variation (see chapters 3 and 4).

The value used for γ has varied from 0.64 (Brainerd and Lamb 1984) to 0.56 (Patterson *et al.* 1984). The larger value was obtained from the circular polarisation zero crossing times when the system was in a faint state (Liebert *et al.* 1978). Fig. 5.2 indicates that γ = 0.57 during 1984 from both the intensity data and circular polarisation zero crossing times (and, to a lesser accuracy from the linear polarisation peaks).

Fig. 5.3 shows the results of the above calculations in the (i,β) plane. The solution to the position angle data is shown shaded and the other three curved lines correspond to $(\gamma,\delta,h) = (0.57,0^{\circ},0)$, $(0.65,0^{\circ},0)$ and $(0.57,5^{\circ},0.01)$. The solution found by Brainerd and Lamb (1984) is also shown. The best solution for the February 1984 data is $i = 77^{\circ}\pm7^{\circ}$, $\beta = 155^{\circ}\pm6^{\circ}$. This is close to that found by Brainerd and Lamb (1984) ($75^{\circ}\pm5^{\circ}$, $148^{\circ}\pm5^{\circ}$) and consistent with the values required from the existence of discernible cyclotron features, viz. $0^{\circ}<i\lesssim30^{\circ}$, $90^{\circ}<\beta\lesssim100^{\circ}$ or $80^{\circ}\lesssim i<90^{\circ}$, $150^{\circ}\lesssim\beta<180^{\circ}$ (Wickramasinghe and Meggit 1982).

5.2.3 Is VV Puppis an Eclipsing AM Her Star?

With an inclination so close to 90° it is possible that the accretion column is eclipsed by the secondary. This suggestion was first made by Warner and Nather (1972) in order

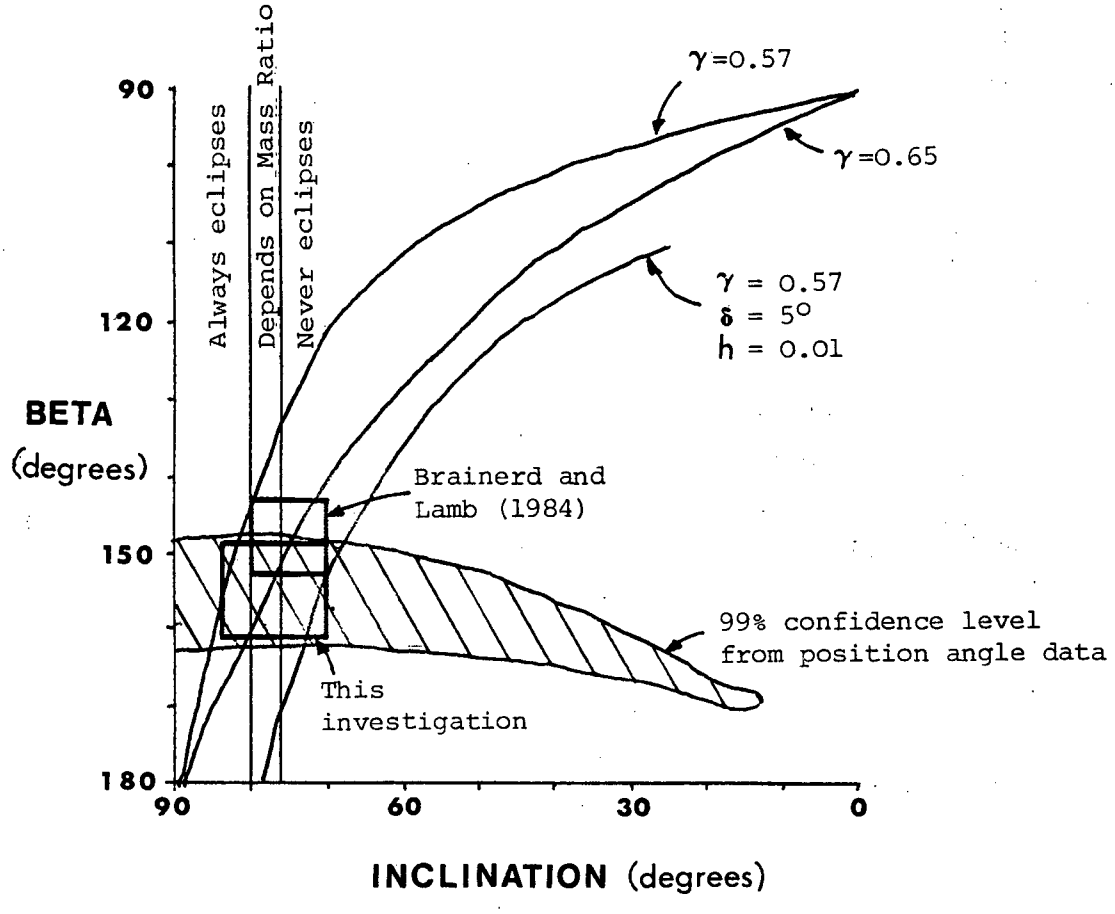

Figure 5.3 Constraints on i and β showing the loci of the best fits for this investigation and that of Brainerd and Lamb (1984)

to account for $\gamma \gtrsim 0.5$ (in terms of the accretion disk model they proposed). For mass ratios (M_2/M_{WD}) $0.013 \lesssim q \lesssim 1.4$ an eclipse of the primary will always take place if $i \gtrsim 85^\circ$ and never takes place if $i \lesssim 72^\circ$ (Horne 1983). The mass ratio can be constrained a little by calculating the mass of secondary. Using the empirical zero age main sequence relationship determined by Patterson (1984) and his M_2 - Period relationship (equation 7), the secondary mass is $M_S \sim 0.13 M_\odot$. Spectroscopy by Cowley *et al.* (1982) indicates that the mass function $f(M) \gtrsim 0.33$ implying $M_{WD} \gtrsim 0.52 M_\odot$ (for $M_S \sim 0.13 M_\odot$ and worst case $i = 90^\circ$) and $0.09 \lesssim q \lesssim 0.25$, while spectroscopy by Schneider and Young (1980) indicates $f(M) \gtrsim 0.606$ implying $M_{WD} \gtrsim 0.82 M_\odot$ and $0.09 \lesssim q \lesssim 0.16$. For a primary mass $0.52 \lesssim M_{WD} \lesssim 1.4 M_\odot$ the system will always eclipse if $i \gtrsim 80^\circ$ ($M_{WD} = 1.4 M_\odot$) and never if $i \lesssim 76^\circ$ ($M_{WD} = 0.52 M_\odot$). If the primary mass is $1 M_\odot$ an eclipse will occur for $i \gtrsim 78^\circ$.

From the analysis of γ and the position angles it is possible, but not essential, that an eclipse of the accretion column by the secondary occurs. It is necessary to search in the intensity and polarisation data for other clues.

The position of the secondary has been located from infra-red photometry by Szkody and Capps (1980), Allen and Cherepashchuk (1982) and Szkody *et al.* (1983). It is at inferior conjunction at $\phi \approx 0.1$ (Patterson *et al.* 1984). This coincides roughly with the rapid and eclipse-like decline at the the end of the bright phase (fig. 5.1 and WN figs. 2,3 and 5). It is notable that the phase of the decline has been constant relative to Walker's (1965) ephemeris, although at the same time there were variations in the phase of the onset of the

bright part of the orbit (see Patterson *et al.* 1984, Table 1). It is possible that the stability in the phase of the decline to minimum light (despite the fact that accretion may take place at slightly different locations on the primary) is caused by an eclipse by the secondary.

The behaviour of the position angle at this phase is also unusual as it does not follow the increasing trend observed during the linear polarisation peak. Whether this is the result of an eclipse is not certain. As the circular polarisation transition through zero at $\phi \sim 0.14$ is variable in phase, it is not possible that the negative excursion just afterwards is caused by an eclipse.

The calculated percentage polarisations using the shockfront models of Wickramasinghe and Meggitt (see chapter 4) indicate that values closer to $i \simeq 90^{\circ}$ may be more appropriate when a finite spot size is used. This is discussed more fully in section 5.2.3. The eclipse interpretation of the rapid decline in brightness at $\phi \simeq 0.15$ is, however, mediated against by the behaviour of HO139-68 (see section 5.3). This object is not viewed at a high inclination, but has a light curve extremely similar to that of VV Puppis, except that there is a rapid increase in brightness at the beginning of the bright phase and a slow decline at the end of the bright phase. Thus the question of the existence of the eclipse remains unsolved.

There are some important consequences, if, in fact, the system <u>is</u> found to be eclipsing:-

1) The eclipse centre is at ϕ = 0.20 which must also be the phase of inferior conjunction of the secondary. The angle between the line of centres and the plane containing the rotation axis and active magnetic poles, ψ, is then 72^{o}.

2) The fraction of the orbit with the pole invisible behind the limb of the primary, γ, is less than 0.6 ($\gamma \sim 0.5$) because without the eclipse the bright part of the orbit would extend to $\phi \sim 0.25$. Thus the inclination would be even closer to 90^{o} than has been hitherto deduced.

3) As the contribution from the secondary is extremely small at optical wavelengths (confirmed by the absence of strong colour changes at $\phi \sim 0.15$ to 0.20 (Walker 1965)) and the primary is obscured, the residual light from the system at $\phi \sim 0.2$ must arise from the curving accretion stream which climbs out of the orbital plane. This is also probable the source of the background intensity for the rest of faint phase ($\phi \sim 0.2$ to 0.7).

4) This would be only the second known eclipsing AM Her star, and would become an important candidate for tests of asynchronous rotation of the primary (see however section 5.4). As the eclipse locates the position of the secondary precisely, any drift in ψ will be evident from the long term changes in γ. Patterson *et al.* (1984) have provided some of the necessary data in their Table 1. From their calculations γ has decreased since 1964 at a more or less uniform rate from 0.60 to 0.55. If the decrease is secular then ψ would go through 360^{o} in $\sim$300 years. Earlier, less precise light curves by Thackeray *et al.* (1950) and Oosterhoff (1935) do not, however, confirm this trend and indicate that the slip period is greater than $\sim$2500 yrs. Either of the above numbers is considerably longer

than those derived theoretically by Campbell (1984) which are of the order of 10 years. Because of this long baseline of observations, if VV Puppis is an eclipsing system, it will provide strong limits in the class of AM Her variables on asynchronous rotation.

5.2.4 Fits from the Cyclotron Calculations

The extensive investigation undertaken in Chapter 4 indicates that the shock front calculations by Wickramasinghe and Meggitt 1984 provide good fits to the observed percentage polarisations in at least one AM Her star, E1405-451. The same calculations were therefore used for VV Puppis. The magnetic field strength of VV Puppis is $\sim$32 MG (Wickramasinghe and Meggitt 1982); the calculations (which assume a field of 30 MG) are therefore appropriate as far as field strength is concerned.

The fits to the data in chapter 4 were made assuming a point source of emission on the surface of the primary. The model is made more realistic by assuming that the emission region is situated at a height h (in units of primary radius) above the surface of the primary. In order to impart an area to the shock, the single point used in chapter 4 was broken into 9 discrete elements arranged in 3 rows of 3, each with 1/9 of the total flux expected from the single point. This "raft" of 9 emission points, which can be varied in extent and height above the surface, crudely simulates the emission region.

The fit for the following parameters is shown in figure 5.4:

$i = 83^{o}$

$\beta = 150^{o}$

h = 0.01

spot size in longitude = 4^{o}

spot size in latitude = 4^{o}

non-radial tilt = 5^{o} in longitude

harmonics included: 3-10

constant background = 3% of peak flux

variable background = 0

There is close agreement between the observed and calculated circular polarisations and with the linear polarisation between $\phi \sim 0.9$ to 1.7. The calculated linear peak at $\phi \sim 0.75$ is however not observed. There is poorer agreement between the observed and calculated flux as the shape of the latter is too square during the bright part of the orbit.

It was not possible to suppress the calculated linear peak at $\phi \sim 0.75$ by increasing the non-radial tilt of the column. Although this peak was observed in some individual runs, notably run S3109, it was always lower than the peak at $\phi \sim 0.2$. Possibly the same explanation as proposed in chapter 4 for the asymmetry in the data for E1405-451 (section 4.4.2) involving areal temperature structure may again be appropriate.

The negative excursion in the circular polarisation at $\phi \sim 0.2$ is well reproduced for an accretion region height of 0.01 R_{WD} and the difference between the depth of the two dips at $\phi \sim 0.2$ and $\phi \sim 0.75$ is satsifactorily reproduced if a 5^{o} tilt

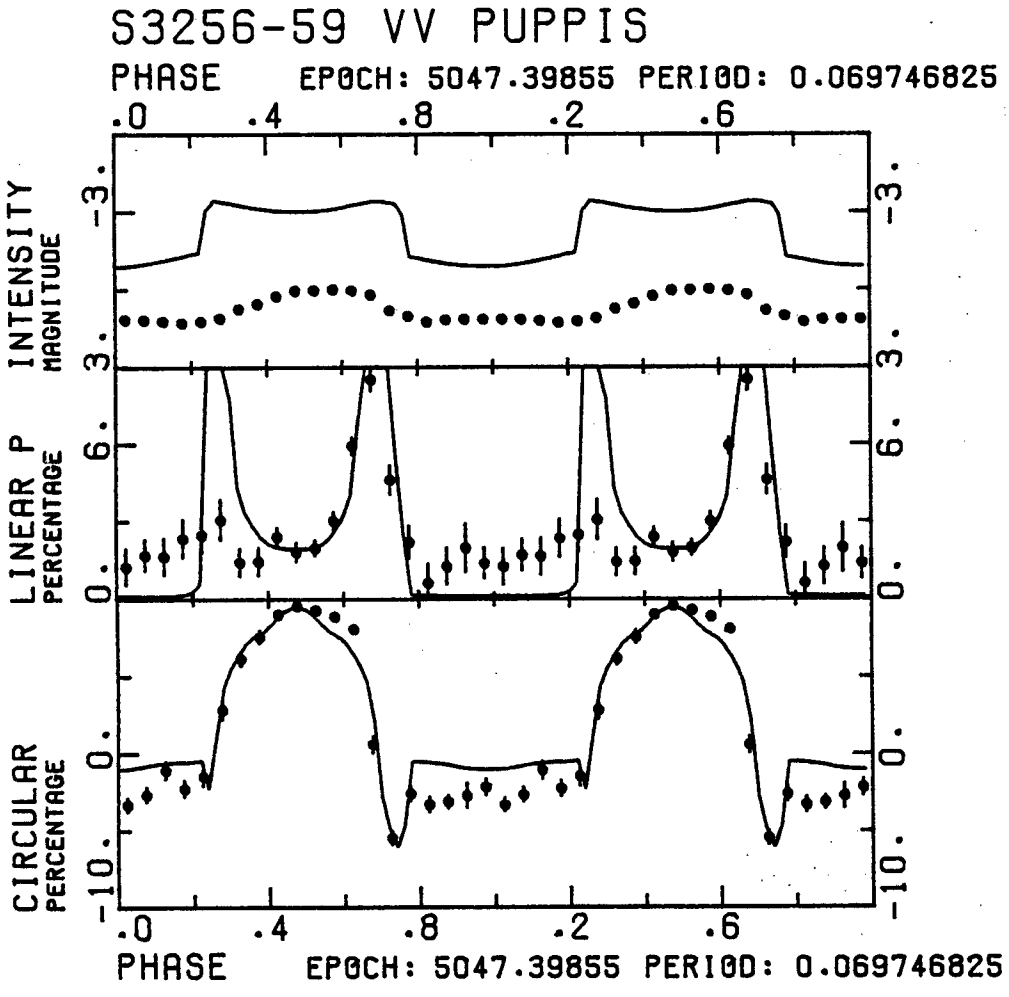

Figure 5.4 The best fit for the 20 keV shock front calculations superimposed on the intensity and polarisation data for runs S3256-S3259. For parameters see text.

(in longitude) from radial is assumed for the accretion. The height is the same as that deduced by Liebert *et al.* (1978) but lower than that found by Liebert and Stockman (1979) ($h \sim 0.1\ R_{WD}$). The latter value is too large to fit the observations presented here. The spot size used here corresponds to $f \sim 3 \times 10^{-4}$.

The inclination and magnetic colatitude required in order to achieve a satisfactory fit to the data were consistent to within the uncertainties with the values deduced in section 5.2.2. If the shock front calculations of Wickramasinghe and Meggitt (1984) are assumed to be reasonably accurate then the lower inclinations and smaller colatitudes within the range of uncertainties are ruled out, and the evidence is stronger that the inclination is large enough for VV Puppis to be an eclipsing system.

The fit provided by the 10 keV shock front model was not as good as that provided by the 20 keV model. The only observational information on the temperature of the shock gives T>5 keV (Patterson *et al.* 1984).

5.2.5 Tests for the Weighted Harmonic Number (WHN).

Because the white dwarf field strength in VV Puppis is known, it is possible to compare the observed WHN with the range of harmonics that are visible in the white light bandpass. For a bandpass of 3500Å to 9000Å and a magnetic field of 32 MG, harmonics 4 to 8 and the tails of harmonics 3 and 9 are encompassed. The WHN varies between 3.6 and 7.8 between $\phi \sim 0.88$ to 0.13 (bright part of the orbit). The average WHN = 5.2 ± 1.4,

corresponding to effective wavelengths 5000Å to 8800Å for the 32 MG field. This agreement is encouraging and indicates that field strengths may be calculated to within a factor of ∿2 by this method. Higher accuracy may be obtained by making narrow band observations, but this would require a longer series of observations or a larger telescope than that used for the white light observations. For those AM Her stars whose primary's field strengths have not been determined accurately by Zeeman spectroscopy, this method allows some estimate of their field strengths to be made.

The WHN calculated from the 20 keV shock front model of Wickramasinghe and Meggitt (1984), which apply to a 30 MG field, lie in the range 4 to 5 during the same phases. Although this value is slightly lower than that obtained for the observed WHN, the agreement is encouraging, lending credence to the field strength estimate for E1405-451 derived in section 4.4.1.

Table 5.1

Run	Date	Duration (cycles)	Telescope (m)	Passband (Å)
S3102	6 Apr 1983	1.4	1.9	3500-9200
S3104	7 Apr 1983	1.0	1.9	3500-9200
S3109	10 Apr 1983	1.1	1.9	3500-9200
S3115	13 Apr 1983	0.25	1.0	3500-9200
S3118	15 Apr 1983	0.75	1.0	3500-9200
S3120	18 Apr 1983	1.6	1.0	3500-9200
S3256	1 Feb 1984	3.2	1.0	3500-9200
S3257	2 Feb 1984	3.8	1.0	3500-9200
S3258	3 Feb 1984	3.2	1.0	3500-9200
S3259	4 Feb 1984	3.8	1.0	3500-9200
S3260	5 Feb 1984	4.2	1.0	3500-9200
S3261	6 Feb 1984	1.5	1.0	3500-9200

5.3 HO139-68

This X-ray source was first detected with the low energy detectors on the HEAO1 A-2 experiment, and was identified optically with a variable star of magnitude 15 to 16.5 possessing a strong emission line spectrum (Agrawal *et al.* 1981). Photometry by Cropper (1982) and Pickles and Visvanathan (1982) showed that the light curve was hump shaped with a minimum lasting approximately 0.3 of the orbit. An orbital period of 113.64 minutes was deduced from the steeply rising onset of of the hump which was called phase zero. Simultaneous photometry and spectroscopy has been presented by Thorstensen *et al.* (1984). Circular polarisation measurements by Bailey *et al.* (1982) and linear polarisation measurements by Visvanathan and Touhy (1982) confirmed the stars AM Her classification. HO139-68 went into a low state ($V \geq 17.5$) at the end of 1982 and has remained at this level. Wickramasinghe *et al.* (1984) have deduced a magnetic field of 30 MG from Zeeman spectroscopy in the low state.

5.3.1 The Observations

These were all made at the Sutherland site of the S.A.A.O. Initial photometric observations were made in 1982 before the polarimeter was commissioned. Unfortunately the star has been in a faint state since the end of 1982 so that all polarimetric observations were hampered greatly by the faintness of the object. Table 5.2 lists the observations made in 1982 and 1983. No observations were made in 1984. In order to maximise the count rate, all observations were made in white light. An RCA 8644 photomultiplier (S20 response)

was used for the photometry in 1982 and a cooled RCA31034A photomultiplier with a glass fabry lens (giving a band pass from 3500Å to 9200Å) was used for the polarimetry in 1983.

Following Pickles and Visvanathan (1982) the steep rise in brightness at the onset of the bright hump was adopted as phase zero. Nine timings from the above paper and six from runs S2932 to S3036 were used to refine the ephemeris of Pickles and Visvanathan (1982) yielding:-

$$\text{time of rise} = \text{HJD } 2444901.972286 \pm 15 + 0.07891648 \pm 35\,E$$

This is sufficiently precise to determine the phases of the 1983 runs to within 0.025 of an orbit.

Examples of the high state photometry are shown in fig. 5.5 and 5.6 (runs S2936 and S3030). The latter was made simultaneously with polarimetry by Dr. S. Tapia (as was S3025) but those data are not available for analysis. The faint state polarimetry is extremely noisy so runs MS003, 5, 8 and S3174, 7, 9 were phase binned with the result shown in fig. 5.7. It can be seen that the linear polarisation has a value consistent with zero over the whole orbit, whereas the circular polarisation is slightly negative between $\phi \sim 0.0$ and 0.2 ($\sim -2.5\%$) and zero for the rest of the orbit (except for another possible slightly negative excursion at $\phi \sim 0.55$). These excursions are apparent in both the July 1983 and August/September sets of data. The hump-shaped structure of the light curve has disappeared as can be seen from the nearly flat phase-averaged light curve. The variations visible in the latter data are more likely to be the result of night to night and week to week

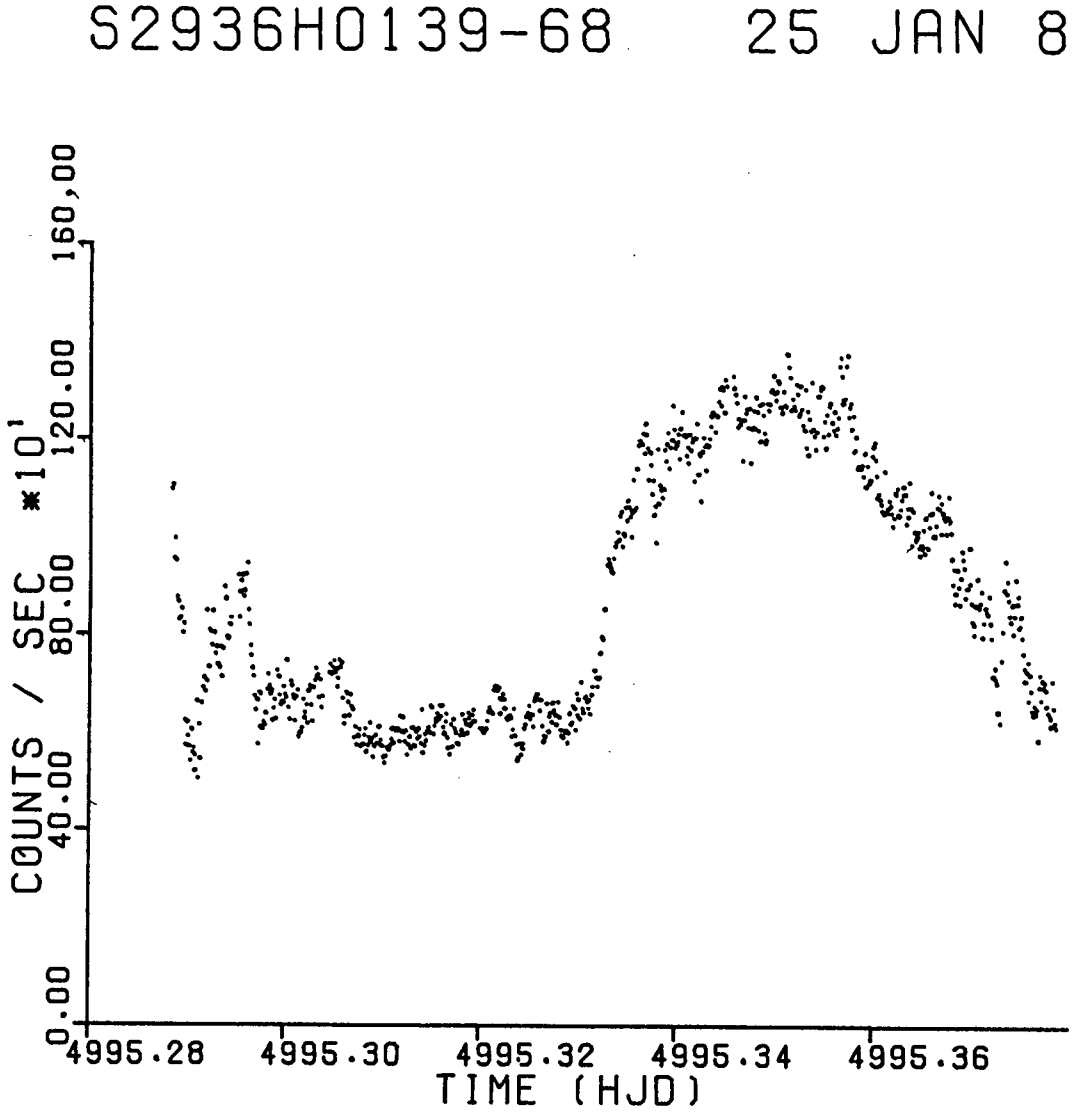

Figure 5.5 High state photometry of HO139-68 run S2936

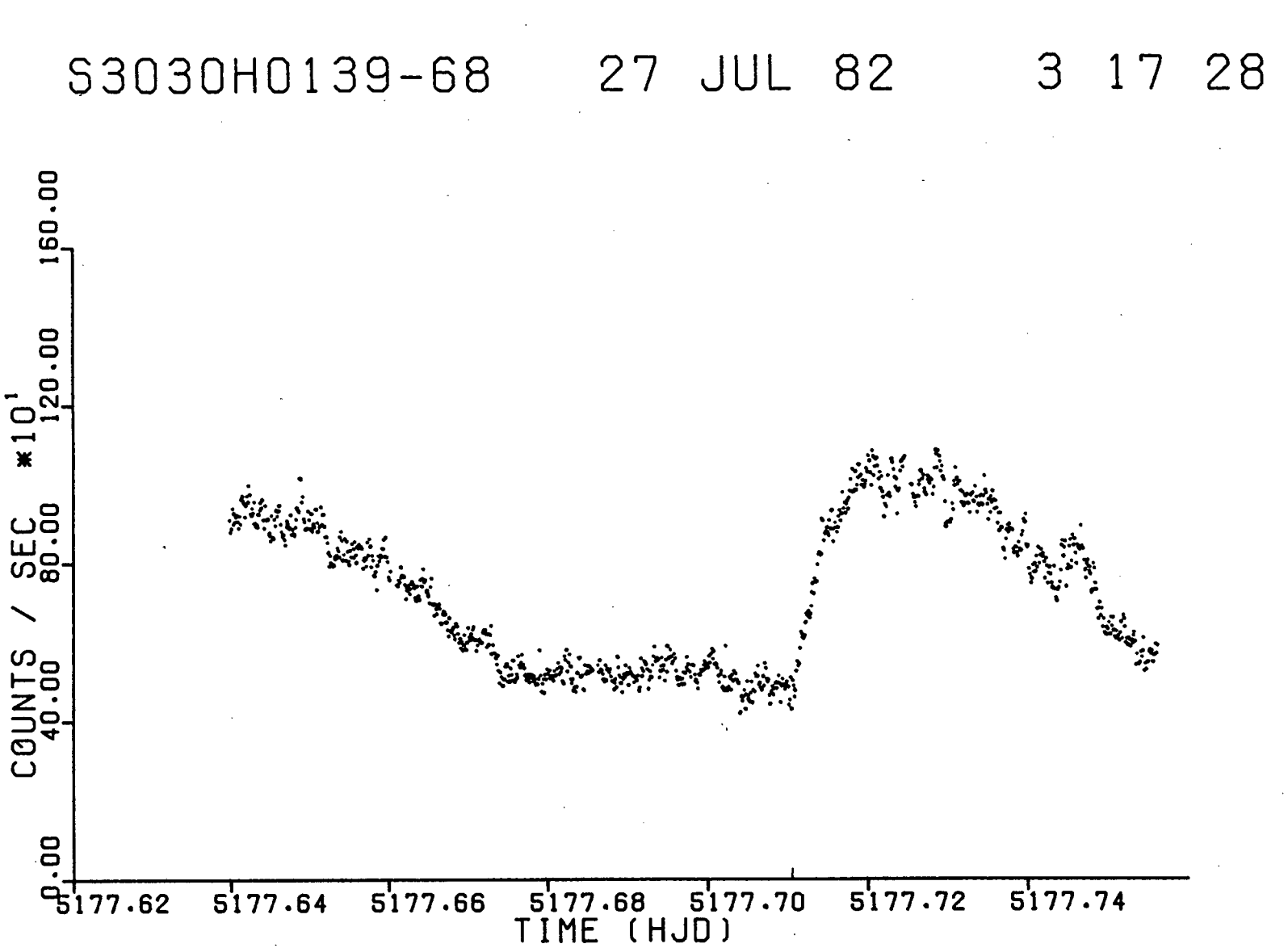

Figure 5.6 High state photometry of HO139-68 run S3030

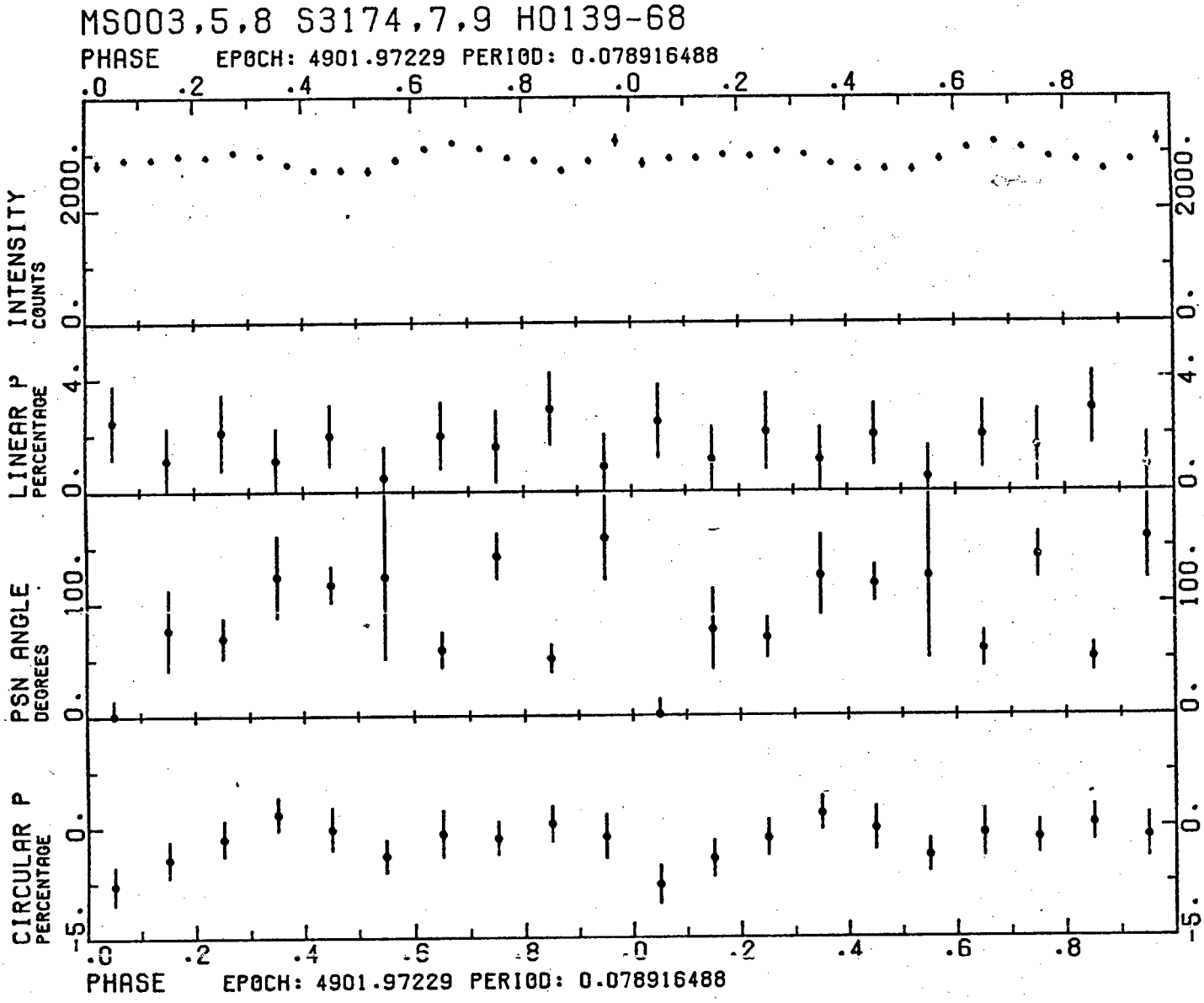

Figure 5.7 The low state intensity and polarisation data for H0139-68 folded on the orbital period.

variations and the small apertures used. Sky variations were minimised by alternate star-sky measurements.

5.3.2 Geometrical Considerations

In the absence of high quality linear polarisation data it is difficult to deduce i and β with any accuracy. Some progress may be made however by comparing HO139-68 to VV Puppis. The light curves of both of these objects are very similar, although the minimum lasts for a shorter fraction of the orbit in HO139-68. At first sight $\gamma < 0.5$ would indicate that $\beta < 90^{o}$ but this is contradicted by the fact that the circular polarisation is negative for only 30 percent of the orbit (during the bright phase) and positive for the rest of the orbit (Bailey *et al.* 1982). The pole is therefore on the hemisphere of the primary visible to the observer for 0.3 of the orbit. This is confirmed by the spacing of the linear polarisation peaks (0.4 of an orbit). The height and extent of the accretion column must therefore be taken into account, as both of these factors will extend the bright phase of the orbit. This provides a consistent picture, with the circular polarisation reaching large positive values as the column is viewed from underneath at each limb before dropping to zero as it is eventually entirely obscured by the primary. Thus $\beta > 90^{o}$.

It is interesting to speculate as to why the accretion column is visible (when over the limb) for so much longer in this star than in VV Puppis. This may be caused by a tall accretion column, indicating that the accretion rate is low. However, as i and β are not well determined for this system (see later), the alternative explanation - that i and β are such that the column

remains fairly close to the limb - cannot be ruled out.

It is apparent from the linear polarisation measurements of Visvanathan and Tuohy (1983) that the position angle increases continually, passing through 360° in one orbit, indicating that $i<(180^{\circ}-\beta)$. In addition the breadth of the linear polarisation peak and the existence of linear polarisation during the entire bright phase indicates that the angle to the column, α, does not deviate much from 90° during the bright phase. Values of $60^{\circ}\lesssim\beta-i\lesssim90^{\circ}$ would probably be appropriate.

The resultant locus of i and β fulfilling the above conditions is shown in figure 5.8 as a shaded region. Some further progress can be made by adopting $0.6\lesssim\gamma\lesssim0.7$ from the circular and linear polarisations. This is shaded at right angles to the loci from the previous considerations. The resultant cross hatched region contains the (i,β) loci consistent with all of the above conditions. This indicates that $i\lesssim60^{\circ}$ and the magnetic pole is within 35° of the orbital plane. As no previous estimates of i and β exist for this star it is appropriate to provide the following approximate relationships from fig. 5.8:

$$0\lesssim i\lesssim60^{\circ}$$

$$\beta = 80^{\circ}+0.78i\pm0.2i \quad (35^{\circ}\lesssim i\lesssim60^{\circ})$$

$$\beta = 90^{\circ}+0.49i\pm0.2i \quad (0^{\circ}\lesssim i\lesssim35^{\circ})$$

5.3.3 The Low State Polarisations

The phase-averaged low state polarisations are very small (fig. 5.7). The linear polarisations are inconsistent with the values reported by Visvanathan *et al.* (1983) of 6 percent at a constant position angle over the orbit, as they

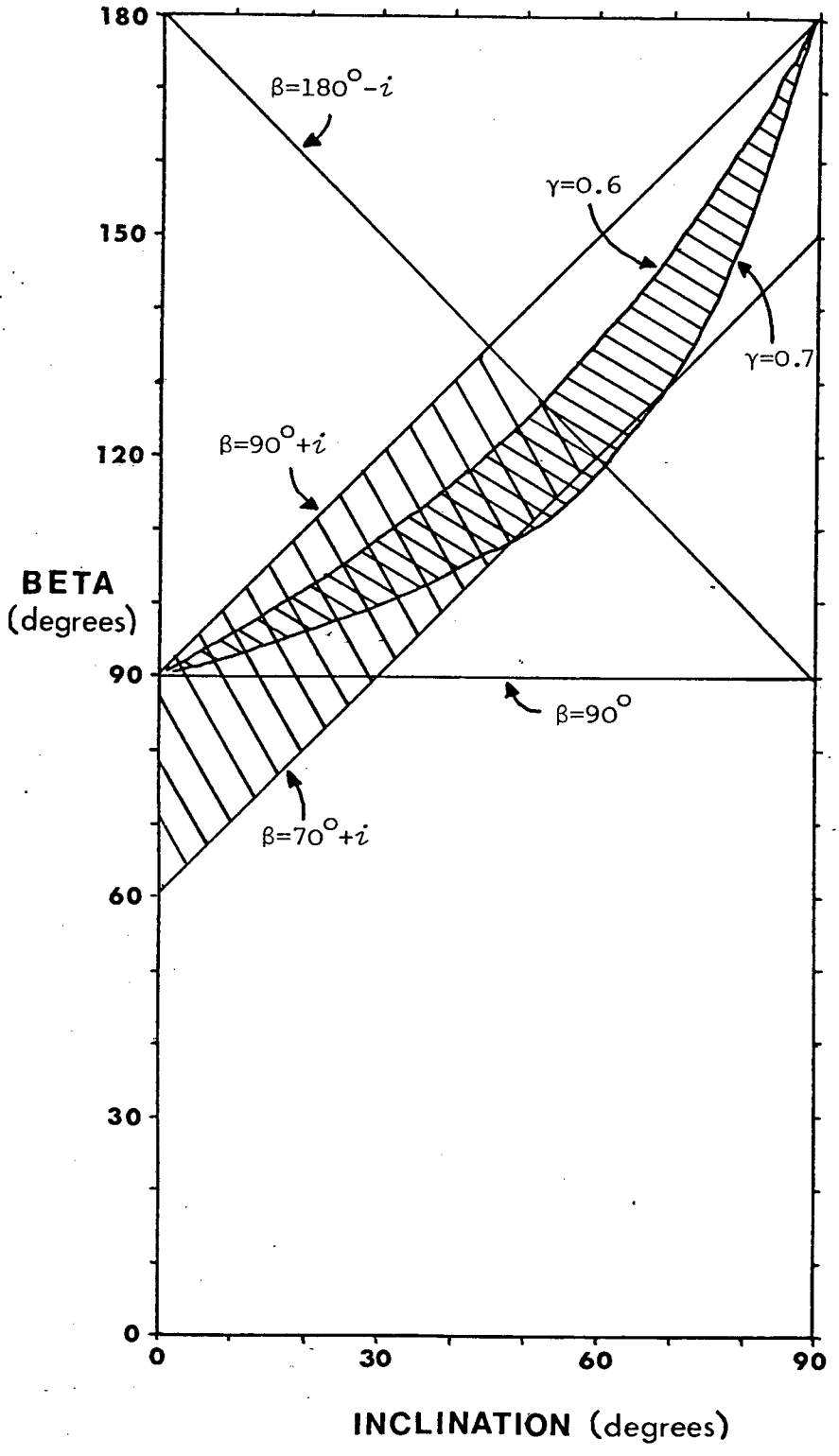

Figure 5.8 Constraints on i and β. The cross-hatched region contains the (i,β) loci consistent with all the conditions available from the data.

are systematically less than 3 percent at widely scattered position angles.

The circular polarisation is slightly negative at the same phase as that occurring in the high state and the excursion appears to last for ∿0.25 of an orbit. It is at only ∿1/3 of the high state value of 9% (Bailey *et al.* 1982). This is in contrast to the behaviour in AM Her and VV Puppis (Latham *et al.*, 1981, and Liebert *et al.*, 1979) during faint states. (In common with these two stars, however, spectra of HO139-68 taken during the low state show much weakened emission lines (Wickramasinghe *et al.*, 1984). As the drop in brightness is ∿2½ magnitudes in all three cases it is unclear why the polarisation is so reduced in HO139-68 and not in the other two objects. However, from the almost total absence of any modulation in the light curve at the orbital period and the lower values of circular polarisation it appears that the accretion process is almost entirely shut down during the low state in HO139-68.

Table 5.2

Run	Date	Duration Cycles	Telescope (m)	Passband Å
S2932	23 Jan 1982	0.5	0.75	3300-7800
S2933	24 Jan 1982	1.1	0.75	3300-7800
S2936	25 Jan 1982	0.8	0.75	3300-7800
S3025	25 Jul 1982	1.3	0.75	3300-7800
S3030	26 Jul 1982	1.4	0.75	3300-7800
S3036	17 Sept 1982	1.7	0.75	3300-7800
MS003	15 Jul 1983	0.8	1.9	3500-9200
MS005	16 Jul 1983	0.6	1.9	3500-9200
MS008	17 Jul 1983	1.3	1.9	3500-9200
S3174	30 Aug 1983	2.6	1.9	3500-9200
S3177	31 Aug 1983	1.7	1.9	3500-9200
S3179	01 Sept 1983	1.7	1.9	3500-9200

5.4 E2003+225

This object was also first discovered by the HEAO 1 A-2 detectors, and catalogued as H2005+22 (Nugent *et al.* 1983). It was located more precisely by the Einstein Observatory and identified optically by Nousek *et al.* (1982). The X-ray observations, and spectroscopy, polarimetry and high speed photometry were described in a comprehensive paper by Nousek *et al.* (1984) hereafter N. This system, the tenth and most recent AM Her variable to be confirmed, has the longest orbital period in the class (222.5 min).

5.4.1 Observations

Continuous observations of more than a full orbit are difficult to obtain at the latitude of Sutherland; our observations of the object are therefore not very extensive. They are listed in Table 5.3. The U.C.T. Polarimeter with RCA31034A/glass fabry lens was used to gather the data on the 1.9 and 0.75m telescopes. The passband was 3500Å-9200Å.

Run MS007, covering 0.8 of the orbital cycle, is shown in fig. 5.9. Moonset occurred halfway through the run so 60 sec sky observations were made every 240 sec to ensure that the correct sky subtractions were made. Fig. 5.10 shows runs S3344 and S3348 phase folded. These are the most extensive observations available here, covering an orbital cycle each, but they suffer from increased photon noise resulting from the use of a small telescope (0.75m). The polarisation behaviour is similar to that depicted in N. The circular polarisation varies almost sinusoidally from zero at $\phi \approx 0$ to -6% at $\phi \approx 0.5$ in white light (the phasing is discussed in Section 5.4.2) while there is a linear polarisation peak at $\phi \approx 0.0$ visible in run MS007 (fig. 5.9). In the May 1984 observations (fig. 5.10) the linear peak appears to have smeared out into two low peaks

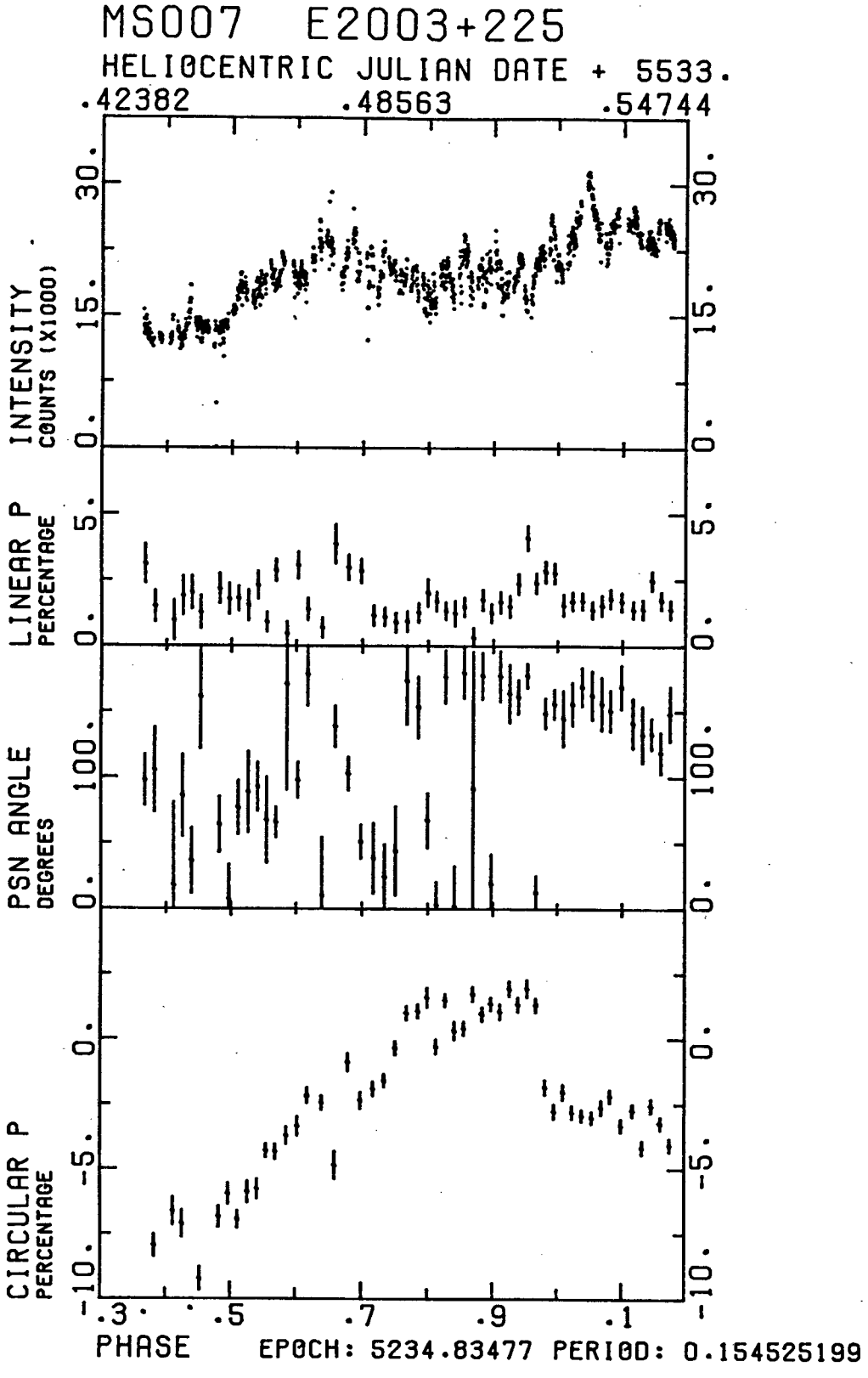

Figure 5.9 Run MSOO7 taken on 17 July 1983

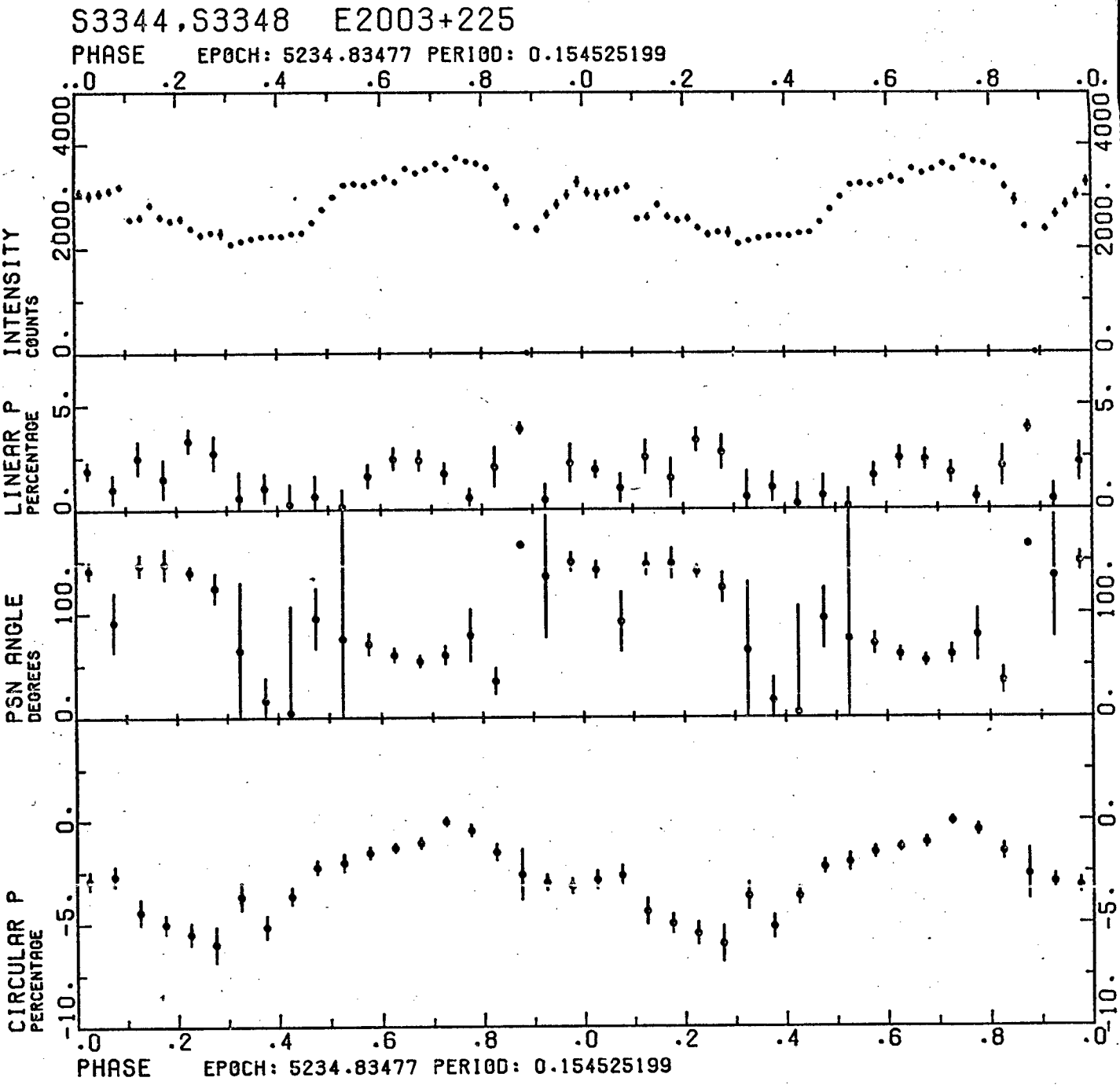

Figure 5.10 Runs S3344 and S3348 taken on 30 May and 1 June 1984, phase folded. The position angles have been offset by +60° to enhance clarity. The linear ephemeris of N has been used to phase the data.

each side of $\phi \sim 0.0$. Another peak is evident at $\phi \sim 0.5$ (it is also evident in the data published by N). The position angle decreases gradually from a peak at $\phi \sim 0.4$, rising steeply again at $\phi \simeq 0.2$. The I band circular polarisation data of N show a notch at $\phi \simeq 0.4$ which is not visible in the white light data shown here. A comparison between the maximum circular polarisations attained in figures 5.9 and 5.10 reveals that these declined from $\sim 9\%$ in July 1983 to $\sim 5.5\%$ in May 1984.

The light curve is similar to that of E1405-451 (chapter 4 fig. 4.3) in that it has a double humped structure. Flickering on a short timescale is also evident.

5.4.2 The Orbital Period

Fifteen linear polarisation peaks spaced over 1515 orbital cycles observed by N yielded the following ephemeris for the midpeak:

$$\text{HJD} = 2445234.8348 \underset{\pm 4}{} + 0.1545252E \underset{\pm 3}{}$$

Initially the May 1984 runs (fig. 5.10) were phased according to this ephemeris, but it was found that phase shippage of ~ 0.25 had occurred during the 4000 cycles since the above epoch and an orbital period of 0.1545148 days was required, a much greater change than that allowed by the above quoted uncertainties. Similarly, it was found from runs MS007 and S3200 that a period of 0.1545192 days was appropriate, again outside the allowed range of periods quoted above. This indicated that a period change had taken place.

Fig. 5.11 shows an O-C diagram with the above information. Unfortunately the 15 linear polarisation peak timings referred to above are not available, so the following estimates were made:-

1) The uncertainty in the epoch, when scaled by $\sqrt{N}$ (the number of observations) corresponds to an uncertainty in the O-C diagram of $\sim$0.01 cycles.

2) The uncertainty in the period accumulated over 1515 cycles and scaled by $\sqrt{N}$ also indicates an uncertainty of $\sim$0.01 cycles.

Two points were therefore available, one at the epoch and the other at cycle 1515, both with an O-C of 0 and uncertainty of 0.01 cycles. The O-C timings, with estimates of their uncertainties, of phase zero in runs MS007, S3200 and S3344 and S3348 provided three other points in the diagram.

A linear fit was found to be inconsistent with the observations of N, as an error in the epoch of 0.1 cycles would result (a factor of 40 over the standard error), but a quadratic fit was found to be acceptable, and consistent with the estimated uncertainties of the individual points in the O-C diagram. Before proceeding, however, one other piece of evidence must be considered. Soft X-ray data presented by N were taken with the EINSTEIN satellite $\sim$3424 cycles before the above epoch. If it is possible to phase these observations the period change would be constrained more strongly. Fortunately preliminary results of soft X-ray observations by EXOSAT are available from Maraschi *et al.* (1985) and Osborne *et al.* (1985). These observations were made starting at

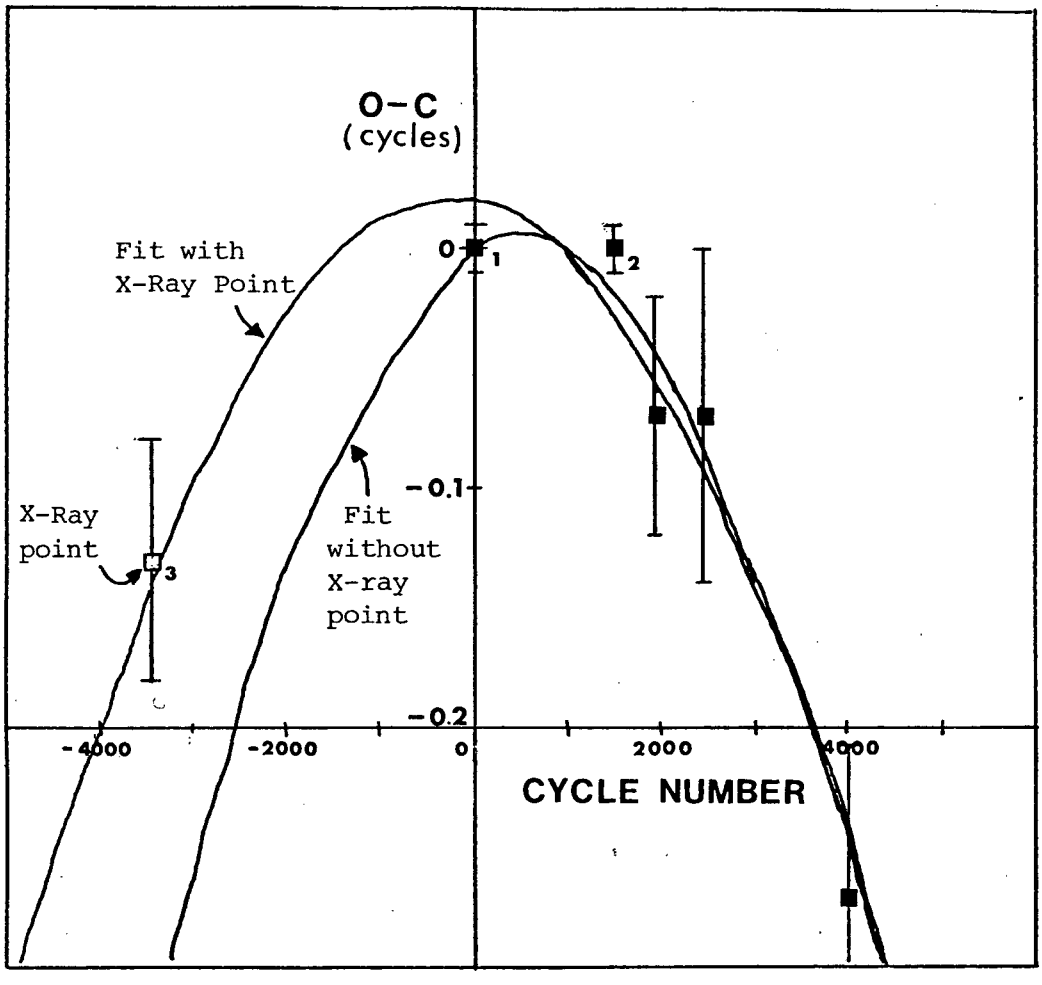

Figure 5.11 O-C Diagram for E2003+225 showing best quadratic fits including and excluding the X-ray point (3). Points 1, 2 and 3 are from Nousek *et al.* (1984).

HJD 2445619.757 i.e. ∿2491 cycles after the epoch and at a time when the O-C can be calculated easily from the optical observations as ∿-0.1 (linear or quadratic fits). A comparison of these observations with the soft X-ray light curves presented by N shows that the curves are remarkably similar. The EXOSAT data are phased according to the ephemeris of N by Osborne *et al.* (1984) and the beginning of the EINSTEIN observation, according to the same ephemeris, is at $\phi = 0.254$. By comparison of several features in the two light curves it can be ascertained that the features occur ∿0.03 cycles earlier in the EINSTEIN curve than in the EXOSAT curve. Thus the O-C of the point at -3424 cycles is -0.1+(-0.03) or ∿-0.13 cycles. This point is also plotted in fig. 5.11 and indicates that a quadratic fit is essential for fitting the times of maxima of the linear polarisation. One further timing in 1985 will be sufficient to confirm this finding.

A formal quadratic fit of the form:

$$O\text{-}C = A + BE + CE^2$$

was made to the points in fig. 5.11. The points at E=0 and E=1515 cycles were assigned double the weight of the other four points. This yielded the following values for A, B and C in units of orbital period:

$A = 0.021$

$B = -6.695 \times 10^{-6}$

$C = -1.548 \times 10^{-8}$

Translated into days this gives a revised ephemeris for E2003+225 of:

$$\text{HJD } 2445234.8380 \underset{\pm 20}{} + 0.1545242E \underset{\pm 7}{} - 2.39 \times 10^{-9} E^2 \underset{\pm 0.26 \times 10^{-9}}{}$$

This is not substantially different from the fit without the X-ray point at -3424 cycles.

The above discussion provides strong evidence that the period of the linear polarisation peaks is decreasing (i.e. the primary is being spun up). It is instructive to compare the spin-up rate with that predicted by theory.

The spin-up rate from the above expression is:

$\dot{P} = 2C = -3.1 \times 10^{-8}$ s s^{-1}

This can be compared with the value of -2.5×10^{-8} obtained from equation 3 of Lamb and Patterson (1983), assuming a 1 $M_\odot$ primary of radius 5×10^8cm and moment of inertia 10^{50}gcm^2, and that the star is near its equilibrium spin-up rate and has an accretion luminosity of 10^{34} ergs s^{-1}. For $M_{WD} = 0.5\ M_\odot$, $\dot{P}_{eq} \simeq -1 \times 10^{-7}$ and for $M_{WD} = 1.3\ M_\odot$, $\dot{P}_{eq} \simeq -7 \times 10^{-9}$ (still assuming an accretion luminosity of 10^{34} ergs s^{-1} in the absence of any better value). Thus the spin-up rate observed here is consistent with the expected values from the discussion by Lamb and Patterston (1983) (although these do not place very strong constraints on $\dot{P}$, as the primary mass is unknown). Other predictions from Lamb and Patterson (1983) are:

1) upper bound to the magnetic field $\lesssim$ 70MG;

2) an upper bound to the inner radius of the disk r_o of $r_o/R_{WD} \lesssim 80 \simeq a/2$ where a is the binary separation if P is the orbital period.

3) If B $\simeq$ 30MG $r_o/R_{WD} \lesssim 50 \simeq a/3$.

All of the above are calculated assuming a $1M_\odot$ primary.

The above $\dot{P}$ corresponds to $\dot{P}/P \simeq 7.3 \times 10^{-5}$ yr^{-1} which is considerably larger than the values found for the orbital

periods of other cataclysmic variables of similar periods ($<5 \times 10^{-8}$ yr^{-1}, Patterson 1984) and indicates that the primary and secondary in E2003+225 are not phase locked. In fact, the timings used above, derived from linear polarisation peaks and X-ray light curves, give no indication of the orbital period of the system at all; this is always inferred from the polarisation timings assuming synchronous rotation. If the line emitting region is close to the secondary, the orbital period could be obtained from the period of the radial velocity variations. However the spectroscopy of Nousek *et al.* (1984) is not of high enough resolution to determine the period of the narrow emission line peaks. Ellipsoidal variations in the infra-red light curve, if detected, would locate the secondary (Szkody *et al.* 1983). No such observations are available. The degree of asynchronism therefore remains unknown if the rotation axis of the primary is parallel to the orbital rotation axis. If it is not parallel the effective β will vary. As the polarisation curves vary only over a time scale of months (see section 5.4.1) it is likely that the orbital period of the system is close to the rotation period of the primary.

5.4.3 The Geometry of the System

Unfortunately the data available here are not of sufficient quality to place firm constraints on i and β. However, the following may be noted:-

1) The circular polarisation is small (<10%) at all phases. This indicates that $|i-\beta| \gtrsim 40^{\circ}$.

2) The position angle follows a wave shaped curve (see Brainerd and Lamb 1983) and does not increase indefinitely, so $\beta < i$.

3) The circular polarisation is at a maximum at $\phi \simeq 0.5$ and the linear polarisation peak occurs at $\phi \simeq 0.0$, indicating that the column is closest to the limb at $\phi \simeq 0.0$ and closest to the line of sight at $\phi \simeq 0.5$.

4) The position angles have their maximum rate of change (corresponding to the column closest to the line of sight) at $\phi \simeq 0.3$ in contradiction to (3) above and the rate of change at this phase is fairly rapid indicating $|i-\beta| < 40^{\circ}$.

The first two points above indicate that the values of i and β are consistent with those proposed by N, i.e. $46^{\circ} < i < 74^{\circ}$, $10^{\circ} < \beta < 27^{\circ}$. The position angle data, usually the most reliable indicator for i and β, to some extent contradict the above interpretation, especially with regard to the phasing of the position angle curve. More extensive observations will be required to resolve these difficulties.

5.4.4 The Phasing of the X-Ray Data

N claim that the period calculated from 15 linear polarisation peaks is not sufficiently accurate to determine the phasing of the X-ray light curve, despite an accumulated error from the quoted uncertainties over the intervening 3424 cycles of only $\sim$0.01 of a period. Using the ephemeris from Section 5.4.2 it is possible to determine that the start of the EINSTEIN observation is at $\phi = 0.39$. This indicates that

the deep minimum in the X-ray light curve extends from phases 0.4 to 0.47, exactly the phases at which N found a deep notch in the I band circular polarisation data. The phasing of both of these minima indicates that they are likely to be caused by the accretion stream passing in front of the accretion column as in EF ERI (Patterson, Williams and Hiltner 1981). It is unlikely that the minima are caused by an eclipse of the accretion region by the secondary, as proposed by N, because the minima are highly wavelength dependent. The stream is also likely to be responsible for the brief dip at the same phase observed in some blue light curves by N.

Table 5.3

Run	Date	Duration (cycles)	Telescope (m)
MS007	17 July 1983	0.9	1.9
S3200	6 Oct 1983	0.4	1.9
S3344	30 May 1984	1.2	0.75
S3348	1 June 1984	1.2	0.75

5.5 PG 1550+191

Stockman *et al.* (1981) announced the discovery of linear and circular polarisation in this CV candidate from the Palomar Green survey. A comprehensive investigation by Liebert *et al.* (1982) included photometry, polarimetry and spectroscopy.

5.5.1 The Observations

The system was observed polarimetrically on only three occasions as its time of visibility coincided with that

of E1405-451. The log of observations all of which were made at the Sutherland site of the S.A.A.O. is set out in Table 5.4. Photometric observations, made on the 0.75m telescope, were taken at high time resolution in order to detect excess high frequency noise, but none was found at the limit of the scintillation noise. A larger telescope than the 0.75m is required.

One additional linear polarisation peak at HJD 2445818.54785 enables the emphemeris obtained by Liebert *et al.* (1982) to be refined to:

$$\text{HJD } 2444763.758312 + 0.0788745E$$
$$\pm 9 \qquad\qquad \pm 3$$

Although the above peak occurs 13373 cycles after the epoch and 12322 cycles after the last published timing, there appears to be no cycle count ambiguity and the two ephemerides agree to within their uncertainties.

Run S3297, phase folded, is shown in fig. 5.12. The circular polarisation is very similar to the "red" and "blue" data presented by Liebert *et al.* (1982), except that the amplitude of the orbital modulation is slightly larger in the white light run. The linear polarisation and the position angle data, however, are somewhat different. Whereas there is a single linear polarisation peak at $\phi = 0.0$ in the data of Liebert *et al.* (1982) there appears to be linear polarisation over most of the orbit in fig. 5.12, although it still peaks at $\phi = 0.0$. The position angles of Liebert *et al.* (1982) have a larger amplitude of variation than that in fig. 5.12. These differences are similar to those found in

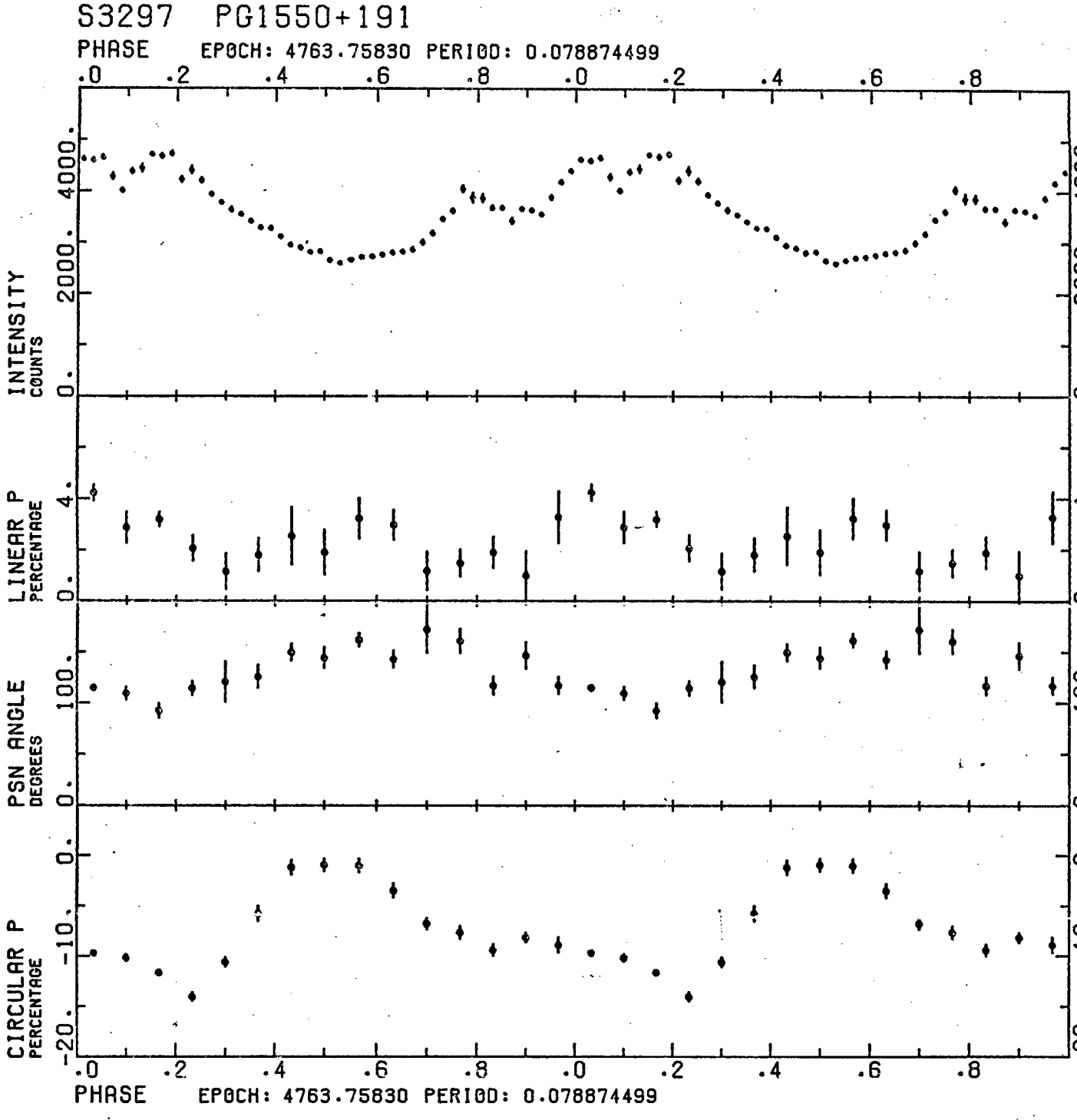

Figure 5.12 Phase folded data for run S3297 taken on 27 April 1984

E1405-451 (Chapter 4, figs. 4.8 and 4.9) and constitute further evidence for shifts in the location of the accretion region. Inversion of the PG1550+191 circular polarisation curves (Liebert *et al.* 1982, fig. 5.2) indicates that the orbital modulation is very similar to that of E1405-451; the two colour data of Liebert *et al.* 1982) show the same self-absorption/ dilution by constant background dip as seen in E1405-451 (Chapter 4) at $\phi \simeq 0.5$, and again it is wider in the blue than in the red as predicted by the Wickramasinghe and Meggitt (1984) calculations (fig. 4.7).

The similarity in the photometric and polarimetric behaviour of the two stars indicates that they are observed at similar inclinations and have similar magnetic colatitudes. The data available here for PG 1550+141 are sparce but $i=55^{\circ}$, $\beta=30^{\circ}$ is consistent with the position angle variation. Liebert *et al.* (1982) deduce $i \lesssim 42^{\circ}$, $\beta \simeq 30^{\circ}$-40°, which is probably more accurate. In both sets of observations $i \gtrsim \beta$, from the position angle data.

More observations must be made of this system before a more thorough investigation can be carried out.

Table 5.4

Run	Date	Duration	Telescope	Type of Observation	Filter
S3107	9 April 1983	0.1	1.9	SLC	-
S3126	18 April 1983	0.8	1.0	SCL	red, blue
S3156	3 August 1983	0.3	0.75	HS Phot	-
S3166	8 August 1983	0.3	0.75	HS Phot	-
S3297	27 April 1984	1.8	1.9	SLC	-

REFERENCES

Agrawal, P.C., Rao, A.R., Riegler, G.R., Pickles, A.J. and Visvanathan, N., 1981. *I.A.U. Circ.* No. 3649.

Allen, D.A. and Cherepashchuk, A.M., 1982. *Mon. Not. R. astr. Soc., 201,* 521.

Bailey, J., 1978. *Mon. Not. R. astr. Soc., 185,* 73P.

Bailey, J., Giles, A.B., Watts, D.J. and Greenhill, J.G., 1982. *I.A.U. Circ.* No. 3720.

Biermann, P., Kühr, H., Liebert, J., Stockman, H., Strittmatter, P. and Tapia, S., 1982. *I.A.U. Circ.* No. 3680.

Brainerd, T.J. and Lamb, D.Q., 1983. Preprint.

Campbell, C.G., 1984. *Mon. Not. R. astr. Soc., 211,* 66.

Cowley, A.P., Crampton, D. and Hutchings, J.B., 1982. *Astrophys. J., 259,* 730.

Cropper, M.S., 1982. *I.B.V.S.*, No. 2096.

Herbig, G.H., 1960. *Astrophys. J., 132,* 76.

Home, K., 1983. Ph.D. Thesis, California Institute of Technology, Pasadena, California.

Lamb, D.Q. and Patterson, J., 1983. *Proc. I.A.U. Coll. 72,* 229, eds. Livio, M. and Shaviv, G., D. Reidel Publishing Company.

Latham, D.W., Liebert, J. and Steiner, J.E., 1981. *Astrophys. J., 246,* 919.

Liebert, J., Stockman, H.S., Angel, J.R.P., Woolf, N.J., Hege, K. and Margon, B., 1978. *Astrophys. J., 225,* 201.

Liebert, J. and Stockman, H.S., 1979. *Astrophys. J., 229,* 652.

Liebert, J., Stockman, H.S., Williams, R.E., Tapia, S., Green, R.F., Rautenkranz, D. and Ferguson, D.H., 1982. *Astrophys. J., 256,* 594.

Maraschi, L., Beuermann, K., Bonnet-Bidaud, J.M., Charles, P.A., Chiappeti, L., Hammerschlag, G., Howarth, I., Motch, C., Mouchet, M., Osborne, J., Stella, L., Tanzi, E.G., Treves, A., Van Paradijs, J., Willis, A.J. and Wilson, R., 1984. *Proc. 4th European I.U.E. Conference*, Rome. In press.

Nousek, J.A., Luppino, G. and Gajar, S., 1982. *I.A.U. Circ.* No. 3733.

Nousek, J.A., Takalo, L.O., Schmidt, G.D., Tapia, S., Hill, G.J., Bond, H.E., Grauer, A.D., Stern, R.A. and Agrawal, P.C., 1984. *Astrophys. J., 277*, 682.

Nugent, J.J., Jensen, K.A., Nousek, J.A., Garmire, G.P., Mason, K.O., Walter, F.M., Bowyer, C.S., Stern, R.A. and Riegler, G.R., 1983. *Astrophys. J. Suppl. Ser. 51*, 1.

Oosterhoff, P. Th., 1935. *Publ. astr. Soc. Pacif., 47*, 322.

Osborne, J., Maraschi, L., Beuermann, K., Bonnet-Bidaud, J.M., Charles, P.A., Chiapetti, L., Motch, C., Mouchet, M., Tanzi, E.G., Treves, A. and Mason, K.O., 1984. *Symp. X-Ray Astronomy*, Bologna. In press.

Patterson, J., Williams, G. and Hiltner, W.A., 1981. *Astrophys. J., 245*, 618.

Patterson, J., 1984. *Astrophys. J. Suppl. Ser., 54*, 443.

Patterson, J., Beuermann, K., Lamb, D.Q., Fabbiano, G., Raymond, J.C., Swank, J. and White, N.E., 1984. *Astrophys. J., 279*, 785.

Pickles, A.J. and Visvanathan, N., 1982. *Proc. astr. Soc. Austr., 4*, 425.

Schneider, D.P. and Young, P., 1980. *Astrophys. J., 240*, 871.

Stockman, H., Liebert, J., Tapia, S., Green, R., Williams, R., Ferguson, D. and Szkody, P., 1981. *I.A.U. Circ.* No. 3616.

Szkody, P. and Capps, R.W., 1980. *Astronom. J., 85,* 882.

Szkody, P., Bailey, J.A. and Hough, J.H., 1983. *Mon. Not. R. astr. Soc., 203,* 749.

Tapia, S., 1977. *I.A.U. Circ.* No. 3054.

Thackeray, A.D., Wesselink, A.J. and Oosterhoff, P.Th., 1950. *B.A.N., 11,* 193.

Thorstensen, J.R., Schommer, R.A. and Charles, P.A., 1983. *Publ. astr. Soc., Pacif., 95,* 564.

Van Gent, H., 1931. *B.A.N., 6,* 93.

Visvanathan, N. and Wickramasinghe, D.T., 1979. *Nature, 281,* 47.

Visvanathan, N. and Wickramasinghe, D.T., 1981. *Mon. Not. R. astr. Soc., 196,* 275.

Visvanathan, N. and Tuohy, I., 1982. *I.A.U. Circ.* No. 3720.

Visvanathan, N. and Tuohy, I., 1983. *Astrophys. J., 275,* 709.

Walker, M.F., 1965. *Mitt. der Stern. Budapest,* No. 57.

Wickramasinghe, D.T. and Meggitt, S.M.A., 1982. *Mon. Not. R. astr. Soc., 198,* 975.

Wickramasinghe, D.T., Reid, I.N. and Bessell, M.S., 1984. *Mon. Not. R. astr. Soc., 211,* 37P.

Wickramasinghe, D.T. and Meggitt, S.M.A., 1984. Preprint.

Wickramasinghe, D.T., Visvanathan, N. and Tuohy, I.R., 1984. *Astrophys. J., 286,* 328.

CHAPTER 6

OBSERVATIONS OF OTHER CATACLYSMIC VARIABLES

6.1 Introduction

In addition to the observations made on the AM Her stars, detailed in chapters 3 to 5, observations were made on a variety of other cataclysmic variables (CV's). Some of these are presented and briefly discussed in this final chapter.

The first object, V603 Aql, is a classical nova and the second, E1013-477, is a strong candidate for membership in the AM Her class of CV's. The remaining objects - AE Aqr, EX Hya, H2252-035 and V1223 Sgr - are members of the DQ Her class (Lamb and Patterson 1983). V603 Aql was chosen in order to investigate reports of polarisation at roughly the orbital period. The DQ Her stars were chosen in order to try to confirm the period of the primary. As this was a secondary program to the AM Her class program, observations were mostly made in poorer conditions. No polarisation variations at orbital or primary rotation periods were found in any of these objects.

6.2 V603 Aql

6.2.1 Introduction

This old nova (Nova Aquilae 1918) was reported by Metz (1982) to have small polarisation variations at nearly the orbital period (deduced from radial velocity observations - Kraft 1964). The linear and circular polarisation variations were reported to have periods of 0.1485 and 0.1376 days respectively; these differ from the period of 0.1448 days, determined from a repeating hump feature in the light curve reported by Haefner

(1981) and the spectroscopic period of 0.1385 days. Observations were therefore carried out in an attempt to confirm the validity of the reported polarisations.

6.2.2 Observations

Three runs each covering almost the spectroscopic period, were taken on consecutive nights ($JD_{\odot}$2445819,20,21) with the U.C.T. Polarimeter on the 1.9m reflector at S.A.A.O. A white light passband of 3500-9200Å was used to maximize the count rate. Conditions on the third night were not photometric, but not poor enough to affect significantly the polarisation results.

The polarisation variations are too small to be seen in individual observations which were taken at a 60 sec time resolution. Therefore the light curves only are shown in figure 6.1. As it is not possible to extrapolate to the era of our observations from the ephemeris given by Haefner (1981) or that of Rahe *et al.* (1980), ϕ = 0 is taken arbitrarily as $JD_{\odot}$2445819.0, and phases are calculated with the radial velocity period (0.1385 days).

6.2.3 Results

The three nights of polarisation data were transformed to Stokes Parameters Q,U and V and each data set searched for periodicities using the Discrete Fourier Transform technique (Deeming 1975, Kurtz 1984) up to the Nyquist frequency ($1/\frac{1}{120}$ sec^{-1}). The results of this analysis are shown in figure 6.2. As can be seen, there are no significant periods in any of the Stokes Parameters at the periods quoted by Metz (1982) (marked by small arrows). Moreover, there are no significant peaks at any period

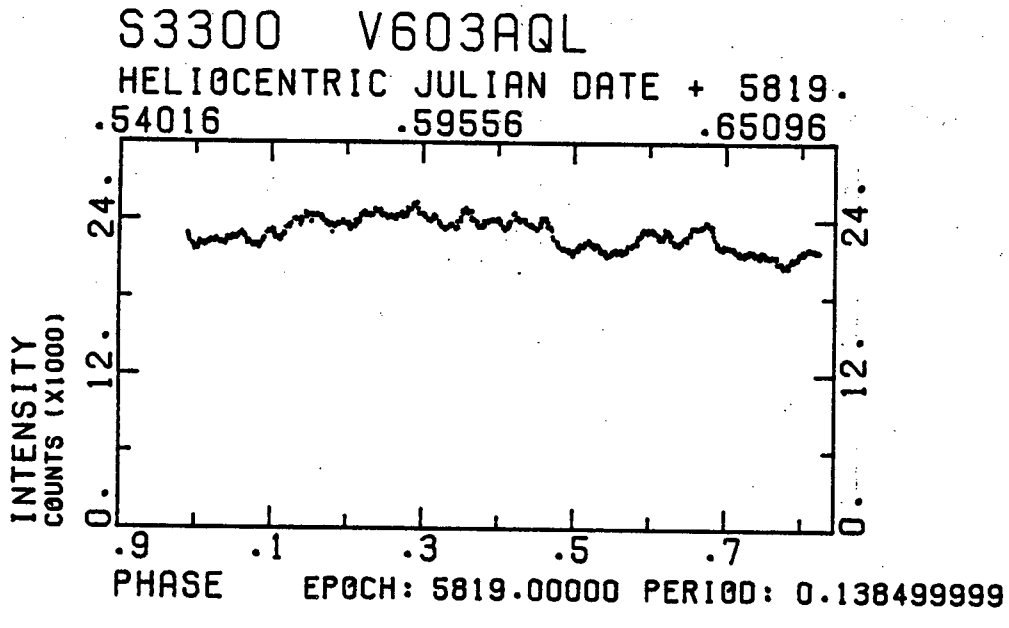

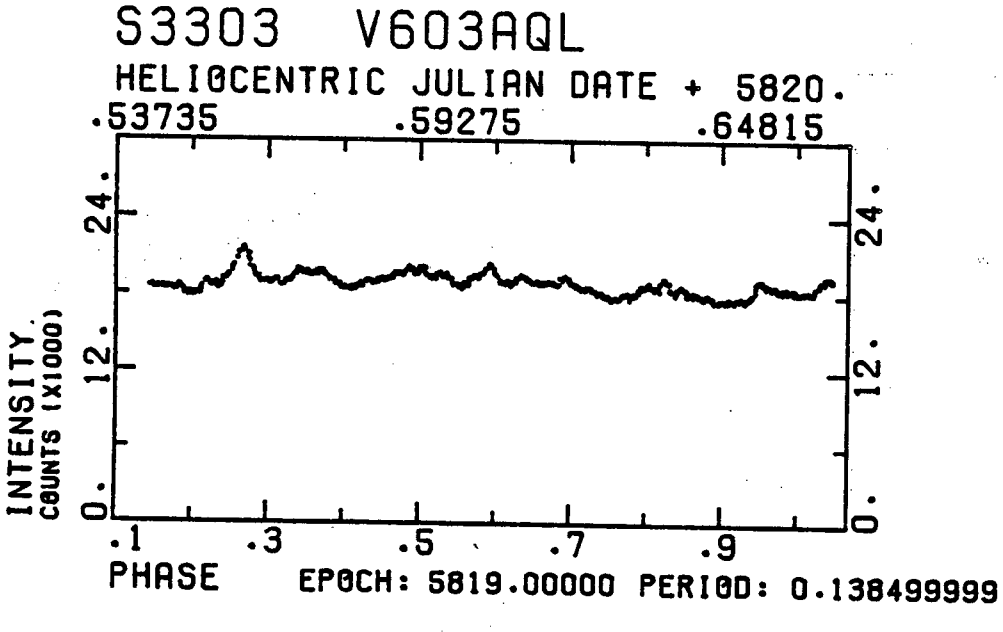

Figure 6.1 Examples of light curves for V603 Aql on the nights starting 29th and 30th April 1984

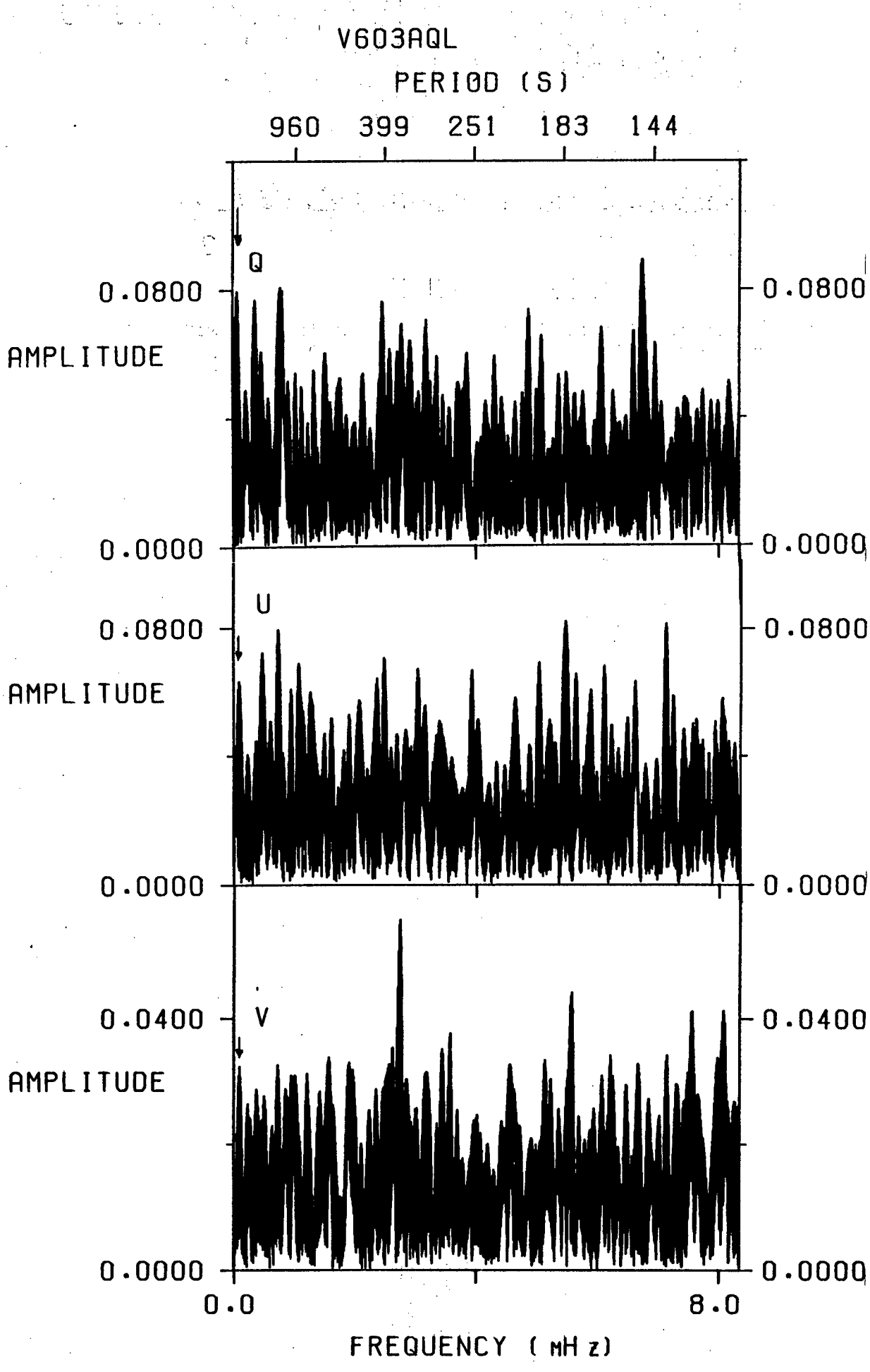

Figure 6.2 Power spectra for the three Stokes Parameters of runs S3300, S3303 and S3304 combined. Ordinate scale is in percent.

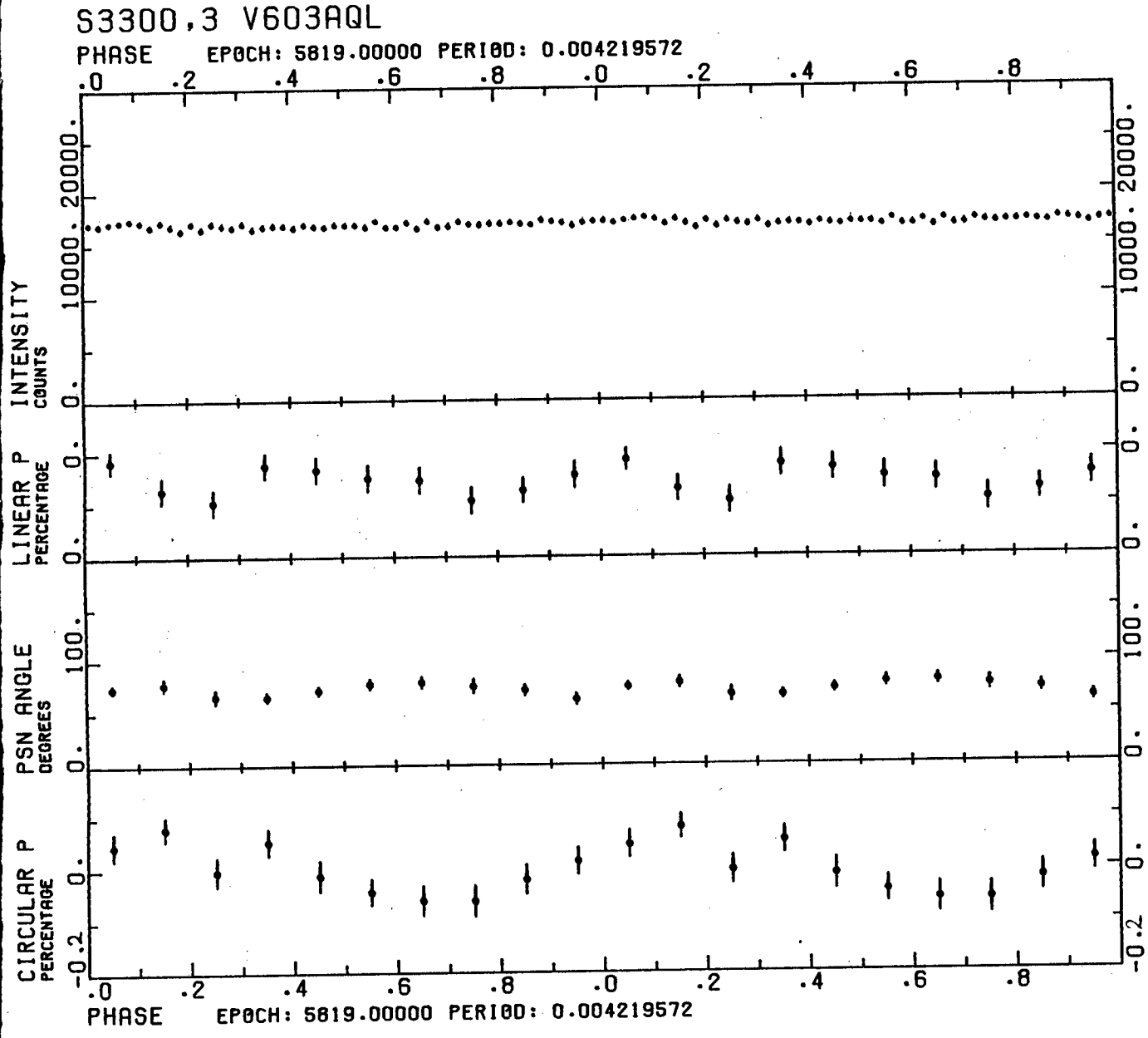

Figure 6.3 Runs S3300 and S3303 (with S3304 polarisation information only) folded on the 366 second period discussed in the test.

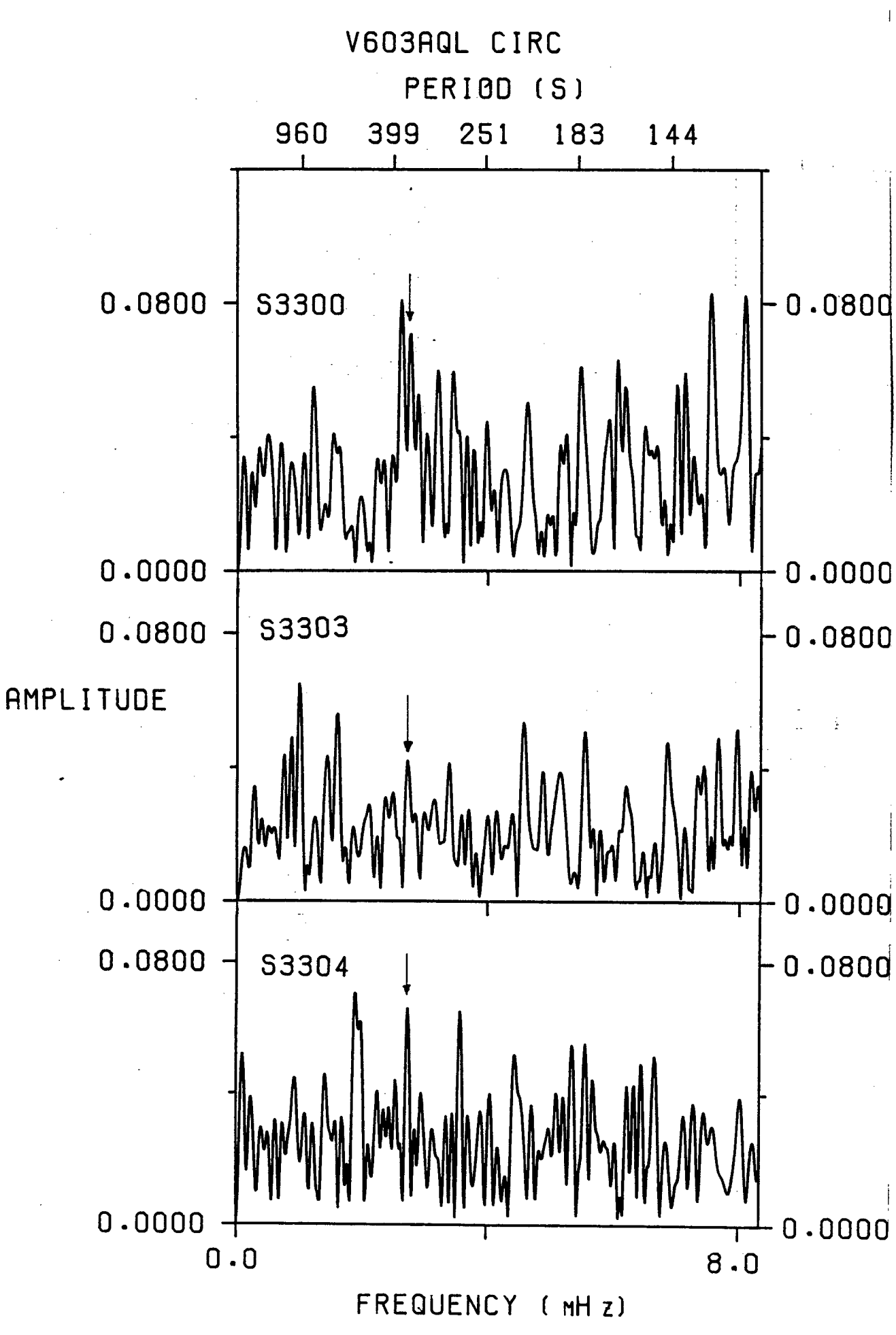

Figure 6.4 Power spectra of the circular polarisation for the three individual runs S3300, S3303 and S3304. The 366 second peak is arrowed in each case.

down to 120 seconds, with one possible exception - that at 366 seconds in the circular polarisation with an amplitude of $\sim$0.055 percent. Figure 6.3 shows the entire data set folded at this period. There is no variation in the intensity at this period, although some (non-sinusoidal) variation is evident in the linear polarisation.

It is difficult to quantify the significance of the above period (Scargle 1982). Thus the amplitude spectra of the circular polarisation in the three individual nights of data are shown in figure 6.4 and the question left open.

To summarise therefore, no evidence is found in the data for significant polarisation variations at any of the previously proposed periods, and a search down to 120 sec shows that the only possibly significant variations take place in the circular polarisation at a period of 366 seconds.

The average polarisations for all three runs together are: $p = 0.390\% \pm 0.020\%$, $\theta = 70^{\circ}.8 \pm 2^{\circ}.6$ and $q = -0.001\% \pm 0.008\%$. The linear polarisation is consistent with the value and orientation expected for interstellar polarisation (Mathewson and Ford 1970).

6.3 E1013-477

6.3.1 Introduction

This X-ray source was identified as a blue $\sim 17^{m}$ star by Mason *et al.* (1982) and proposed as an AM Her type variable on the basis of the spectrum, which contained strong emission lines of H, HeI and HeII. Mason *et al.* (1983) reported that the count rate during the Einstein observations between December 1979 and June 1980 was at least a factor of 10 lower than that

detected by HEAO 1 (H1011-47) in December 1977, and also that the star had faded to $\sim 19^m$ in May 1982 from $16\overset{m}{.}6$ in June 1981 and April 1982. Maraschi *et al.* (1984) reported that the UV flux was weaker by a factor of 2 in March 1984 compared with the observation by Mason *et al.* (1983) in January 1982.

6.3.2 Observations and Results

Three runs were made on this proposed AM Her candidate with the UCT Polarimeter on the 1.9m reflector at the SAAO - S3112 in April 1983 and S3294 and S3298 in April 1984. As the source was found to be very faint, at magnitude 18.6 $\pm$ 0.5, a white light (3500Å - 9200Å) passband was used, to maximize the count rate. This brightness is consistent with that found by Mason (1983) in May 1982 and indicates that the star has almost certainly remained in a faint state between May 1982 and April 1984.

The polarimetric observations were of 1000 sec duration, but were interruped every 200 sec for sky measurements. Polarisation measurements of such a faint source are difficult to make but averaging the circular polarisation for each run yields 1.0 $\pm$ 1.9, 2.6 $\pm$ 2.3 and 0.7 $\pm$ 2.9 percent for S3112 (2 hrs), S3294 (3.6 hrs) and S3298 (1.5 hrs) respectively. Values of circular polarisation $\gtrsim$20 percent are ruled out by the observations, and the above values are consistent with zero. This does not rule out the possibility that E1013-477 is an AM Her star, as H0139-68 in a low state also showed very small values of circular polarisation ($\sim$2 percent, section 5.3). It is not yet known if the proposed 103 min period (Mason *et al.* 1983) is correct so it is not possible to phase the observations to detect a repeating pattern. In short, it is not possible to confirm or

deny the star's membership of the AM Her class from the observations available here. Probably it will be necessary to wait until the star brightens before this will be possible.

6.4 AE Aqr

6.4.1 Introduction

This extensively studied nova-like variable was found to have periodic oscillations at 16.5 and 33 seconds in the optical cal and X-ray light curves by Patterson (1979) and Patterson *et al.* (1980) and was therefore classified as a DQ Her star. Spectroscopic investigations by Joy (1954), Chincarini and Walker (1974), Chincarini and Walker (1981) established that the orbital period was 9.88 hrs, and provided a number of orbital elements. Linear polarisation variations from one year to the next were reported by Szkody *et al.* (1982). Polarisation observations were therefore made to investigate variations on a time scale of seconds and the longer timescale of months.

6.4.2 Observations

The U.C.T. Polarimeter with an RCA 31034A photomultiplier/crown glass fabry was used in two separate ways to obtain polarisation measurements with high enough time resolution to detect any modulation at 16.5 and 33 sec. The log of observations is set out in Table 6.1. Runs S3390, S3394 and S3405 were taken in the circular only mode of the polarimeter at a time resolution of 5 seconds. A $CuSO_4$ filter was used, which gave in a bandpass from 3500Å - 5500Å. Conditions were relatively poor during the runs. Runs S3342 and S3386 were taken in white light (3500Å - 9200Å) and the I_C band respectively in the simultaneous linear

and circular mode of the polarimeter. In order to achieve enough time resolution in this mode, 10 second integrations (with 1 sec dead time) were made consecutively into 3 buffers. At the end of 363 sec (S3342) or 198 sec (S3386), the accumulated counts in each of the three buffers were reduced individually. The polarisations were therefore "folded" with the 33 sec period for 363 or 198 sec, and the reduction yielded groups of three polarisation measurements with a time resolution of 11 seconds, 363 or 198 seconds apart. Conditions were non-photometric during S3386.

6.4.3 Short Timescale Variations

The intensity data, taken at 1 sec in all 5 runs, were Fourier analysed (Deeming 1975, Kurtz 1984) to derive the amplitude of the 16.5 and 33 sec oscillations reported by Patterson (1979). None was found down to an amplitude of $\sim$0.18 percent of the mean level in any of them, a lower level than the 0.2 - 0.3% amplitude oscillations found by Patterson (1979). The circular polarimetry of runs S3390, S3394 and S3405 was then analysed separately and together. No significant oscillations were found down to the 0.08% level. A least squares fit to all of the above data at the two periods yielded the following amplitudes:-

16.5 sec - 0.064% $\pm$ 0.030%

33 sec - 0.007% $\pm$ 0.030%

These values are consistent with zero.

The circular and linear polarisations from runs S3342 and S3386 were also analysed at periods down to 22 sec and no significant oscillations were found at the 0.2% level in Q and U and the 0.1% level in the circular polarisation. In summary, no

variations were found in any of the three bandpasses, in any Stokes Parameter.

Although there are indications that the amplitudes of the intensity modulations at 33 and 16 sec are lower than found previously, further observations will be necessary before any firm conclusions can be drawn.

Table 6.1

Observations of AE Aqr

Run	Date	Duration	Mode	Telescope	Filter
S3342	29 May 84	140 min	SLC	0.75m	None
S3386	2 Jul 84	150 min	SLC	1.9 m	I_c
S3390	15 Aug 84	140 min	CO	1.0 m	$CuSO_4$
S3394	16 Aug 84	160 min	CO	1.0 m	$CuSO_4$
S3405	20 Aug 84	90 min	CO	1.0 m	$CuSO_4$

6.4.4 Longer Timescale Variations

Linear polarisation variations on a timescale of months were detected by Szkody *et al.* (1982). They found the linear polarisation to be $\sim$0.16% at $\sim 70^{\circ}$ in the B, V and R bands during 1976 and $\sim$0.69% at $\sim 80^{\circ}$ in U, B and V bands in 1977.

The data gathered above were averaged for each run and the results are summarised in Table 6.2.

The mean circular polarisation was -0.054 ± 0.010 percent.

The linear polarisations are found to be consistent with the 1976 observations of Szkody *et al.* (1982), but less than the 1977 observations. The position angle has remained

Table 6.2

Averaged Results for AE Aqr

Run	Filter	p (percent)	θ degrees	q (percent)
S3342	none	0.196±0.066	70°±15°	-0.029±0.023
S3386	I_C	0.15 ±0.10	70°±28°	-0.058±0.034
S3390	$CuSo_4$	-	-	-0.075±0.028
S3394	$CuSo_4$	-	-	-0.051±0.028
S3405	$CuSo_4$	-	-	-0.19 ±0.10

constant within the uncertainties in the measurements. Circular polarisation measurements show the star to be significantly circularly polarised at approximately the -0.05% level in all five runs. Szkody *et al.* (1982) tentatively attribute the polarisation to the effects of scattering off an accretion disk. While the position angle of the linear polarisation is consistent with that expected from interstellar polarisation (to within 20^{o}), multicolour observations by Szkody *et al.* (1982) show an unusual wavelength dependence of polarisation as compared to interstellar polarisation. In view of the above and also the variations in the percentage linear polarisation and the detection of circular polarisation, the cause of the polarisation is probably intrinsic to AE Aqr itself.

6.5 EX Hya

6.5.1 Introduction

EX Hya is an eclipsing dwarf nova with an orbital period of 98.3 run (Mumford 1964, Warner 1972) and a brightness modulation with a period of 67.0 min (Vogt *et al.* 198o). On this basis it was classified as a DQ Her star (Warner 1983, Lamb and Patterson 1983). As with AE Aqr, polarisation observations were made to detect, if possible, any variations at either of the above periods.

6.5.2 Observations and Results

Only one polarimetric observation was made on EX Hya. A red filter was used in the UCT Polarimeter, resulting in a passband of 5500Å to 9200Å. The run S3296, was made on the 1.9m telescope on 27 April 1984 and was of 3.3 hrs duration, or two orbital cycles.

The power spectrum of the intensity data shows a strong peak at 67 min as expected, but there are no significant peaks in the circular polarisation data down to the 0.3% level. Least squares fits at the 67 and 98 minute periods determined by Gilliland (1982) assuming a linear ephemeris give a red band semiamplitude of 0.08% $\pm$ 0.08% for the 67 minute and 0.10% $\pm$ 0.08% for the 98 minute periods in the circular polarisation data. Taking a 2σ upper limit to the above values indicates that the 67 minute intensity variation, which has an amplitude of $\sim$15% of the mean brightness is less than 1.5% polarised.

The average red band polarisations over the entire run were found to be:

$$p = 0.30\% \pm 0.12\%,\ \theta = 71^{\circ} \pm 13^{\circ},\ q = -0.018\% \pm 0.038\%$$

6.6 H2252-035

6.6.1 Introduction

This DQ Her star identified by Griffiths *et al.* (1980) has an orbital period of 3.6 hr and two other periods, one thought to result from the rotation of the magnetic primary, and the other the orbital sideband of the rotation period (Patterson and Price, 1980, Warner, O'Donoghue and Fairall, 1981). A previous lower limit on the linear polarisation of 2% and the circular polarisation of 1% was set by Bailey and Axon (1979) communicated in Griffiths *et al.* (1980) and another limit of 0.2% in the modulated linear polarisation was set by Williams and Johns (1980). Neither of the above reports specified the bandpass used for the observations.

6.6.2 Observations and Results

Two runs were taken on this object. The first was run S3195 with the 1.9m telescope on 4 October 1983 using a red bandpass of 6700Å - 9200Å. The second, S3215, with the 1.0m telescope on 26 October 1983 used an I_C bandpass. Both runs lasted for ∿3 hrs, or ¾ of an orbital period.

Power spectra of the intensity data show a peak at 858 seconds of amplitude 3.0% for the red run and 2.7% for the I_C run. No significant peaks occur in the circular or linear polarisation data of either runs. The noise level in run S3195 is ∿0.18% for the linear polarisation and ∿0.14% for the circular polarisation, while that in S3215 is ∿1.1% and ∿0.8%. An upper limit to the polarisation of the pulsed component is therefore ∿6% and ∿5% for the red band data and ∿40% and ∿30% for the I_C band data.

The average polarisations for run S3195 are:

$p = 0.44\% \pm 0.06\%$

$\theta = 172^{\circ} \pm 5^{\circ}$

$q = 0.028\% \pm 0.027\%$

The values expected from interstellar polarisation are $p \sim 0.3 - 0.5\%$ and $\theta \sim 157^{\circ} - 180^{\circ}$ and thus the linear polarisation measured above is consistent with that expected from an interstellar origin.

6.7 V1223 Sgr

6.7.1 Introduction

This DQ Her type cataclysmic variable was identified with the X-ray source 4U1849-31 by Steiner *et al.* (1980). Extensive white light photometry by Warner and Cropper (1984) showed

modulation at three periods - the orbital period at 0.140239 days and two other periods of 794 sec and 850 sec. Watts *et al.* (1984) reported upper limits to the polarisations of ±3% in V, ±0.5% in R, +0.5/-1.0% in J and ±6% in K.

6.7.2 Observations and Results

Seven polarimetric runs were taken on this object during 1983 and 1984. Most of the runs were made during non-photometric conditions and are therefore of poor quality. One run, S3175 on 31 August 1983 with the 1.9m telescope, was taken in white light and the other 6 were taken through R_C and I_C filters on a variety of telescopes. The observing log is set out in Table 6.3.

More than 100 hrs of high speed photometry was obtained and analysed in collaboration with B. Warner. These results have been reported elsewhere (Warner and Cropper 1984).

In order to extract as much information as possible from the R_C and I_C runs, they were Fourier analysed together. No coherent variation was observed in these or the white light runs to the following level:

a) white light, linear 0.2% circular 0.15%

b) R_C and I_C merged, linear 0.8% circular 0.6%.

This sets limits on the polarisation in the pulsed component of the intensity of ∿5% and ∿4% for the white light and ∿27% and ∿20% for the R_C and I_C runs.

The above limits to the R_C and I_C polarisation variations are at the same level as those reported by Watts *et al.* (1984) for their R band data in the circular polarisation. The photon flux in the white light run above is weighted heavily

towards the blue by the flux distribution of the star and the photomultiplier response. The limit therefore principally places constraints on the polarisation of the pulsed fraction at the blue end of the spectrum.

The average polarisations for V1223 Sgr are:

a) white light - $p = 0.51\% \pm 0.18\%$

$\theta = 35^{\circ} \pm 42^{\circ}$

$q = -0.056\% \pm 0.030\%$

b) R_C and I_C data - $p = 0.49\% \pm 0.16\%$

$\theta = 87^{\circ} \pm 9^{\circ}$

$q = -0.037\% \pm 0.066\%$

These values are consistent with those expected from interstellar polarisation ($p \simeq 0.5\%$, $\theta \simeq 93^{\circ}$ - Matthewson and Ford 1970, and $E(B-V) \simeq 0.15$ - Warner 1984).

Table 6.3

Observations of V1223 Sgr

Run	Date	Duration	Telescope	Filter
S3175	31 Aug 83	144 min	1.9m	None
S3207	9 Oct 83	172 min	1.9m	R_C
S3210	10 Oct 83	50 min	1.9m	R_C
S3221	29 Oct 83	100 min	1.0m	I_C
S3223	30 Oct 83	86 min	1.0m	I_C
S3350	2 Jun 84	40 min	0.75m	I_C
S3384	27 Jun 84	115 min	1.9m	I_C

6.8 Implications of the Results for DQ Her Stars

Although the DQ Her class of cataclysmic variables are thought to contain a magnetic white dwarf primary (see Warner 1983, 1984 for reviews), no intrinsic polarisation at the rotation

or any other period has been observed in these objects, with the possible exception of the prototype itself (Swedlund, Kemp and Wolstencroft 1974, Kemp, Swedlund and Wolstencroft 1974, Nather, Smak and McGraw 1974). These observations were made more than 10 years ago and no further polarimetric observations have been reported (see the comment in Patterson, Robinson and Nather, 1978). Polarisations of ∿30% were reported for the modulated component, principally at 142 sec in both linear and circular polarisation by the first set of authors and at 71 sec in the linear by the second set. An unfiltered S11 passband (∿3500Å - 5800Å) was probably used by both groups; the detection was therefore made predominantly at the blue end of the spectrum.

It is not yet known whether the lack of observed polarisation variations in these objects implies smaller magnetic fields than those of the AM Her objects, or whether any cyclotron radiation is being diluted to very low levels (Barrett and Chanmugam 1984). The data from H2252-035 and V1223 Sgr indicate upper limits of ∿5% to the pulsed component, nearly an order of magnitude lower than the level reported in DQ Her. However, the pulsed component referred to here is not at the same period as the X-ray period (Warner *et al.* 1981, Osborne, reported in Watts *et al.* 1984) and is therefore reprocessed radiation, which is not significantly polarised (Barrett and Chanmugam 1984). Unfortunately no intensity modulation was detected at the X-ray period in the relatively small data sets of either of the above stars, so no limit can be set to the percentage polarisation of this pulsed fraction. It is therefore not possible to place an upper limit on the magnetic field strength which might have been possible (given the above limits) if the principal modulation in the optical was at the X-ray period. The one DQ Her object

for which a modulation was detected at the X-ray period - EX Hya - is likely to have a much smaller field strength than the AM Her objects (because the primary does not rotate synchronously although the orbital separation is comparable to those of the short period AM Her systems).

The prime candidate for the detection of polarisation variations at the rotation period is H2215-086 (Patterson and Steiner 1983, Shafter and Targon 1982). Not only does the principal modulation frequency in the light curve occur at the X-ray and hence rotation frequency, the amplitude of the modulation is some ten times that of H2252-035 or V1223 Sgr.

The maximum polarisation one could expect from the presence of the magnetic field in DQ Her stars can be calculated, roughly, by assuming 10% polarisation in the pulsed fraction at the X-ray period (by analogy with the AM Her stars) and then calculating the diluted polarisation. If no polarisation variation is detected at this level, it indicates that:

a) the accretion process is different in the two classes of star (e.g. the accretion region is substantially larger in the DQ Her stars - King and Shaviv 1985);

b) the magnetic field is weaker and the polarisation occurs principally at other (longer) wavelengths; or

c) the light is substantially reprocessed off an axisymmetric disc.

The limits which have to be reached in the DQ Her stars with known X-ray period are set out in Table 6.4.

Table 6.4

Expected Maximum Polarisations from
DQ Her Stars with Known X-Ray Periods

Star	X-Ray Period sec	Amplitude of Pulsations %	Max. Pol^{n} %	Best limit for Modulated Component %	Best limit for Average Circular %	Refs.
AE Aqr	33	0.25	0.02	0.08	-0.054±0.010	1,3,10
H2252-035	805	1.5	0.15	0.15	0.028±0.027	1,4,7
H2215-086	1239	∿30	∿3	-	-	6,9
TV Col	1943	3	0.3	-	0.07	2,8
EX Hya	4022	15	1.5	0.3	-0.018±0.038	1,5

References

1 - This thesis
2 - Stockman *et al.* (1982), reported in Warner (1983)
3 - Warner, private communication
4 - Warner *et al.* (1981)
5 - Cordova *et al.* (1985)
6 - Patterson and Steiner (1983)
7 - White and Marshall (1981)
8 - Bonnet-Bidaud *et al.* (1984)
9 - Cook *et al.* (1984)
10 - Patterson (1979)

It is evident from the above that we are only now reaching the polarisation levels required for detection of the polarisation, assuming the best case conditions. To be pessimistic, if case (b) or (c) above turns out to be correct, it may never be possible to reach the required level of sensitivity to detect polarisation in these objects, and their magnetic field strengths will have to be inferred from other effects.

REFERENCES

Barrett, P.E. and Chanmugam, G., 1984. *Mon. Not. R. astr. Soc., 210*, 15P.

Bonnet-Bidaud, J.M., Motch, C. and Mouchet, M., 1984. Preprint.

Chincarini, G. and Walker, M.F., 1974, in Electronography and Astronomical Applications, ed. Chincarini, G., Griboral, P.J. and Smith H.J., University of Texas Press, Austin.

Chincarini, G. and Walker, M.F., 1981. *Astron. Astrophys., 104*, 24.

Cook, M.C., Watson, M.G. and McHardy, I.M., 1984. *Mon. Not. R. astr. Soc., 210*, 7P.

Cordova, F.A., Mason, K.O., Kahn, S.M., 1984. Preprint.

Deeming, T.J., 1975. *Astrophys. Space Sci., 36*, 137.

Gilliland, R.L., 1982. *Astrophys. J., 258*, 576.

Griffiths, R.E., Lamb, D.Q., Ward, M.J., Wilson, A.S., Charles, P.A., Thorstensen, J., McHardy, I.M. and Lawrence, A., 1980. *Mon. Not. R. astr. Soc., 193*, 25P.

Haefner, R., 1981. *I.B.V.S.* No. 2045.

Joy, A.H., 1954. *Astrophys. J., 120*, 377.

Kemp, J.C., Swedlund, J.B. and Wolstencroft, R.D., 1974. *Mon. Not. R. astr. Soc., 193*, L15.

Kraft, R.P., 1964. *Astrophys. J., 139*, 457.

Kurtz, D.W., 1985. *Mon. Not. R. astr. Soc.*, in press.

Lamb, D.Q. and Patterson, J., 1983. *Proc. I.A.U. Coll., 72*, 229.

Maraschi, L., Beuermann, K., Bonnet-Bidaud, J.M., Charles, P.A., Chiapetti, L., Hammerschlag, G., Howarth, I., Motch, C., Mouchet, M., Osborne, J., Stella, L., Tanzi, E.G., Treves, A., van Paradijs, J., Willis, A.J. and Wilson, R., 1984. *Proc. 4th European I.U.E. Conf.*, Rome.

Mason, K.O., Middleditch, J., Cordova, F.A., Jensen, K., Reichert, G.A., Bowyer, S., Murdin, P. and Clark, D., 1982. *I.A.U. Circ.* No. 3684.

Mason, K.O., Cordova, F.A., Middleditch, J., Reichert, G.A., Bowyer, S., Murdin, P. and Clark, D., 1983. *Publ. astr. Soc. Pacif., 95,* 370.

Mathewson, D.S. and Ford, V.L., 1970. *Mem. R. astr. Soc., 74,* 139.

Metz, K., 1982. *I.B.V.S.* No. 2201.

Mumford, G.S., 1964. *Publ. astr. Soc. Pacif., 76,* 57.

Nather, R.E., Smak, J.I. and McGraw, J.T., 1974. *I.A.U. Circ.* No. 2677.

Patterson, J., Robinson, E.L. and Nather, R.E., 1978. *Astrophys. J., 224,* 570.

Patterson, J., 1979. *Astrophys. J., 234,* 978.

Patterson, J., Branch, D., Chincarini, G. and Robinson, E.L., 1980. *Astrophys. J., 240,* L133.

Patterson, J. and Price, C.M., 1981. *Astrophys. J., 243,* L83.

Patterson, J. and Steiner, J.E., 1983. *Astrophys. J., 264,* L61.

Rahe, T., Boggess, A., Drechsel, H., Holm, A. and Krautter, J., 1980. *Astron. Astrophys., 88,* L9.

Scargle, J., 1982. *Astrophys. J., 263,* 835.

Shafter, A.W. and Targon, D.M., 1982. *Astron. J., 87,* 655.

Steiner, J.E., Watson, M.G., McHardy, I.M. and Pye, J.P., 1980. *I.A.U. Circ.* No. 3529.

Swedlund, J.B., Kemp, J.C. and Wolstencroft, R.D., 1974. *Astrophys. J., 193,* L11.

Szkody, P., Michalsky, J.J. and Stokes, G.M., 1982. *Publ. astr. Soc. Pacif., 94,* 137.

Vogt, N., Krzeminski, W. and Sterken, C., 1980. *Astr. Astrophys., 85,* 106.

Warner, B., 1972. *Mon. Not. R. astr. Soc., 158,* 425.

Warner, B., O'Donoghue, D. and Fairall, A.P., 1981. *Mon. Not. R. astr. Soc., 196,* 705.

Warner, B., 1983. *Proc. I.A.U. Coll., 72,* 155.

Warner, B., 1984. In Cataclysmic Variables and Low Mass X-ray Binaries, eds. Lamb, D.Q. and Patterson, J., Cambridge, Massachusetts. In press.

Warner, B. and Cropper, M., 1984. *Mon. Not. R. astr. Soc., 206,* 261.

Watts, D.J., Giles, A.B., Greenhill, J.G., Hill, K. and Bailey, J., 1984. Preprint.

White, N.E. and Marshall, F.E., 1981. *Astrophys. J., 249,* L25.

Williams, G. and Johns, M., 1980. *I.A.U. Circ.* No. 3519.

EPILOGUE

Some Final Comments

Polarisation information is crucial for the analysis of AM Her stars. It may have been evident that there is a severe shortage of this information for all of the members in the class (possibly excepting the prototype itself). Even in so well studied a star as EF Eri, much interpretation has been based on only a small amount of polarisation information. There is obviously a great need for more polarimetry, extending over a longer baseline, before substantial progress can be made. It is also amply clear that in order to cover a representative range of behaviour of these stars, a very extensive set of observations is required. At no stage of this investigation were any data found to be redundant.

In order for more progress to be made with the theory of the cyclotron emission, observations will have to be made in specific bandpasses. The polarisation expected in those bandpasses should then be calculated from theory, taking into account the harmonic structure of the radiation and filter transmissions. Only then can direct comparisons be made. Because of the narrower bandpasses necessary these observations will inevitably require large telescopes. In view of the shifts in the apparent position of the accretion region found in some of the data presented here, the accretion geometry should preferably be well determined from simultaneous linear polarisation observations.

Other important questions (among many) arising from this thesis which have been addressed here and elsewhere, but need to be investigated further before any conclusions can be reached are:-

a) What is the source of the basically unpolarised component of the light which is present in the "off" parts of the orbital cycle in stars such as VV Puppis and CW1103+254, and which must be included in order for reasonable fits to be made to the cyclotron calculations?

b) Do the narrow peaks in the emission lines originate in the stream or on the heated face of the secondary, and what is the origin of the multiple emission components seen in the spectra of some objects such as EF Eri?

c) What causes the low states in the AM Her and DQ Her stars, and why is the percentage polarisation reduced in some AM Her stars, and increased in others during the low state?

d) What does the real accretion column look like i.e. does it have areal structure and can cylindrical symmetry about the dipole axis be assumed?

e) What does the real accretion stream look like?

f) What is the cause of the high frequency fluctuations found in the intensity power spectra of some AM Her stars?

More specifically, the following observations need to be carried out:

a) The spinup in the rotation rate of the primary in E2003+225 should be confirmed;

b) H2215-086 should be observed intensively to detect any polarisation modulation at the white dwarf rotation period;

c) The membership of E1013-477 in the AM Her class should be confirmed or rejected as soon as possible.

These observations are planned for the very near future.

It is also possible to look back and comment on the capabilities of the polarimeter. It is apparent that the data produced have been of high quality, and further, that the simultaneous measurement of linear and circular polarisation, and the recording of a light curve at a high time resolution, have proved to be extremely important. However, the instrument was built as a general purpose polarimeter, capable of the highest accuracy; it was not specifically designed for rough ($\sim$1%) measurements of polarisation at low light levels - the regime in whch it has been used almost exclusively in this investigation. A "second generation" polarimeter, designed particularly for this regime would have to use both ordinary and extraordinary beams from the analyser and would have to use a detector of the highest quantum-efficiency, i.e. a CCD. In addition the polarisation should be retrievable at a high time resolution (if this is required) and the sky intensity and polarisation be made available simultaneously. In common with the UCT Polarimeter, retarders effective over a wide wavelength range and an ability for simultaneous linear and circular polarimetry should be retained.